Molecular and cellular mechanisms underlying adult blood-brain barrier maintenance

HARVARD UNIVERSITY
Graduate School of Arts and Sciences

DISSERTATION ACCEPTANCE CERTIFICATE

The undersigned, appointed by the

Division of Medical Sciences

in the subject of Biological and Biomedical Sciences

have examined a dissertation entitled

Molecular and cellular mechanisms underlying adult blood-brain barrier maintenance

presented by Xavier J. du Maine

candidate for the degree of Doctor of Philosophy and hereby certify that it is worthy of acceptance.

Signature: Thomas L. Schwarz
Thomas L. Schwarz (Nov 10, 2021 10:46 EST)

Typed Name: Dr. Thomas Schwarz

Signature: Xi He
Xi He (Nov 10, 2021 10:50 EST)

Typed Name: Dr. Xi He

Signature: Patricia A. D'Amore

Typed Name: Dr. Patricia D'Amore

Signature: Shawn Ferguson
Shawn Ferguson (Nov 17, 2021 09:44 EST)

Typed Name: Dr. Shawn Ferguson

Date: October 29, 2021

Molecular and cellular mechanisms underlying adult blood-brain barrier maintenance

A dissertation presented

by

Xavier J. du Maine

to

The Division of Medical Sciences

in partial fulfillment of the requirements

for the degree of

Doctor of Philosophy

in the subject of

Biological and Biomedical Sciences

Harvard University

Cambridge, Massachusetts

October 2021

Dissertation Advisor: Dr. Chenghua Gu Xavier J. du Maine

Molecular and cellular mechanisms underlying adult blood-brain barrier maintenance

Abstract

To ensure optimal neuronal function, the blood-brain barrier (BBB) maintains a homeostatic brain microenvironment free from harmful agents and delivers nutrients to the brain to support metabolic needs. Although the BBB was first identified more than a century ago, the molecular and cellular mechanisms underlying its formation and maintenance have only recently begun to be uncovered. To date, studies that have examined BBB function in adult mice have largely focused on injury, aging, pathological, or therapeutic models. Thus, the molecular and cellular mechanisms underlying physiological BBB maintenance in adulthood remain largely unknown.

The goal of this dissertation is to uncover novel mechanisms of adult BBB maintenance. First, we provide a mechanism of how canonical Wnt signaling regulates BBB integrity in adulthood. Following acute attenuation of canonical Wnt signaling in mouse brain endothelial cells (ECs) *in vivo*, we find that there is an increase in transcytosis, which correlates with a rapid loss of the caveolae-mediated transcytosis inhibitor MFSD2A. Strikingly, EC-specific overexpression of MFSD2A in Wnt signaling-deficient brain ECs is not sufficient to rescue increased transcytosis, indicating that canonical Wnt signaling regulates multiple transcytosis pathways to maintain BBB integrity. Second, we make progress toward the development of small molecular weight tracers to evaluate the permeability of tight junctions (TJs) at the

ultrastructural level. In Wnt signaling-deficient brain ECs, we find that TJs are impermeable to the smallest molecular weight tracer assayed (1.9 kDa) despite reductions in TJ protein levels.

Third, we investigate the role of nutrient transporters in establishing and maintaining BBB integrity. This class of genes, which is highly expressed and enriched in brain ECs compared to peripheral ECs, delivers a wide variety of nutrients and substrates to the brain to meet the metabolic and energetic needs of neurons. We use a combination of mouse genetics, BBB leakage assays, and electron microscopy to investigate the roles of *Slc16a1* (monocarboxylate transporter 1, MCT1) and *Slc7a5* (large neutral amino acid transporter 1, LAT1) in regulating BBB integrity, finding that neither are required for BBB integrity.

Table of Contents

Title Page……..……i

Copyright Page……ii

Abstract……...iii

Table of Contents……..……v

Acknowledgements……vi

Chapter 1: Introduction……1

Chapter 2: Experimental Procedures……..33

Chapter 3: Molecular and Cellular Mechanisms Governing Canonical Wnt Signaling Regulation of Adult BBB Maintenance: Transcytosis…….41

Chapter 4: Molecular and Cellular Mechanisms Governing Canonical Wnt Signaling Regulation of Adult BBB Maintenance: Tight Junctions…….62

Chapter 5: Nutrient Transporters: Candidate Novel Regulators of BBB Integrity……85

Chapter 6: Conclusions and Outlook……..95

Acknowledgements

I am profoundly grateful for so many people who have enriched, positively shaped, and aided me in my journey through graduate school and my path leading up to graduate school.

I would like to thank my academic community and colleagues. I thank my thesis advisor and mentor Chenghua Gu for giving me the freedom to explore topics of interest to me, teaching me how to do rigorous science, and being a model of bold resilience in the midst of rejection. I thank my fellow members of the Gu Lab, past and present, for their support, guidance, camaraderie, and friendship. I thank my dissertation advisory committee members Tom Schwarz, Gary Yellen, and Timothy Hla for their great advice, humor, and guidance as I navigated the ups and downs of multiple projects. I thank my dissertation defense committee members Tom Schwarz, Xi He, Patricia D'Amore, and Shawn Ferguson for generously agreeing to review my dissertation. I thank Thomas Philips and Jeffrey Rothstein (Johns Hopkins) for opening up the door to a collaboration to study MCT1 in the context of the BBB. And I thank the members of the HMS Electron Microscopy Core – Anja Nordstrom, Maria Ericsson, Louise Trakimas, Peg Coughlin, and Liz Benecchi – for their tireless work that made my research possible, for their warmth and kindness, and most of all for their friendship, which I cherish.

I would not be here today were it not for the mentorship, time, and investment of so many. I thank my parents Jessica and Danny du Maine for making sure I had access to quality public education and instilling in me the importance of education from a young age. I thank my high school anatomy and physiology teacher Kerry Zimmerman for introducing me to the exciting mysteries of the human body and encouraging me to pursue laboratory research. I thank the lab and program mentors, PIs, and program coordinators who provided me with crucial exposure to hands on research, sparking a fire in me to eventually pursue a PhD: Jennifer

Mosher, Stephanie Rodriguez, Erica Koval, Timothy Miller, and the Young Scientist Program (Washington University School of Medicine); Mark Kunitomi, Lauren Shields, Ken Nakamura, and the Summer Research Training Program (UCSF); Roger Lefort and Michael Shelanski (Columbia); and Stephen Zhang, Mike Crickmore, Dragana Rogulja, and the Summer Honors Undergraduate Research Program (Harvard Medical School).

I would like to thank everyone who has supported and empowered me throughout graduate school. I thank my BBS (PPS) classmates for infusing graduate school with fun, supportive community. I thank my Minority Biomedical Scientists of Harvard and Harvard Coalition for Black Lives friends and peers for constantly encouraging, inspiring, and uplifting me through Black joy, Black excellence, Black resilience, and Black power. I thank my HPREP and SHURP families for giving me the opportunity to give back and be of service to others. I thank my fellow GSAS Diversity and Inclusion Fellows for being my diversity "partners" throughout graduate school, especially Lara Roach and José Del Río Pantoja. I thank Sheila Thomas and Karina Gonzalez for being a constant source of support and mentorship throughout graduate school and equipping me with the resources and guidance to realize my dreams and ideas about making Harvard a more diverse and inclusive training, learning, and teaching environment.

I thank my faith communities at Aletheia Church, Calvary Chapel in the City, Boston Healthcare Fellowship, and the Christian Medical and Dental Association for helping me to pause, reminding me of the greater purpose of my work and life, and supporting me in my spiritual and personal growth. I thank my health providers Nyssa Boardman, Meg Schrier, and Carmen Cruz for gently teaching me how to practice self-care and prioritize mental health. I thank my family for being there, and especially my sister Maxine for being my biggest supporter

and loudest cheerleader. I thank my dearly beloved friends for their unconditional agape love, which has shaped me into who I am today. Lastly, and most of all, I thank my Creator for giving me the strength and persistence to sustain me throughout graduate school.

CHAPTER 1

Introduction

1.1. Vascular Heterogeneity

Endothelial cells (ECs) throughout the body display a remarkable heterogeneity in their structure and function, adapting to the needs of their underlying tissues and organs (Aird, 2007b). Structural differences include the organization of the basement membrane, the presence or absence of pores (i.e. fenestrations) and gaps in the endothelium, the architecture of cell-cell junctions, and the presence of vesicular structures and organelles. Despite this striking diversity of features, all blood vessels can be broadly placed into three structural categories: discontinuous, continuous fenestrated, and continuous non-fenestrated (Aird, 2007a).

Discontinuous vessels are characterized by gaps, fenestrations, and a poorly formed basement membrane. These vessels primarily include the sinusoid vessels of the liver, whose blood filtering function necessitates the presence of large gaps and fenestrations that permit the exchange of blood contents between the circulation and the liver parenchyma. Continuous vessels, as their name suggests, are characterized by a continuous basement membrane and an endothelium that is free of gaps. Continuous vessels can be further subdivided into fenestrated and non-fenestrated. Fenestrated continuous vessels include vessels in the endocrine glands, GI tract mucosa, and the kidney glomerulus. The presence of fenestrations makes these vessels more permeable to blood contents relative to their continuous non-fenestrated counterparts, which include vessels in the skin, lung, heart, and brain.

Even among the continuous non-fenestrated vessels, there is a heterogeneity in structure and function. In particular, continuous non-fenestrated vessels in the brain that comprise the blood-brain barrier have a unique set of properties.

1.2. Specialized Properties of the Blood-Brain Barrier

The blood-brain barrier, or BBB, is a set of specialized properties possessed by brain capillary ECs that enable them to maintain a homeostatic brain environment for optimal neuronal function (Chow and Gu, 2015; Langen et al., 2019). These properties, which tightly regulate the entry and exit of agents to and from the brain parenchyma, have two main functions: protection and nourishment. First, the BBB prevents the entry of potentially harmful molecules, cells, and pathogens into the brain, protecting it from agents that can perturb normal physiology. Second, the BBB delivers a variety of nutrients and molecules to the brain, supplying the energetic substrates and precursors required for proper neuronal and glial function. The molecular and cellular properties of brain capillary ECs, discussed below, enable them to carry out these protective and nutritive functions (**Figure 1.1**).

1.2.1. Tight junctions

One crucial property of brain ECs is the presence of specialized tight junctions (TJs). These cell-cell junctions are comprised of interlocked extracellular protein complexes anchored in the plasma membrane by the cytoskeleton. BBB TJs, in particular, are characterized by very close apposition of adjacent EC membranes. Notably, the apposition of these membranes in brain ECs is closer than that observed in peripheral ECs (e.g. cardiac), which is an ultrastructural correlate of functionally tighter junctions (Muir and Peters, 1962; Reese and Karnovsky, 1967). The tightness of BBB TJs prevents the paracellular diffusion of substances between the blood and the brain, creating a size- and charge-based permeability barrier between adjacent brain ECs.

TJs are primarily composed of claudins, occludin, zonula occludens, and junctional adhesion molecule (JAM) proteins. Claudin-5 (CLDN5), occludin (OCLN), and zonula

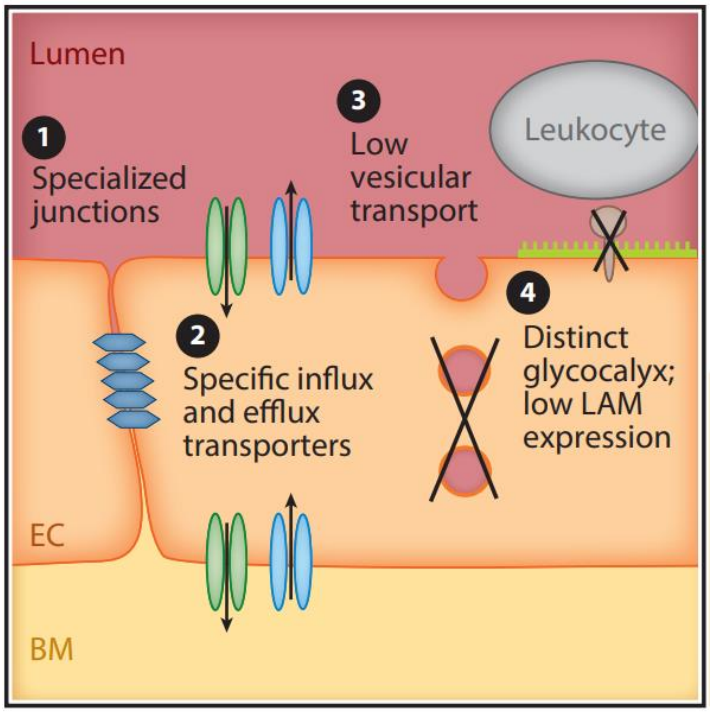

Figure 1.1. Specialized Properties of the Blood-Brain Barrier. The four main specialized properties of brain ECs that confer BBB function are specialized tight junctions, suppression of transcytosis, expression of influx and efflux transporters, and suppression of leukocyte adhesion molecules. Adapted from (Langen *et al.*, 2019).

occludens-1 (ZO-1) are expressed in brain ECs and localize to junctions during embryonic CNS angiogenesis as ECs enter the cortex, and their expression persists into adulthood (Daneman et al., 2010b). Claudins and occludin form interlocking homomeric and heteromeric "zipper" structures that tightly seal the space between adjacent ECs.

Cldn5$^{-/-}$ mice, while displaying brain EC TJs with normal morphology, have a size-selective BBB leakage phenotype (leakage threshold between 742 Da and 1.9 kDa) and mice die perinatally (Nitta et al., 2003). Although earlier studies claimed that CLDN1, CLDN3, and CLDN12 are also expressed at the BBB, recent studies have shown that mRNA for these claudins are either undetectable or at extremely low levels in brain ECs, and that these claudins are dispensable for barrier function (Castro Dias et al., 2019a; Castro Dias et al., 2019b; Pfeiffer et al., 2011).

Ocln$^{-/-}$ mice also display normal TJ morphology but, in contrast to CLDN5 KO mice, survive into adulthood and have calcification in the cerebellum and basal ganglia (Saitou et al., 2000). While this phenotype may suggest aberrant calcium homeostasis due to altered TJ permeability, neither BBB leakage nor TJ permeability have been directly examined in these mice. Also, because OCLN is widely expressed in epithelial cells, it cannot be ruled out that the brain calcification is due to epithelial cell defects.

ZO-1 (*Tjp1*) acts a cytoplasmic adaptor that anchors extracellular TJ complexes to the actin cytoskeleton, providing them with a stabilizing intracellular scaffold. *Tjp1*$^{-/-}$ mice, in contrast to *Cldn5*$^{-/-}$ and *Ocln*$^{-/-}$, have severe developmental phenotypes, including impaired yolk sac angiogenesis, growth defects, and apoptosis, resulting in lethality by E10.5 (Katsuno et al., 2008). Thus, the specific mechanisms of ZO-1's role in BBB TJ formation and function remain unknown. Overall, tamoxifen-inducible and tissue-specific ablation of TJ proteins at different

timepoints during pre- and post-natal development, as well as adulthood, will help shed light on these mechanisms.

1.2.2. Suppression of transcytosis

Another essential cellular feature of BBB ECs is the suppression of transcellular vesicular trafficking, or transcytosis. Some of the earliest observations of this phenomenon occurred in the 1960s in the pioneering electron microscopy (EM) studies of Thomas Reese and Morris Karnovsky (Reese and Karnovsky, 1967). The suppression of transcytosis prevents the movement of large macromolecules, including serum proteins, from the blood to the brain, creating a transcellular permeability barrier. To date, the only known molecular regulator of transcytosis in the central nervous system (CNS) is major facilitator superfamily domain-containing 2a, or MFSD2A. MFSD2A expression is observed at E13.5, exclusively in the barrier-containing brain and spinal cord vasculature (Ben-Zvi et al., 2014). Mice with global knockout of *Mfsd2a* have a dysfunctional BBB and blood-retinal barrier characterized by increased permeability to a variety of exogenous tracers, including sulfo-NHS-LC-biotin (557 Da), 10 kDa and 70 kDa dextran, and horseradish peroxidase (HRP, 44 kDa) (Ben-Zvi *et al.*, 2014; Chow and Gu, 2017). Notably, while *Mfsd2a*$^{-/-}$ mice display increased transcytosis, they have TJs that are impermeable to HRP, providing evidence according to current standards that their BBB leakage phenotypes are due to transcytosis and not TJs. We have previously identified the upregulated vesicle subtype in *Mfsd2a* mutants as caveolae, a flask-shaped vesicular organelle that is abundant in peripheral ECs, especially in continuous non-fenestrated blood vessels (Andreone et al., 2017).

Mechanistically, MFSD2A functions as a transporter for long-chain fatty acid–containing lysophosphatidylcholine lipid species, notably those containing docosahexaenoic acid (DHA)

(Nguyen et al., 2014). Our work shows that DHA incorporation into brain EC plasma membranes favors a liquid disordered state of the plasma membrane, which suppresses the formation of caveolae vesicles (Andreone *et al.*, 2017). Importantly, genetic ablation of caveolae vesicles in *Mfsd2a*$^{-/-}$ mice is sufficient to rescue BBB leakage, further supporting a model in which MFSD2A suppresses transcytosis by preventing caveolae formation.

1.2.3. Transporters

Given the BBB's relative impermeability, it requires mechanisms for delivering nutrients to the brain. This is primarily accomplished through the expression of substrate-specific influx transporters, which mediate passive transport of sugars, amino acids, lipids, monocarboxylic acids, nucleotide derivatives, organic ions, and other molecules from the blood to the brain (Campos-Bedolla et al., 2014). These influx transporters are primarily in the 400-member solute carrier (SLC) family of transporters, around 50 of which are expressed in brain ECs (Campos-Bedolla *et al.*, 2014). One of the most highly expressed nutrient transporters is the glucose transporter GLUT1 (*Slc2a1*), which is important for BBB integrity, cerebral blood flow, and angiogenesis (Tang et al., 2021; Veys et al., 2020; Winkler et al., 2015).

In addition to influx transporters, the BBB expresses a variety of efflux transporters that facilitate the removal of toxins and metabolic waste products from the brain (Campos-Bedolla *et al.*, 2014). These efflux transporters are primarily in the ATP-binding cassette (ABC) family of transporters and include, most notably, P-glycoprotein or PGP (*Abcb1a*), which is also known as multidrug resistance gene 1 (MDR1). PGP has a broad pool of substrates that includes many small lipophilic molecules and drugs. Lastly, BBB ECs expresses ion pumps/exchangers that actively maintain extracellular sodium and potassium ion gradients to ensure proper neuronal function (Campos-Bedolla *et al.*, 2014).

1.2.4. Suppression of leukocyte adhesion molecules

Leukocyte adhesion molecules (LAMs) are required for the immobilization of circulating leukocytes on the luminal vessel wall, initiating the subsequent steps that facilitate their migration across the endothelium and into the underlying parenchyma (Ransohoff and Engelhardt, 2012). In the brain, the presence of leukocytes can trigger inflammation, which may perturb normal brain physiology. To minimize the entry of harmful, proinflammatory leukocytes into the brain, BBB ECs suppress expression of LAMs (Rossler et al., 1992).

1.3. The Neurovascular Unit

The specialized molecular and cellular properties of the BBB are not intrinsic to brain ECs. Rather, they require close interaction with other cell types in the brain to be induced and maintained. The primary cell types that brain ECs interact with are pericytes, astrocytes, and neurons, which, together with ECs, form the neurovascular unit (NVU).

1.3.1. Pericytes

Pericytes are a type of mural cell that sit on the outer wall of capillaries, embedded in the EC basement membrane. They extend various processes along the blood vessel wall, increasing the physical contact between these two cell types. During embryonic development, brain ECs secrete platelet-derived growth factor B (PDGFB), which binds to heparan sulfate proteoglycans in the endothelial extracellular matrix. PDGFB recruits pericytes to the blood vessel wall through binding to pericyte-expressed PDGF receptor β (PDGFRβ) (Hellstrom et al., 1999). Genetic manipulations that perturb this ligand-receptor interaction result in reduced pericyte coverage of brain capillaries (Armulik et al., 2010; Daneman *et al.*, 2010b).

Reduced pericyte coverage causes BBB dysfunction and leads to perinatal lethality for *Pdgfrb*$^{-/-}$ mice (Daneman *et al.*, 2010b). Both these mice, as well as pericyte-deficient mouse

models that are adult viable, display leakage of a variety of small and large molecular weight exogenous tracers and endogenous plasma proteins (Armulik *et al.*, 2010; Bell et al., 2010; Daneman *et al.*, 2010b). While some studies argue that increased BBB permeability in pericyte-deficient mice is due to increased transcytosis, rigorous, quantitated ultrastructural evidence for this claim is lacking. However, the reduction of endothelial MFSD2A expression in pericyte-deficient mice lends credence to this hypothesis (Ben-Zvi *et al.*, 2014). Importantly, a potential role for TJ dysfunction in inducing increased permeability in pericyte-deficient has not been ruled out.

While pericytes are embedded within the EC basement membrane, they also secrete basement membrane proteins that are important for BBB function, including laminin (Gautam et al., 2016), as well as the recently characterized vitronectin (Ayloo *et al*., bioRxiv 2021), which provides the first evidence for a specific mechanism of pericyte-EC signaling that regulates BBB integrity without ablating pericytes or reducing pericyte coverage.

In addition to their role in BBB formation, pericytes are also required for maintenance of the BBB in adulthood. Specifically, *Pdgfrb*$^{+/-}$ mice, which don't have reduced pericyte coverage or increased BBB permeability during development, display an age-dependent gradual loss of pericytes beginning at one month of age, resulting in increased BBB permeability to exogenous tracers and endogenous serum proteins (Bell *et al.*, 2010). In addition, in a recent study that acutely deleted the pericyte-specific transcription factor FOXF2 in adult mice, there was an increase in BBB leakage of the tracer Evans Blue (Reyahi et al., 2015).

1.3.2. Astrocytes

Just outside of the EC basement membrane, astrocytes extend endfeet processes that ensheath blood vessels (Mathiisen et al., 2010). This physical proximity puts them in an ideal

position to signal to brain ECs and regulate their function. Unlike pericytes, astrocytes are not required for induction of barrier properties during embryogenesis since gliogenesis occurs postnatally, after the BBB has already functionally formed. In fact, astrocyte endfeet only begin to physically associate with blood vessels during the first week after birth in mice and rats (Daneman *et al.*, 2010b).

One of the established functions of astrocyte-EC interactions is the regulation of brain water flux through the astrocytic water channel aquaporin-4 (AQP4), which is expressed in astrocytic endfeet (Nielsen et al., 1997). Notably, AQP4 global or glial-specific KO mice have a decrease in brain edema following experimental conditions that increase brain water uptake (Haj-Yasein et al., 2011; Manley et al., 2000). Another posited role of astrocytes is the enhancement of TJ ultrastructural properties, such as the total number of endothelial TJs and TJ length (Tao-Cheng et al., 1987), though the evidence for this is lacking *in vivo*.

Although astrocytes do not play a role in BBB formation, they are important for BBB maintenance. One of the primary mechanisms of astrocyte-mediated BBB maintenance is through the secretion of Wnt factors WNT7A, WNT7B, and Norrin (Wang et al., 2018) (see **1.8.2. Canonical Wnt Signaling Components in the Central Nervous System** for more details). In addition, like pericytes, astrocytes secrete basement membrane proteins that are important for BBB maintenance. Specifically, knockout of astrocytic laminin causes BBB breakdown through altered TJ protein expression and perturbed pericyte differentiation (Yao et al., 2014). A recent study also found that acute, sparse astrocyte ablation in adult mice leads to BBB leakage and loss of ZO-1 expression (Heithoff et al., 2021). Altogether, these findings demonstrate a requirement for astrocytes for BBB maintenance.

1.3.3. Neurons

While the role of mature, fully differentiated neurons in BBB maintenance is unclear, neuronal precursors play a well-defined role in BBB formation. Specifically, the CNS neuroepithelium expresses and secretes Wnt factors that activate canonical Wnt signaling in CNS ECs, inducing barrier properties (see **1.9.2. Canonical Wnt Signaling in CNS Vascular Development** for more details). In addition, a recent study characterized a neuro-glia-vessel intercellular communication pathway dependent on the neuronal guidance cue reelin and endothelial Dab1 that is important for barrier properties associated with EC interaction with astrocytes (Segarra et al., 2018).

1.4. Blood-CNS Barriers

In addition to the BBB, the central nervous system (CNS) contains two other functionally analogous barriers – the blood-retinal barrier (BRB) and the blood-spinal cord barrier (BSCB) – which possess many of the same properties (Chow and Gu, 2017; Winkler et al., 2012). The retina, which is a part of the CNS along with the brain and spinal cord, contains a highly stereotyped architecture of neurons and glia that enables vision. Unlike the BBB and BSCB, development of the retinal vasculature and BRB begins after birth.

At P1, brain ECs invade the optic nerve head (ONH) and grow radially along the vitreal surface of the retina during the first week after birth (Stahl et al., 2010). By P8, this superficial vascular plexus is formed, which later gives rise to the deeper plexus, followed by the intermediate plexus. Mirroring the spatiotemporal development of the retinal vasculature, BRB formation occurs first in the mature vessels proximal to the ONH and progresses to the immature vessels distal to the ONH (Chow and Gu, 2017). For example, at P5, injected tracers are confined

within the proximal vessels but leak from the distal vessels. By P10, the distal vessels are also sealed, concluding BRB formation.

Within the retina, there are two functional BRBs. Specifically, the inner BRB (iBRB) is comprised of blood vessels in the superficial vascular plexus. In addition, there is an outer BRB formed by the layer of retinal ganglion cells that are connected by TJs. The iBRB, like the BBB, is characterized by TJs, suppression of transcytosis, expression of influx and efflux transporters, and suppression of LAMs. Thus, the iBRB is functionally analogous to the BBB, with many of the same genetic perturbations that disrupt BBB integrity and function also having the same effect on the iBRB.

1.5. Assaying Blood-Brain Barrier Permeability

To determine if blood vessels are functionally "sealed," (i.e. barrier-competent) we employ blood-CNS barrier leakage assays. These assays involve the injection of exogenous tracers into the blood circulation or the detection of endogenous serum proteins. Exogenous tracers circulate for a given amount of time in the blood prior to sacrificing the animal to perform histology on the brain. Next, we examine the spatial relationship between the tracer or endogenous protein and the blood vessels.

The basic principle underlying these assays is that if a blood vessel has a functional barrier, exogenous injected tracers and endogenous serum proteins will be confined within the vascular compartment. However, if a blood vessel does not have a functional barrier, the tracer will leak out of the blood vessel and enter the parenchymal space. These assays are widely used to determine if blood-CNS barriers are functional ("sealed") or dysfunctional ("leaky") at the level of gross permeability to blood contents. However, it is worth noting that they do not reflect all aspects of blood-CNS barrier physiology and are not meant to do so.

Exogenous tracers have a wide range of chemical properties (e.g. molecular weight, atomic radius) and include multiple types of biomolecules: proteins (e.g. horseradish peroxidase – 44 kDa), polysaccharides (e.g. dextrans – 3 to 2000 kDa), and small molecules (e.g. sulfo-NHS-LC-biotin - 557 Da). Common endogenous serum proteins used for leakage assays are albumin (~67 kDa), fibrinogen (340 kDa), and immunoglobulin G, or IgG (150 kDa). Another general principle of leakage assays is that permeability to larger tracers or endogenous proteins is indicative of a more severe barrier defect. However, there is vigorous debate in the field surrounding whether certain tracers cross the barrier through a paracellular-selective or transcellular-selective route, with little definitive evidence of the ultrastructural level (see **4.1. Assessing Tight Junction Permeability** for more details). A major technological need is smaller molecular weight tracers that are compatible with electron microscopy imaging, which I make progress toward developing in my work (see **4.2. The Development and Optimization of Tools to Assess the Permeability of Tight Junctions at the Ultrastructural Level**).

1.6. BBB Development

Multiple studies have characterized BBB formation using leakage assays. Specifically, our group has described the spatiotemporal development of the BBB using injection of the tracer 10 kDa dextran into the liver of embryos (Ben-Zvi *et al.*, 2014). At E13.5, we find that the vasculature in the entire brain is permeable to 10 kDa dextran. At E14.5, functional BBB formation begins and is complete by E15.5, as indicated by the confinement of 10 kDa dextran within the brain vasculature. This temporal finding of BBB formation has been independently confirmed in separate studies. One study examining the developing mouse spinal cord vasculature dated the initiation of barriergenesis (i.e. impermeability to sulfo-NHS-biotin) to

E14.5 (Sohet et al., 2015). Another study examining the developing rat brain vasculature found that the BBB was impermeable to sulfo-NHS-biotin as early as E15 (Daneman *et al.*, 2010b).

Interestingly, we also observe a caudal-to-rostral and ventrolateral to dorsomedial pattern of spatial barrier acquisition (Ben-Zvi *et al.*, 2014). This pattern of BBB formation mirrors CNS vascularization, which also occurs in a caudal-to-rostral spatiotemporal pattern. For example, at E14.5 the hindbrain and midbrain vasculature are sealed, as well as the ventral-lateral cortex. However, the dorsal-medial cortex is still leaky. At E15.5, the dorsal-medial cortex becomes sealed, indicating a fully formed BBB (Ben-Zvi *et al.*, 2014).

As described above, the induction and maintenance of these barrier properties depends on the neural environment in which brain ECs reside. A previous study mapped out the generation of different cell types in the brain during embryogenesis and early postnatal development. It found that pericytes, which are generated by E10, are recruited to blood vessels at E11, around the time of cortical angiogenesis (Daneman *et al.*, 2010b). The neuroepithelium also plays a role in the induction of these properties through the production and secretion of Wnt factors (see below for details). Astrocytes are generated later after birth (P1) and begin to make contacts with blood vessels during the first week after birth. This occurs by P5 in rats and P7 in mice (Daneman *et al.*, 2010b).

1.7. BBB Maintenance

To date, there have been very few studies investigating the molecular and cellular mechanisms of adult BBB maintenance under physiological conditions (Chang et al., 2017; Tran et al., 2016; Wang et al., 2012). Among studies that have examined BBB function in sexually mature adult mice, there has been a large focus on disease, injury, aging, or pathological models (Banks et al., 2021; Bell et al., 2012; Deane et al., 2003; Elahy et al., 2015; Kiss et al., 2020;

Montagne et al., 2020; Munji et al., 2019; Park et al., 2018; Sagare et al., 2013; Shibata et al., 2000; Soto et al., 2015; Stamatovic et al., 2019; Sweeney et al., 2018; Yamazaki et al., 2016; Yang et al., 2020; Zhao et al., 2020). In addition, other studies have relied on ablation or altering the abundance of entire cell types (Bell *et al.*, 2010; Heithoff *et al.*, 2021; Reyahi *et al.*, 2015), leaving the specific intercellular signaling–mediated and cell-autonomous mechanisms of BBB maintenance largely unknown. One of the major exceptions to this large gap in knowledge is the canonical Wnt signaling pathway, which is discussed in detail below. Although this pathway plays an important role in BBB maintenance, it is unclear which other signaling pathways are required for BBB maintenance in adulthood, which brain regions they are active in, and how cell-autonomous and non-cell-autonomous mechanisms mediate their effects on the BBB.

1.8. Canonical Wnt Signaling

1.8.1. Pathway Overview

The highly conserved canonical Wnt pathway is dependent on the transcriptional mediator β-catenin, which acts downstream of Wnt ligands and Wnt receptors at the cell surface to orchestrate expression of Wnt target genes (Nusse and Clevers, 2017). This is in contrast to the non-canonical Wnt pathways, which signal through Wnt but operate independently of β-catenin. Under baseline conditions, cytosolic β-catenin (encoded by the gene *Ctnnb1*) is constitutively degraded via targeting to the proteasome following its phosphorylation by a cytoplasmic protein complex, termed the destruction complex.

The destruction complex has four core components: casein kinase 1α (CK1α), glucose synthase kinase 3 (GSK3), AXIN1, and adenomatous polypolis coli (APC). CK1α and GSK3 are serine/threonine kinases that sequentially phosphorylate β-catenin to initiate its ubiquitination by E3 ubiquitin ligase β-TrCP, while AXIN1 functions as a scaffold to bring the components of the

destruction complex together (Stamos and Weis, 2013). The role of APC is not well understood but putative functions include destruction complex cycling and localization, mediating β-TrCP interactions with β-catenin, and cytoplasmic sequestration of β-catenin (Stamos and Weis, 2013). Upon Wnt ligand binding to the Wnt receptor Frizzled and Wnt co-receptors low-density lipoprotein receptor–related proteins 5/6 (LRP5/6), the destruction complex is inactivated. This inactivation occurs at least in part via Dishevelled (DVL) polymerization and AXIN1 recruitment to the phosphorylated cytoplasmic tail of LRP5/6.

Inactivation of the destruction complex allows β-catenin to accumulate in the cytoplasm and translocate to the nucleus. In the nucleus, it binds to transcription factors (TFs) belonging to the T-cell factor (TCF) and lymphoid enhancer-binding factor (LEF) families. These TF heteromers facilitate gene expression in concert with a host of transcriptional co-activators via TCF/LEF-binding sites in regulatory elements of target genes (Valenta et al., 2012).

1.8.2. Canonical Wnt Signaling Components in the Central Nervous System

The basic components of the canonical Wnt signaling pathway at the cell surface are the ligands, receptors, co-receptors, and co-activators (**Figure 1.2**). In the CNS, the primary brain EC-relevant ligands are WNT7A/7B and Norrin (*Ndp*). For the sake of simplicity, I will refer to WNT7A/7B and Norrin as "Wnt ligands". The primary CNS Wnt ligand receptor in ECs is Frizzled-4 (FZD4, encoded by *Fzd4*), although there are other Frizzled receptors (e.g. *Fzd6*) expressed in the CNS vasculature (Daneman et al., 2009). The primary CNS Wnt ligand co-receptors in ECs are LRP5 and LRP6. Finally, the known CNS Wnt ligand co-activators in ECs are GPR124, RECK, and TSPAN12. There is a great deal of genetic interaction and redundancy among these components in a region- and tissue-specific manner (Wang *et al.*, 2018). In **Table 1.1**, I provide a summary of tissue and cell type expression for each of these components at

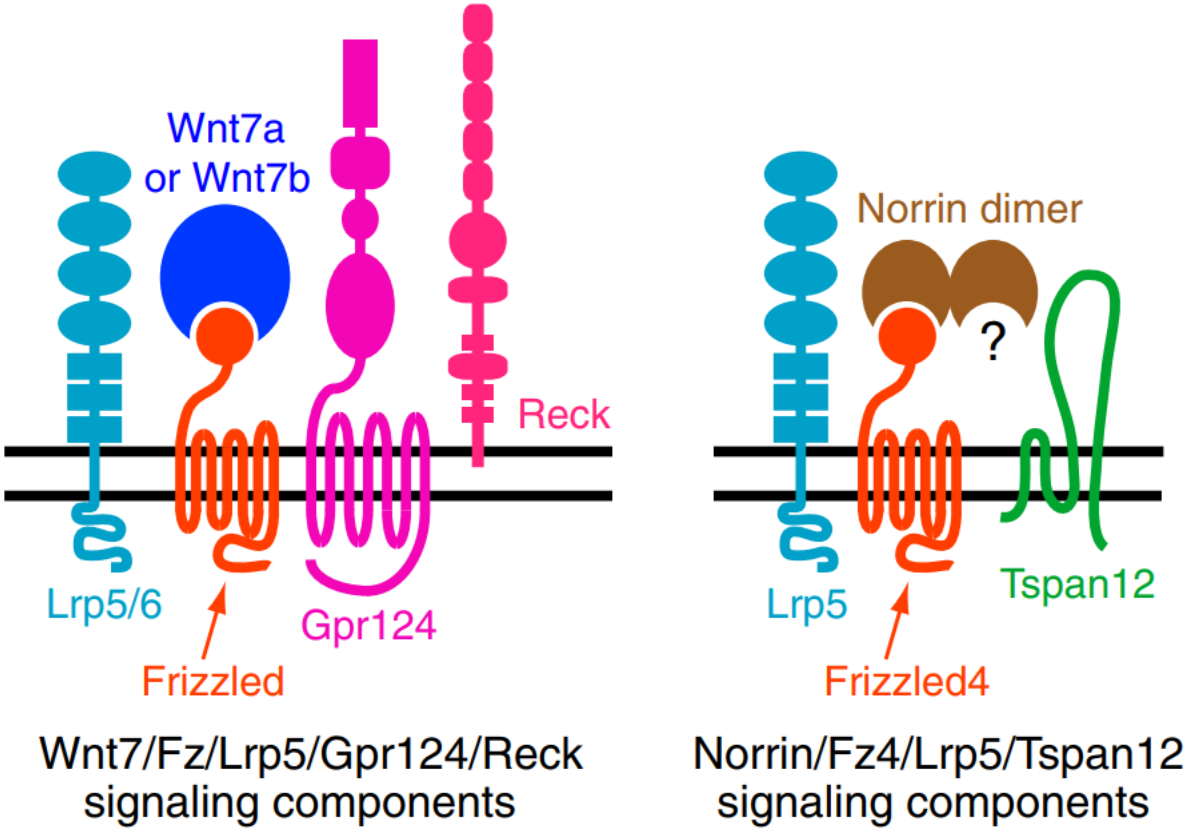

Figure 1.2. Canonical Wnt Signaling Components in Central Nervous System Endothelial Cells. The major BBB-relevant components of the canonical Wnt signaling pathway in the CNS include WNT7A/7B, FZD4, LRP5/6, GPR124, RECK, and TSPAN12. While the Wnt7/Fz/Lrp5/Gpr124/Reck signalosome (left) is functionally predominant in most of the CNS vasculature, the Norrin/Fz4/Lrp5/Tspan12 signalosome (right) is functionally predominant in the retinal vasculature. Adapted from (Wang *et al.*, 2018).

Table 1.1. CNS Tissue and Cell Type Expression of BBB-Relevant Canonical Wnt Pathway Components in Mouse. Each cell type is color-coded: **endothelial cells** (ECs), **mural cells** (pericytes and smooth muscle cells [SMCs]), **other perivascular cells** (microglia and fibroblasts), **glia** (astrocytes, oligodendrocytes, oligodendrocyte precursor cells [OPCs], and Muller glia), and **neural cells** (neural progenitors, neurons)

Pathway component	Timepoint	Tissue/cell type expression	Method of detection	References
Wnt ligands				
WNT7A/7B	E11.5	Ventral-lateral spinal cord: **neural progenitors** in the ventricular zone Cortical forebrain: **neural progenitors**	*In situ* hybridization of embryonic CNS tissue sections	(Daneman *et al.*, 2009)
WNT7A	P7	**Astrocytes:** predominant expression **OPCs:** moderate expression **Neurons:** low expression	Bulk RNA-seq of FACS-purified cell types in the cerebral cortex	(Zhang et al., 2014)*
WNT7B	P7	**Neurons:** predominant expression **Astrocytes:** slightly lower expression **OPCs:** slightly lower expression	Bulk RNA-seq of FACS-purified cell types in the cerebral cortex	(Zhang *et al.*, 2014)*
WNT7A	Adult (10-19 weeks)	**Astrocytes:** predominant expression	Single-cell RNA-seq of brain vascular cells	(Vanlandewijck et al., 2018)**
WNT7B	Adult (10-19 weeks)	**Astrocytes:** predominant expression	Single-cell RNA-seq of brain vascular cells	(Vanlandewijck *et al.*, 2018)**
WNT1	E11.5	Dorsal neural tube: **neural progenitors** in the ventricular zone	*In situ* hybridization of embryonic CNS tissue sections	(Daneman *et al.*, 2009)
WNT3	E11.5	Dorsal neural tube: **neural progenitors** in the ventricular zone	*In situ* hybridization of embryonic CNS tissue sections	(Daneman *et al.*, 2009)
WNT3A	E11.5	Dorsal neural tube: **neural progenitors** in the ventricular zone	*In situ* hybridization of embryonic CNS tissue sections	(Daneman *et al.*, 2009)

Table 1.1 (Continued)

WNT4	E11.5	Dorsal and intermediate spinal cord: **neural progenitors**	*In situ* hybridization of embryonic CNS tissue sections	(Daneman *et al.*, 2009)
WNT5A	E11.5	Cortical forebrain: **neural progenitors** (spatially complementary to Wnt7a/7b)	*In situ* hybridization of embryonic CNS tissue sections	(Daneman *et al.*, 2009)
Norrin	E10.5	Spinal cord: Dorsal **neuroepithelium** Hindbrain: Mid-dorsal **neuroepithelium**	*Ndp* alkaline phosphatase knock-in reporter	(Ye et al., 2011)
Norrin	P4/P7	Retina: **Muller glia**	*Ndp* alkaline phosphatase knock-in reporter	(Ye et al., 2009)
Norrin	P7	**Astrocytes:** predominant expression **OPCs:** moderate expression	Bulk RNA-seq of FACS-purified cell types in the cerebral cortex	(Zhang *et al.*, 2014)*
Norrin	Adult (10-19 weeks)	**Astrocytes:** predominant expression **Oligodendrocytes:** lower expression	Single-cell RNA-seq of brain vascular cells	(Vanlandewijck *et al.*, 2018)**
Norrin	Adult	Cerebellum: **Bergmann glia** Forebrain and diencephalon: **astrocytes**	*Ndp* alkaline phosphatase knock-in reporter	(Ye *et al.*, 2011)
Wnt receptors				
FZD4	Midgesation embyro	Widely expressed	*Fz4* lacZ reporter mouse	(Wang et al., 2001)
FZD4	Early postnatal	P8: no expression in the cerebellum P15: expression observed in cerebellum	*Fz4* lacZ reporter mouse	(Wang *et al.*, 2001)
FZD4	P7	**ECs:** predominant expression **Astrocytes:** much lower expression	Bulk RNA-seq of FACS-purified cell types in the cerebral cortex	(Zhang *et al.*, 2014)*
FZD4	Adult	Brain, lung, and liver **ECs**	Micorarray of FACS-sorted ECs from Tie2-GFP mice	(Daneman *et al.*, 2009)
FZD4	Adult	Brain, lung, liver, eye, heart, kidney, and testis	*Fz4* mRNA probe	(Wang et al., 1996)

Table 1.1 (Continued)

FZD4	Adult (10-19 weeks)	Expression across multiple cell types: highest in **ECs**, lower in **SMCs**, **fibroblasts**, and **astrocytes**	Single-cell RNA-seq of brain vascular cells	(Vanlandewijck *et al.*, 2018)**
FZD6	E11.5	Forebrain and spinal cord: **ECs**	*In situ* hybridization of embryonic CNS tissue sections	(Daneman *et al.*, 2009)
FZD6	Adult	Cerebral cortex: **ECs**	Microarray of FACS-purified ECs in the cerebral cortex	(Daneman *et al.*, 2009)***
FZD6	Adult	Expression across multiple cell types: highest in **ECs**, **pericytes**, and **SMCs**	Single-cell RNA-seq of brain vascular cells	(Vanlandewijck *et al.*, 2018)**
FZD8	Adult	Cerebral cortex: **ECs** (expression is much lower than Frizzled-4 and Frizzled-6)	Microarray of FACS-purified ECs in the cerebral cortex	(Daneman *et al.*, 2009)***
Wnt co-receptors				
LRP5	P7	**Microglia/macrophages:** predominant expression **ECs**, **OPCs**, and **astrocytes**: lower expression	Bulk RNA-seq of FACS-purified cell types in the cerebral cortex	(Zhang *et al.*, 2014)*
LRP6	P7	Broad expression, in order of expression level: **astrocytes**, **OPCs**, **ECs**, **newly formed oligodendrocytes**, **neurons**	Bulk RNA-seq of FACS-purified cell types in the cerebral cortex	(Zhang *et al.*, 2014)*
LRP5	Adult	Broad tissue expression in brain, calvarium, fat, kidney, heart, liver, lung, muscle, skin, spleen, testis	Northern blot	(Kato et al., 2002)
LRP5	Adult (10-19 weeks)	Expressed at similar levels across **ECs**, **pericytes**, **SMCs**, **microglia**, **fibroblasts**, and **astrocytes**	Single-cell RNA-seq of brain vascular cells	(Vanlandewijck *et al.*, 2018)**
LRP6	Adult (10-19 weeks)	Expressed at similar levels across **ECs**, **pericytes**, **SMCs**, **microglia**, **fibroblasts**, **oligodendrocytes**, and **astrocytes** (with overall higher expression than LRP5)	Single-cell RNA-seq of brain vascular cells	(Vanlandewijck *et al.*, 2018)**

Table 1.1 (Continued)

Wnt co-activators				
GPR124	E12.5	Forebrain, midbrain, and neural tube **ECs** and **pericytes** Expressed to a lesser extent in liver, heart, and kidney vessels, lung and esophagus epithelium, and mesenchyme	GPR124 immunofluorescence staining	(Kuhnert et al., 2010)
GPR124	P7	**ECs:** predominant expression	Bulk RNA-seq of FACS-purified cell types in the cerebral cortex	(Zhang *et al.*, 2014)*
GPR124	Adult	Exclusively vascular in tissues examined: brain and retina **ECs** and **pericytes**; kidney, pancreas, and corpus luteum **pericytes**	GPR124 immunofluorescence staining	(Kuhnert *et al.*, 2010)
GPR124	Adult (10-19 weeks)	Expression in **ECs**, **pericytes**, **SMCs**, and **fibroblasts**	Single-cell RNA-seq of brain vascular cells	(Vanlandewijck *et al.*, 2018)**
RECK	E10.5	Widely expressed in mesenchymal tissues Relatively abundant in **ECs** and **SMCs** of large blood vessels (e.g. dorsal aorta)	Whole mount immunostaining and immuno-electron microscopy	(Oh et al., 2001)
RECK	P7	Widely expressed in **ECs**, **astrocytes**, **OPCs**, **newly formed oligodendrocytes**, and **neurons**	Bulk RNA-seq of FACS-purified cell types in the cerebral cortex	(Zhang *et al.*, 2014)*
RECK	Adult (10-19 weeks)	Highest expression in **ECs**; next highest in **pericytes**, **SMCs**, and **fibroblasts**; lowest expression in **microglia**, **oligodendrocytes**, and **astrocytes**	Single-cell RNA-seq of brain vascular cells	(Vanlandewijck *et al.*, 2018)**
TSPAN12	P7	Highest expression in **ECs**, with moderately high levels in **astrocytes** and **OPCs**	Bulk RNA-seq of FACS-purified cell types in the cerebral cortex	(Zhang *et al.*, 2014)*
TSPAN12	P14	Expression in retinal **capillaries** and **neural retina** (ganglion cell layer and inner nuclear layer)	Branched DNA amplification *in situ* hybridization in the retina	(Zhang et al., 2018)

Table 1.1 (Continued)

TSPAN12	Adult (10-19 weeks)	Widely expressed, with highest levels in **ECs** and **SMCs**, followed by **pericytes**, **microglia**, and **astrocytes**	Single-cell RNA-seq of brain vascular cells	(Vanlande wijck *et al.*, 2018)**

*Dataset does not include pericytes or SMCs

**Dataset does not include neurons

***Dataset is limited to FACS-purified ECs from cerebral cortex

various developmental timepoints in the CNS.

1.9. Canonical Wnt Signaling Regulation of CNS Vasculature

1.9.1. Canonical Wnt Signaling: Orchestrator of a Brain Endothelial Transcriptional Program

β-catenin orchestrates a gene expression program via binding to TCF/LEF TFs, as well as a variety of other transcriptional co-activators (Valenta *et al.*, 2012). As a result, canonical Wnt pathway mutations lead to an array of gene expression changes in the CNS vasculature. This includes genes which are canonical targets of Wnt signaling, such as *Axin2*, as well as genes with a known role in regulating BBB function (e.g. *Cldn5*, *Plvap*, *Slc2a1*, *Mfsd2a*). In **Table 1.2**, I compile data from a multitude of studies summarizing gene expression changes in canonical Wnt pathway mutants across different genetic models, timepoints, and CNS regions of interest. Given the requirement of canonical Wnt signaling for BBB formation and maintenance (see **1.9.3. Canonical Wnt Signaling in BBB Development** and **1.9.4. Canonical Wnt Signaling in BBB Maintenance**), identifying genes that are regulated by the pathway can yield insights into the molecular and cellular mechanisms through which canonical Wnt signaling regulates the BBB. Multiple studies have performed transcriptomic analyses in mice harboring null mutations in canonical Wnt signaling pathway components to identify these 'Wnt-regulated BBB genes' (Chen et al., 2012; Schafer et al., 2009; Zhou et al., 2014) (see **Table 1.2**). In addition, a recent study identified genes regulated by β-catenin in adult brain ECs by expressing a stabilized, non-degradable form of β-catenin in ECs of the posterior pituitary gland, a circumventricular organ that is deficient in canonical Wnt signaling and does not contain a functional barrier (Wang et al., 2019). RNA-seq analyses revealed transcripts that were upregulated in posterior pituitary ECs by this gain of function genetic manipulation. These genes were then cross-

Table 1.2. Summary of CNS Endothelial Gene Expression Changes in Canonical Wnt Pathway Mutants. Gene expression phenotypes reflect changes in protein unless otherwise noted. Studies that employed genetic manipulations in sexually mature adult mice (e.g. cell type-specific tamoxifen-inducible Cre activation) are highlighted in yellow, to distinguish them from studies observing phenotypes in sexually mature adult mice where genetic manipulations were performed at earlier time points.

Pathway component	Mutation/ genetic model	Timepoint	CNS region of interest	Gene expression phenotype
Wnt ligands				
WNT7A/7B (Stenman et al., 2008)	*Sox2-Cre; Wnt7a*$^{-/-}$*; Wnt7b*$^{fl/-}$	E12.5	Neural tube (PNVP)	↓Glut1
Norrin (*Ndp*) (Schafer *et al.*, 2009)	*Ndp*^{KO}	P7	Retina	↓mRNA*: *Slc38a5, Panx2, Mfsd2a, Aass, Cldn5, Vwa1, Apcdd1, Slc7a1* ↑mRNA*: *Mdm2, Wdr67, Seh11, Adm, Lilrb4, Plvap, Foxp1*
Norrin (*Ndp*) (Zhou *et al.*, 2014)	*Ndp*^{KO}	P10	Retina	↓mRNA*: *Slco1c1, Cldn5, Foxq1, Ly6a, Abcb1a, Slc38a5, Sox17, Fzd6* ↑mRNA*: *Egr3, Emp1, Marveld2, Cdh5, Adm*
Norrin (*Ndp*) (Wang *et al.*, 2012)	*Ndp*^{KO}	Adult	Cerebellum (molecular layer), olfactory bulbs (nerve fiber layer)	↓Cldn5, ↑Plvap, ↓Glut1 (rare in molecular layer, common in nerve fiber layer)
Norrin (*Ndp*) (Wang *et al.*, 2012)	*Ndp*^{KO}*; GLAST-Cre*^{ERT2}*; Z/Norrin*	Adult	Cerebellum	↑Cldn5, ↓Plvap
Wnt receptor				
FZD4 (*Fzd4*) (Wang *et al.*, 2012)	*Pdgfb-Cre*^{ER}*; Fzd4*$^{fl/-}$	Postnatal (early postnatal 4-OHT treatment)	Retina	↓Cldn5, ↑Plvap, ↓Sox17, ↓Glut1

Table 1.2 (Continued)

FZD4 (*Fzd4*) (Wang *et al.*, 2012)	*Tie2-Cre; Fzd4$^{fl/-}$*	Adult	Cerebellum (molecular layer); olfactory bulbs (nerve fiber and glomerular layers); cerebral cortex (surface vessels); spinal cord	↓Cldn5, ↑Plvap, ↓Glut1 (variable) (rare in spinal cord)
FZD4 (*Fzd4*) (Wang *et al.*, 2012)	*Pdgfb-Cre^{ER}; Fzd4$^{fl/-}$*	Adult (early postnatal 4-OHT treatment)	Cerebellum	↓Cldn5, ↑Plvap, ↓Sox17, ↓Zic3
FZD4 (*Fzd4*) (Wang *et al.*, 2012)	*Pdgfb-Cre^{ER}; Fzd4$^{fl/-}$*	Adult	Cerebellum	↓Cldn5, ↑Plvap
Wnt co-receptors				
LRP5 (Chen *et al.*, 2012)	*Lrp5$^{-/-}$*	P8	Retina	↓mRNA*: *Cldn5, Slc38a5, Mfsd2a, Spp1, Icam2, Gja1, Sox18* ↑mRNA*: *Plvap*
Wnt co-activators				
GPR124 (Kuhnert *et al.*, 2010)	*Pdgfb-Cre^{ER}; Gpr124$^{fl/-}$*	E12.5	Forebrain	↓Glut1
GPR124 (Cullen et al., 2011)	*Tie2-Cre; Gpr124$^{fl/-}$*	E13.5	Forebrain	↓Glut1, ↑Plvap
RECK (Cho et al., 2017)	*Tie2-Cre; Reck$^{fl/-}$*	P0	Brain	↑Plvap
TSPAN12 (Zhang *et al.*, 2018)	*Cdh5-Cre^{ERT2}; Tspan12$^{fl/-}$*	P16 (TAM at P1-P3)	Retina	↑Plvap
β-catenin				
β-catenin (Daneman *et al.*, 2009)	*Tie2-Cre; Ctnnb1$^{fl/fl}$*	E11.5	CNS (unspecified)	↓Glut1
β-catenin (Stenman *et al.*, 2008)	*Flk-Cre; Ctnnb1$^{fl/-}$*	E12.5	Neural tube (PNVP)	↓Glut1

Table 1.2 (Continued)

β-catenin (Liebner et al., 2008)	*Pdgfb-Cre^{ER}; Ctnnb1$^{fl/fl}$*	P4, P7, P14 (4-OHT at P1-4, P4-7, P7-14)	Brain	↓Cldn5, ↑Plvap ↑Plvap (mRNA) at P7
β-catenin (Zhou *et al.*, 2014)	*Pdgfb-Cre^{ER}; Ctnnb1$^{fl/fl}$*	P10, P23-24 (4-OHT at P7/P16-17)	Cortex, thalamus, cerebellum	↓Cldn5, ↑Plvap
β-catenin (Wang *et al.*, 2019)	*Pdgfb-Cre^{ER}; Ctnnb1$^{flex3/+}$*	P60 (4-OHT at P10)	Circumventricular organs: area postrema (AP), choroid plexus (CP), subfornical organ (SFO), posterior pituitary gland (PP)	AP and CP: ↑Lef1, ↑Cldn5, ↓Plvap AP: ↑Pgp, ↑Glut1 SFO and CP: ↑Zo-1 PP: ↑Ocln, ↑Pgp, ↑Glut1, ↑Cldn5, ↑Mfsd2a, ↑Lef1, ↓Plvap
β-catenin (Zhou *et al.*, 2014)	*Pdgfb-Cre^{ER}; Ctnnb1$^{fl/fl}$*	Adult (P55)	Retina	↓Cldn5, ↑Plvap

*Represents a limited selection of some of the most differentially expressed genes, highlighting particular genes of interest

referenced with cerebellar BBB transcripts (defined as the 224 genes ≥2-fold enriched in cerebellar ECs vs. pituitary ECs), yielding a final list of ~100 'Wnt-regulated BBB genes' in adult mice (Wang *et al.*, 2019).

1.9.2. Canonical Wnt Signaling in CNS Vascular Development

At E9.5, the perineural vascular plexus (PNVP) begins to invade the neural tube, initiating CNS angiogenesis (Mancuso et al., 2008). Canonical Wnt signaling is essential for this process to proceed normally (Reis and Liebner, 2013). Null or tissue-specific mutations in specific canonical Wnt signaling components result in severe CNS-specific angiogenesis and vascular patterning defects and hemorrhage, in some cases causing embryonic lethality, including WNT7A/B (Daneman et al., 2009; Stenman et al., 2008), LRP5/6 (Zhou *et al.*, 2014), GPR124 (Cullen *et al.*, 2011), RECK (Cho et al., 2017) and β-catenin (Daneman *et al.*, 2009; Stenman *et al.*, 2008).

Null mutations in other components, while not lethal, lead to retinal angiogenesis defects, including Norrin (Richter et al., 1998), FZD4 (Xu et al., 2004), LRP5 (Xia *et al.*, 2008), and TSPAN12 (Junge et al., 2009). *Fzd4* mutants also present with progressive cerebellar vascular dysmorphology beginning at P30, though whether this is a cause or consequence of the associated progressive cerebellar degeneration is unclear (Xu *et al.*, 2004). Mutations in these latter genes are also associated with familial exudative vitreoretinopathy in humans, which can lead to blindness.

1.9.3. Canonical Wnt Signaling in BBB Development

The embryonic lethality of some canonical Wnt signaling mutants, which occurs before functional BBB formation (E14.5-E15.5), precludes a direct interrogation of their requirement for BBB formation during embryogenesis. However, there are some exceptions. *Gpr124*$^{-/-}$ mice –

which die late in gestation or perinatally – display sulfo-NHS-biotin and fibrinogen leakage in forebrain vessels at E18.5, indicative of a failure of the BBB to form properly. Similarly, mice with EC-specific loss of RECK (*Tie2-Cre;Reck*$^{fl/-}$) – which survive to birth – display widespread BBB leakage of sulfo-NHS-biotin, not only in areas with impaired angiogenesis and severe hemorrhaging (forebrain) but also in areas with normal vascular density (hypothalamus and brainstem) (Cho *et al.*, 2017).

Other canonical Wnt signaling mutants display more restricted BBB defects. *Fzd4*$^{-/-}$ mice, which survive to adulthood, display sulfo-NHS-biotin leakage in the cerebellum, olfactory bulb, and spinal cord, showing impaired BBB and BSCB formation (Wang *et al.*, 2012). Similarly, adult *Tie2-Cre;Fzd4*$^{fl/-}$ mice display Evans Blue leakage in the cerebellum and olfactory bulb (Wang *et al.*, 2012). Adult *Ndp*^{KO} mice display very mild BBB leakage of sulfo-NHS-biotin that is restricted to the cerebellum (Zhou *et al.*, 2014). Finally, null and tissue-specific mutations that cause retinal angiogenesis defects (*Ndp*, *Fz4*, *Lrp5*, and *Tspan12*) also cause impairments in BRB formation (Junge *et al.*, 2009; Luhmann et al., 2005; Xia *et al.*, 2008; Zhang *et al.*, 2018; Zhou *et al.*, 2014).

1.9.4. Canonical Wnt Signaling in BBB Maintenance

Despite the striking decrease in TCF/LEF reporter signal in brain ECs after embryogenesis (Liebner *et al.*, 2008), canonical Wnt signaling is still required for BBB maintenance during postnatal development and in adulthood.

Postnatal development

The requirement of canonical Wnt signaling for BBB integrity during early postnatal development has been shown in P10 *Pdgfb-Cre*^{ER}*;Ctnnb1*$^{fl/fl}$ mice with 4-OHT–mediated EC-specific loss of β-catenin induced at P7 (Zhou *et al.*, 2014). Similar experiments were performed

with P23-24 *Pdgfb-Cre^{ER};Ctnnb1$^{fl/fl}$* and *Pdgfb-Cre^{ER};Lrp5$^{-/-}$;Lrp6$^{fl/fl}$* mice with tamoxifen-mediated EC-specific loss of β-catenin or LRP5/LRP6 induced at P15 or P16 (Zhou *et al.*, 2014). These genetic perturbations resulted in widespread BBB permeability to sulfo-NHS-biotin throughout the brain for β-catenin mutants and a much more restricted pattern of sulfo-NHS-biotin leakage in LRP5/6 mutants (Zhou *et al.*, 2014). Similarly, adult *Pdgfb-Cre^{ER};Fzd4$^{fl/-}$* mice that undergo early postnatal 4-OHT–induced EC-specific loss of FZD4 display sulfo-NHS-biotin leakage in the cerebellum (Wang *et al.*, 2012).

Adulthood

Canonical Wnt signaling is also required for BBB/BRB maintenance in adulthood. Previous studies have shown that EC-specific inducible loss of β-catenin in sexually mature adult mice results in compromised BBB (Tran *et al.*, 2016) and BRB (Zhou *et al.*, 2014) integrity. Similarly, FZD4 is required for maintenance of cerebellar BBB integrity in adulthood (Wang *et al.*, 2012). Across these studies, leakage of sulfo-NHS-biotin and albumin were demonstrated at the BBB, and leakage of sulfo-NHS-biotin was demonstrated at the BRB. However, regional variability across the CNS and size-selectivity of leakage have not yet been characterized. Additionally, while the BRB leakiness at this timepoint is associated with CLDN5^{-}/PLVAP^{+} ECs, it is unknown if the expression of these genes are also altered at the BBB.

1.9.5. Canonical Wnt Signaling Regulation of BBB Subcellular Properties

While many studies have highlighted the role of canonical Wnt signaling in CNS angiogenesis and BBB formation, very few studies have explored its regulation of subcellular EC properties. These properties, which can be analyzed using electron microscopy (EM), include TJ ultrastructure, TJ permeability, vesicular formation/endocytosis/trafficking, and fenestrations.

Tight junctions

Studies in adult mice show that acute knockdown of *Cldn5* leads to size-selective permeability of the BBB to small molecules (Campbell et al., 2012; Greene et al., 2018), similar to what is observed in *Cldn5*$^{-/-}$ embryos (Nitta *et al.*, 2003). Furthermore, canonical Wnt signaling regulates expression of CLDN5 in adulthood and is associated with leakage of sulfo-NHS-biotin (Zhou *et al.*, 2014). These data seem to imply that canonical Wnt signaling may regulate TJ structure in CNS ECs. However, even in *Cldn5*$^{-/-}$ mice, there are no readily apparent defects in TJ ultrastructure. Furthermore, TJ permeability has not been directly evaluated with tracers at the ultrastructural level in these mice (Nitta *et al.*, 2003).

A recent study claimed that adult mice with EC-specific loss of β-catenin lack TJs at the ultrastructural level (Tran *et al.*, 2016). However, these findings are confounded by the fact that these animals succumbed to lethal seizures and petechial hemorrhages, which was the same time point at which ultrastructural analyses were conducted. Thus, the altered TJ ultrastructure may be secondary to this gross pathology rather than a direct consequence of losing β-catenin. In addition, the presence of hemorrhage implies a destabilization of vessels that is likely due to loss of the junctional pool of β-catenin rather than the cytosolic signaling-competent pool of β-catenin. Moreover, this study and others evaluating TJ ultrastructure in *Cldn5* or canonical Wnt pathway mutant mice have not performed tracer injections for their EM analyses. Thus, it remains unknown if canonical Wnt signaling regulates TJ functionality at an ultrastructural level.

Fenestrations

A multitude of studies have shown that canonical Wnt signaling regulates the expression of plasmalemmal vesicle-associated protein (PLVAP), which is a structural component of fenestral and stomatal diaphragms (Stan et al., 1999; Stan et al., 2004). PLVAP is expressed in a

variety of peripheral ECs and is associated with highly permeable fenestrated vessels, as well as some non-fenestrated continuous vessels (e.g. lung and cardiac ECs). Expression of PLVAP is suppressed in CNS ECs by canonical Wnt signaling (see **Table 1.2**).

Accordingly, there is previous EM evidence of fenestrations in retinal vessels of adult Wnt signaling mutant mice (Ndp^{KO} and $Fzd4^{-/-}$), which also widely express PLVAP (Richter *et al.*, 1998; Xu *et al.*, 2004). However, in a different study, $Fzd4^{-/-}$ mouse cerebellar capillaries demonstrated no major ultrastructural differences compared to WT controls (Ye *et al.*, 2009). This discrepancy may be due to a sparser expression of PLVAP in cerebellar capillaries of $Fzd4^{-/-}$ mice, where it is restricted to the molecular layer. Nonetheless, an open question that remains is whether canonical Wnt signaling can dynamically regulate EC fenestrations in adulthood.

Although one study in adult mice showed acquired expression of PLVAP in cerebellar ECs following acute loss of FZD4, the study did not demonstrate whether this was associated with fenestrated ECs (Zhou *et al.*, 2014). In addition, a recent study showed that acutely expressing a stabilized form of β-catenin in mouse ECs at P10 led to a decrease in the number of EC fenestrations by P40 in brain regions that normally have high levels of EC fenestrations (Wang *et al.*, 2019). This demonstrates that repressing PLVAP expression during early postnatal development can indeed influence the abundance of fenestrations even just a month later. However, the specific time window of this Wnt-dependent BBB plasticity and whether it includes the ability of ECs to form *de novo* fenestrations in adulthood remain to be determined.

Transcytosis

Both loss of function and gain of function studies of β-catenin show that it regulates the transcript abundance of MFSD2A (Chen *et al.*, 2012; Schafer *et al.*, 2009; Wang *et al.*, 2019), a

regulator of caveolae-mediated transcytosis in CNS ECs. A recent study even showed that stabilized β-catenin can influence chromatin accessibility within the *Mfsd2a* genetic locus (Wang *et al.*, 2019). These studies indicate that canonical Wnt signaling may regulate transcytosis through the expression of MFSD2A. However, to date, there are no studies that have quantitatively characterized transcytosis in canonical Wnt pathway mutant adult mice using tracer-coupled electron microscopy. Thus, it remains an open question if canonical Wnt signaling regulates transcytosis in CNS ECs, which I address in my work (see **Chapter 3**).

CHAPTER 2

Experimental Methods

Animal Models

All mice were group housed in standard vivarium conditions, with *ad libitum* access to diet and water. *Cdh5-Cre^{ERT2}* mice (MGI:3848982), *Ctnnb1$^{fl/fl}$* mice (JAX:004152, MGI: J:67966), *ROSA26:LSL-Mfsd2a* mice (generated by our lab in a previous study: see (Chow et al., 2020)), *Tie2-Cre* mice (JAX:008863, MGI:2450311), and *Slc7a5$^{fl/fl}$* mice (JAX:027252, MGI:5618433) were all maintained on a C57BL/6 background. *Slc16a1$^{fl/fl}$* mice (Jha et al., 2020) were a gift from Dr. Jeffrey Rothstein.

Tamoxifen Administration

Tamoxifen (Sigma Aldrich, #T5648-1G) was dissolved in peanut oil (20 mg/ml) by brief vortexing followed by heating and rotation at 65°C and mice received five consecutive days of IP injections (0.1 mg/g body weight/day) prior to being sacrificed 3 days after the fifth injection. As a technical note, *Cdh5-Cre^{ERT2};Ctnnb1$^{fl/fl}$;R26:LSL-Mfsd2a* animals (and their *Ctnnb1$^{fl/fl}$* and *Cdh5-Cre^{ERT2};Ctnnb1$^{fl/fl}$* littermates) received a dosage of 0.2 mg/g body weight/day since 0.1 mg/g body weight was insufficient to induce MFSD2A expression from the ROSA26 locus with this combination of alleles.

Immunohistochemistry

Mouse tissues were fixed by immersion in ice-cold 100% methanol (MeOH) overnight at 4°C, sequentially rehydrated in 70% MeOH/PBS, 30% MeOH/PBS, and PBS (at least 4 hrs in PBS) at 4°C, sequentially cryopreserved in 15% and 30% sucrose, and frozen in Neg-50 (Richard-Allan Scientific #6502). 20 µm tissue sections were blocked with 10% goat serum/5% BSA/PBST (0.5% Triton X-100) and stained overnight at 4°C with the following primary antibodies: α-CD31 (1:100, R&D Systems AF3628), α-ERG-488 conjugate (1:200, Abcam ab196374), α-Lef1 (1:100, Cell Signaling #2230S), α-Mfsd2a (1:100, New England Peptide, clone 9590), α-

Claudin-5-488 conjugate (1:200, Thermo Fisher Scientific #352588), α-ZO-1 (1:100, Invitrogen #402200), α-Glut1-647 conjugate (1:200, EMD Millipore #07-1401-AF647), α-Plvap (1:100, BD Biosciences #553849), followed by corresponding Alexa Fluor-conjugated secondary antibodies (1:250, Jackson ImmunoResearch). All sections were mounted with ProLong Gold for imaging.

TUNEL Assay

Brains were dissected and fixed in 4% PFA/PBS overnight at 4°C, cryopreserved in 15% and 30% sucrose, and frozen in Neg-50. 20 µm brain sections underwent TUNEL staining using the Click-iT™ Plus TUNEL Assay for In Situ Apoptosis Detection, Alexa Fluor™ 647 dye (ThermoFisher Scientific #C10619). As a positive control, *Ctnnb1*$^{fl/fl}$ brain slices were treated with DNase I. After the TUNEL reaction, slices were co-stained with α-ICAM2 (1:200, BD Biosciences #553326) to visualize blood vessels.

BBB Leakage Assays

Adult: Adult mice were briefly anesthetized with isoflurane and EZ-Link Sulfo-NHS-LC-Biotin (100 mg/ml in PBS, 0.3 mg/g body weight) was injected into the retro-orbital sinus laterally or bi-laterally (to not exceed 100 µL in each retro-orbital sinus). After 10 minutes of circulation, brains were dissected and fixed as described above. Tissue sections were stained with α-CD31 or α-PECAM overnight to visualize blood vessels, followed by Alexa Fluor-conjugated streptavidin (1:500, ThermoFisher Scientific #S11226) or α-Mouse IgG-conjugated secondary (1:150, ThermoFisher Scientific #A10037) for 2 hours at room temperature to visualize biotin or IgG, respectively. For HRP leakage assays, adult mice were treated as described below (see "Electron microscopy") and slides were mounted with Permount for brightfield imaging.

Early Postnatal: P5-6 pups were anesthetized with isoflurane and a tracer cocktail of 10-kDa dextran tetramethylrhodamine (Thermo Fisher Scientific, #D1817, 10 mg/ml), bovine serum

albumin Alexa-647 conjugate (Invitrogen, #A34785), and EZ-Link Sulfo-NHS-LC-Biotin was injected into the left heart ventricle (10 µl per g body weight) with a Hamilton syringe. After five minutes of circulation, brains were dissected and fixed by immersion in 4% PFA/PBS at 4°C overnight, cryopreserved in 30% sucrose, and frozen in Neg-50. Sections were collected and co-stained with α-PECAM (1:200, BD Biosciences #553370) followed by corresponding Alexa Fluor-conjugated secondary antibodies (1:1000, Thermo Fisher Scientific), or Alexa fluor-conjugated isolectin B4 (1:200, Thermo Fisher Scientific #I21411, #I32450) to visualize blood vessels. Sections co-stained with Alexa Fluor-conjugated streptavidin to visualize biotin. For IgG and fibrinogen leakage, sections were stained with α-Mouse IgG-conjugated secondary (1:200, ThermoFisher Scientific #A31571) and α-fibrinogen (1:1000, Dako #A0080).

Transmission Electron Microscopy

Vesicular transport: Adult mice were briefly anesthetized with isoflurane and HRP type II (Sigma Aldrich, #P8250-50KU, 0.5 mg/g body weight dissolved in 0.2 ml PBS) was injected bi-laterally into the retro-orbital sinus. After 30 minutes of circulation (mice were deeply anesthetized with ketamine/xylazine after 20 minutes), mice were perfused through the heart with ~8 mL room temperature 5% glutaraldehyde/4% PFA/0.1M sodium cacodylate buffer fixative solution (Electron Microscopy Sciences #16300, #15713-S, #11653) by low-pressure gravity-mediated flow. Brains were dissected and post-fixed in 4% PFA/0.1M sodium cacodylate buffer fixative solution overnight at 4°C. Following fixation, sagittal vibratome free-floating sections of 50 µm were collected in 0.1M sodium cacodylate buffer, incubated in 3,3'-diaminobenzidine (DAB, Sigma Aldrich #D5905-50TAB) for 35 minutes, post-fixed in 1% osmium tetroxide and 1.5% potassium ferrocyanide, dehydrated, and embedded in epoxy resin. Ultrathin sections of 70 nm were then cut from the block surface and collected on copper grids.

For vesicular quantification in early postnatal animals, brains were fixed by immersion for one week, prior to tissue processing as described above.

Tight junction permeability: Adult mice were briefly anesthetized with isoflurane and HRP type II, microperoxidase (Sigma Aldrich #M6756-100MG, 20 mg dissolved in 0.2 ml PBS), EZ-Link Sulfo-NHS-LC-Biotin (100 mg/ml in PBS, 0.5 mg/g body weight), biotin ethylenediamine hydrobromide (Sigma Aldrich #B9181-25MG, 50 mg/ml in PBS, 0.2 mg/g body weight), Neurobiotin (Vector Labs #SP-1120-50, 0.5 mg/g body weight), or Omniscan (gadodiamide, GE Healthcare #J-068, 287 mg/ml, 0.2 ml) was injected laterally or bi-laterally into the retro-orbital sinus. After 10 minutes of circulation (or 30 minutes of circulation for HRP), brains were dissected and fixed by immersion in 5% glutaraldehyde/4% PFA/0.1M sodium cacodylate buffer at room temperature for 1 hour, followed by 4% PFA/0.1M sodium cacodylate buffer at 4°C overnight. Following fixation, vibratome free-floating sections of 50 μm were collected in 0.1M sodium cacodylate buffer and incubated in Pierce High Sensitivity Streptavidin-HRP (1:100, ThermoFisher Scientific #21130) or Poly-HRP Streptavidin (1:100, ThermoFisher Scientific #N200) at 4°C overnight (except for the peroxidase tracers and Omniscan), followed by incubation in 3,3'-diaminobenzidine (DAB, Sigma Aldrich #D5905-50TAB, 35 minutes for HRP and biotin tracers, 2 hours for microperoxidase) or Pierce Metal Enhanced DAB (only for biotin ethylenediamine, ThermoFisher Scientific, #34065, 2 hours) at room temperature. As a technical note, microperoxidase was difficult to dissolve and had to be incubated in PBS for 15 minutes at room temperature (no vortexing) in order to go into solution. All tissues were processed for electron microscopy as described above.

Microscopy, Image Processing, and Data Analysis

Vessel density: 5 animals per genotype and 12 images per animal from the cerebellar molecular layer were used for data analysis. Images were acquired using a Leica SP8 laser scanning confocal microscope (25×, 0.75 NA) and were processed using FIJI (NIH). Vessel density was quantified as the $CD31^+$ percentage area using CellProfiler.

LEF1: 5 animals per genotype and 9 images (for cortex) or 12 images (for cerebellar molecular layer) per animal were used for data analysis, with ~70-100 endothelial nuclei captured per image. Images were acquired using a Leica SP8 laser scanning confocal microscope (25×, 0.75 NA) and were processed using FIJI (NIH). With CellProfiler, ERG was used to segment objects (endothelial nuclei) and the LEF1 mean fluorescence intensity was quantified for each individual endothelial nucleus. For each image, the mean fluorescence intensities across all the endothelial nuclei were averaged to generate a value for each image.

Transmission electron microscopy: For quantification of TJ permeability, 5 animals were used per genotype and an average of 23 and 25 vessels were analyzed per animal for HRP and microperoxidase, respectively. Data were quantified as percentage of TJs impermeable to the given tracer. For vesicular transport cohorts with only *Ctnnb1*$^{fl/fl}$ and *Cdh5-Cre*^{ERT2}*;Ctnnb1*$^{fl/fl}$ animals, 5 animals were used per genotype and an average of 25 vessels were analyzed per animal. For vesicular transport cohorts with *Ctnnb1*$^{fl/fl}$, *Cdh5-Cre*^{ERT2}*;Ctnnb1*$^{fl/fl}$, and *Cdh5-Cre*^{ERT2}*;Ctnnb1*$^{fl/fl}$*;R26:LSL-Mfsd2a* animals, 4 animals were used per genotype and an average of 46 vessels were analyzed per animal. Data were quantified as number of HRP-filled vesicles (luminal, abluminal, and cytoplasmic) per μm^2 of endothelial cytoplasm (mean vesicular density), excluding the area of the nucleus.

BBB leakage:

12 images per animal from the cerebellar molecular layer were used for data analysis. Images were acquired using a Leica SP8 laser scanning confocal microscope (25×, 0.75 NA – only biotin and IgG) and an Olympus VS 120 slide scanner (10×, 0.4 NA for biotin and IgG, 20x, 0.4 NA for HRP). For quantification of the biotin or IgG leakage index, confocal images were processed with FIJI (NIH) and the area of the tracer was divided by the area of the $CD31^+$ vessels. For *Tie2-Cre;Slc16a1*$^{fl/fl}$ animals, fibrinogen and IgG leakage images were acquired with a Nikon Eclipse 80i Upright epifluorescence microscope (20×, 0.45 NA).

Quantification of BBB markers: For quantification of CLDN5, ZO-1, MSFD2A, and GLUT1, 12 images per animal from the cerebellar molecular layer were used for data analysis. Images were acquired using a Leica SP8 laser scanning confocal microscope (25×, 0.75 NA) and processed with FIJI (NIH). The ratio of the area of each marker to the area of $CD31^+$ vessels was used to compute the vessel coverage and values were normalized to controls to determine the relative fold change between groups.

Statistical analysis: All statistical analyses were performed using Prism 7 (GraphPad Software). Two group comparisons were analyzed using an unpaired *t*-test or an unpaired *t*-test with Welch's correction. Where appropriate, a nested *t*-test or a Mann-Whitney test was used. Multiple group comparisons were analyzed using a one-way ANOVA followed by a post-hoc Tukey's test, a nested one-way ANOVA, or a Brown-Forsythe one-way ANOVA with Dunnett's T3 multiple comparisons test. Sample size for all experiments was determined empirically using standards generally employed by the field, and no data was excluded when performing statistical analysis. Standard error of the mean was calculated for all experiments and displayed as errors

bars in graphs. Statistical details for specific experiments, including exact *n* values, statistical tests used, and definitions of significance can be found in the figure legends.

CHAPTER 3

Molecular and Cellular Mechanisms Governing Canonical Wnt Signaling Regulation of Adult BBB Maintenance: Transcytosis

3.1. Abstract

Canonical Wnt signaling is essential for the development and maintenance of blood-brain barrier (BBB) integrity. However, the subcellular mechanisms underlying this tight regulation have remained elusive. To address this gap in knowledge, we use a physiological paradigm entailing acute attenuation of canonical Wnt signaling in the adult brain vasculature to investigate how the pathway regulates BBB integrity. Following canonical Wnt signaling attenuation, we find that there is an increase in brain endothelial cell (EC) transcytosis, which correlates with a loss of the caveolae-mediated transcytosis inhibitor MFSD2A. Strikingly, EC-specific overexpression of MFSD2A in Wnt-signaling-deficient brain ECs is not sufficient to rescue increased transcytosis, indicating that canonical Wnt signaling regulates multiple transcytosis pathways. Overall, our findings expand our understanding of brain EC transcytosis and help illuminate subcellular mechanisms of BBB maintenance in adulthood, which is crucial for the advancement of therapeutic delivery to the brain.

3.2. Introduction

The blood-brain barrier (BBB) maintains a homeostatic environment for optimal neuronal function by tightly regulating the movement of ions, molecules, and cells between the blood and brain parenchyma (Andreone et al., 2015). The primary site of the BBB occurs at brain endothelial cells (ECs) that form tightly sealed blood vessels. At the subcellular level, these ECs have specialized properties that determine BBB integrity: highly impermeable tight junctions (TJs), suppression of transcellular vesicular trafficking (transcytosis), and the absence of fenestrations (Langen *et al.*, 2019).

An essential regulator of the BBB is canonical Wnt signaling, which orchestrates a transcriptional program in brain ECs that is dependent on the transcriptional mediator β-catenin

(Reis and Liebner, 2013). Among the dozens of genes regulated by this pathway are some that are known to regulate BBB integrity, including the TJ protein CLDN5 and plasmalemma vesicle-associated protein (PLVAP), which is a structural component of fenestral diaphragms (Nitta *et al.*, 2003; Stan *et al.*, 1999; Stan *et al.*, 2004). More recent studies have shown that the protein MFSD2A, which suppresses caveolae-mediated transcytosis at the BBB (Andreone *et al.*, 2017; Ben-Zvi *et al.*, 2014), is also regulated by the pathway (Sabbagh et al., 2018; Wang *et al.*, 2019).

During embryonic development, canonical Wnt signaling facilitates brain angiogenesis and barriergenesis (Daneman *et al.*, 2009; Liebner *et al.*, 2008; Stenman *et al.*, 2008). In addition, early postnatal brain angiogenesis, as well as maintenance of BBB integrity during early postnatal development and adulthood, all require active canonical Wnt signaling (Martowicz et al., 2019; Wang *et al.*, 2012; Zhou *et al.*, 2014). Accordingly, mouse models with loss of function mutations in the genes encoding brain EC-relevant Wnt ligands, receptors, co-receptors, or β-catenin, display increased BBB permeability to small molecular weight exogenous tracers and large endogenous serum proteins, suggesting an increase in paracellular or transcellular permeability (Cho *et al.*, 2017; Wang *et al.*, 2018; Wang *et al.*, 2012; Zhou and Nathans, 2014; Zhou *et al.*, 2014).

Despite this large body of research, the subcellular mechanisms that govern canonical Wnt signaling regulation of BBB integrity remain elusive. In particular, the contribution of transcytosis has remained underexplored. These mechanisms have been difficult to ascertain due to the pathway's confounding roles in different physiological and pathological processes. First, canonical Wnt pathway mutants have severe CNS angiogenesis defects (Cullen *et al.*, 2011; Daneman *et al.*, 2009; Martowicz *et al.*, 2019; Oh *et al.*, 2001; Stenman *et al.*, 2008; Wang *et al.*, 2012; Wang *et al.*, 2020; Zhou *et al.*, 2014). Therefore, especially at embryonic and early

postnatal stages, it is not possible to rule out if changes in subcellular properties are due to broader gross effects of a malformed vasculature. Second, one week following acute EC-specific ablation of β-catenin in adult mice, there is abundant cell death and lethal seizures (Tran *et al.*, 2016). Therefore, at this time point, it is not possible to rule out if changes in subcellular properties are secondary to pathological seizure induction.

Using a combination of mouse genetics, BBB leakage assays, and tracer-coupled quantitative electron microscopy, we circumvent these confounds to demonstrate that canonical Wnt signaling suppresses transcytosis to maintain BBB integrity.

3.3. Results and Discussion

3.3.1. An acute, EC-specific attenuation of canonical Wnt signaling in adult mice alters BBB permeability

In order to acutely attenuate canonical Wnt signaling in brain ECs, we knocked out the gene encoding β-catenin (*Ctnnb1*) by crossing *Ctnnb1* floxed mice (Brault et al., 2001) (*Ctnnb1*$^{fl/fl}$) with an endothelial-specific tamoxifen-inducible Cre (Sorensen et al., 2009), *Cdh5-Cre*^{ERT2}. Previous studies have shown that endothelial ablation of β-catenin leads to loss of canonical Wnt signaling and defects in vascular development specifically in CNS ECs but not in the ECs of other organs (Daneman *et al.*, 2009; Stenman *et al.*, 2008). To circumvent the confound of angiogenesis defects at earlier developmental time points, we performed tamoxifen injections in sexually mature adult mice (8-10 weeks), when brain ECs are largely quiescent (Ben-Zvi and Liebner, 2021). To circumvent the confound of seizure-induced BBB pathology, which has been observed with a similar experimental paradigm one week following tamoxifen treatment (Tran *et al.*, 2016), we assayed mice three days following the last tamoxifen injection (**Figure 3.1**). At this time point, controls (*Ctnnb1*$^{fl/fl}$) and mutants (*Cdh5-Cre*^{ERT2}*;Ctnnb1*$^{fl/fl}$)

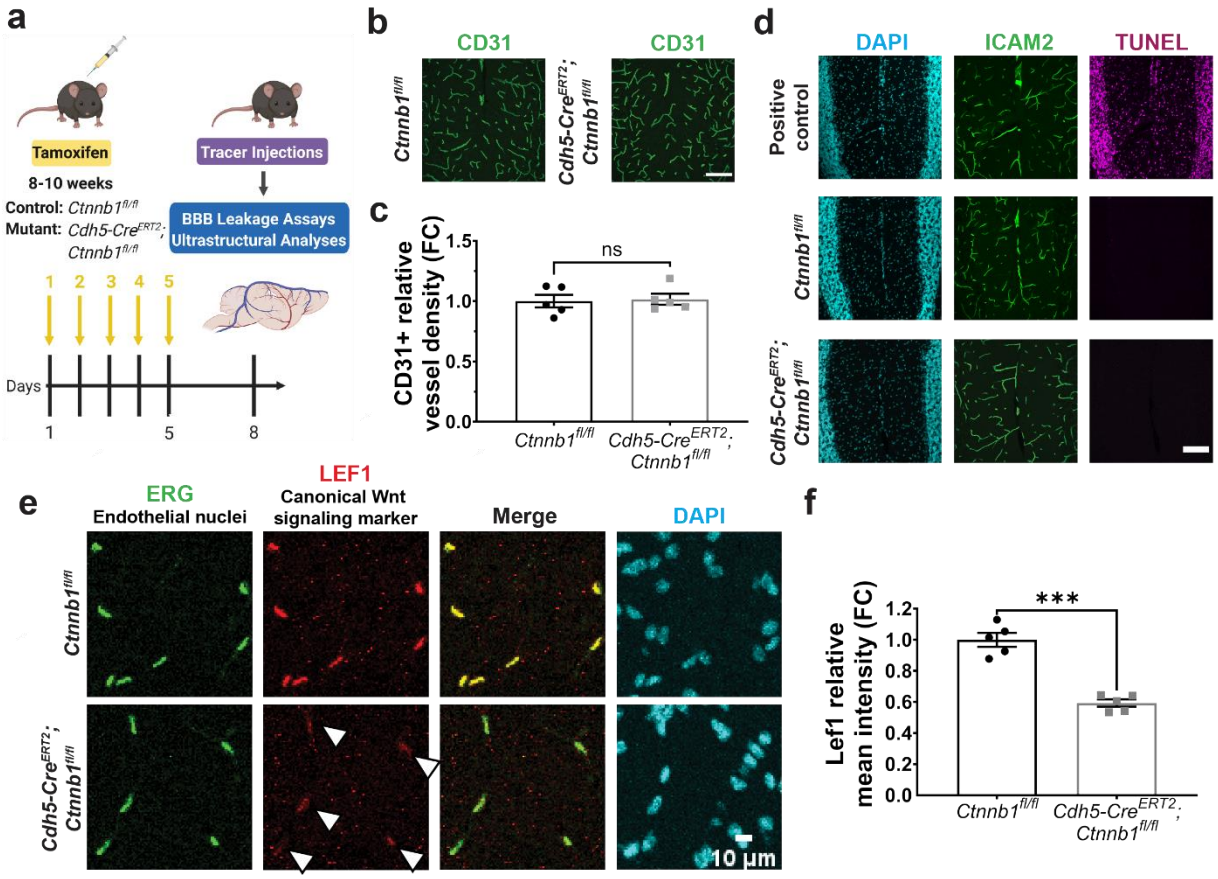

Figure 3.1. A physiological paradigm of acutely attenuated canonical Wnt signaling in the adult brain vasculature. (a) Schematic overview of experimental paradigm: all animals were injected with tamoxifen for 5 consecutive days and assays were performed 3 days after the last injection. Created with BioRender.com **(b)** Immunofluorescence images of brain vasculature (CD31) in controls (*Ctnnb1*$^{fl/fl}$) and mutants (*Cdh5-Cre*^{ERT2}*;Ctnnb1*$^{fl/fl}$). (Scale bar: 100 µm) **(c)** Quantification of vessel density (data are mean ± SEM, n=5 animals per genotype). ns = not significant, unpaired t test. **(d)** TUNEL staining (magenta) in the cerebellum of control (middle) and mutant (bottom) mice, as well as DNase-treated positive control (top), with vessel (ICAM2) and nuclear (DAPI) staining. (Scale bar: 100 µm) **(e)** Immunofluorescence images of endothelial nuclei (ERG), canonical Wnt signaling marker LEF1, and all nuclei (DAPI) in the cerebellar molecular layer of control and mutant mice. White arrowheads denote reduced LEF1 staining in

Figure 3.1 (Continued)

mutant endothelial nuclei. (Scale bar: 10 μm) **(f)** Quantification of the LEF1 mean fluorescence intensity across ERG^+ endothelial nuclei (data are mean ± SEM, n=5 animals per genotype). ***p<0.001, unpaired t test with Welch's correction.

displayed similar brain vessel density and no cell death (**Figure 3.1**), demonstrating that we did not induce angiogenesis defects or seizure pathology.

To assess canonical Wnt signaling in brain ECs, we stained for the transcription factor LEF1, which is a key pathway effector and a transcriptional target of the pathway in ECs (Planutiene et al., 2011). We observed a 40% reduction in LEF1 intensity in brain EC nuclei in mutants relative to controls across multiple brain regions (**Figure 3.1** and **Figure 3.2**). Overall, these results demonstrate that we were able to acutely attenuate canonical Wnt signaling in adult brain ECs.

To assess BBB permeability, we performed BBB leakage assays, injecting tracers into the blood circulation and determining their ability to leak out of the brain vasculature, which would indicate a loss of BBB integrity. We assayed leakage of the small molecular weight tracer sulfo-NHS-LC-biotin (557 Da), the larger tracer horseradish peroxidase (HRP, 44 kDa), and the endogenous serum protein IgG (150 kDa). In mutant mice, biotin leakage was widespread, with the most severe leakage occurring in the cerebellum, hippocampus, and olfactory bulbs (**Figure 3.3** and **Figure 3.4**). The strongest HRP and IgG leakage phenotypes also occurred in the cerebellum, hippocampus, and olfactory bulbs (**Figure 3.3** and **Figure 3.4**).

The occurrence of interregional heterogeneity in BBB leakage (**Figure 3.4**) - despite a similar decrease in mutant EC LEF1 levels across regions with different leakage severity (**Figure 3.2**) - suggests an increased sensitivity to acute attenuation of canonical Wnt signaling in the cerebellum and other affected regions, mirroring an earlier study of endothelial loss of the Wnt receptor FZD4 in adult mice (Wang *et al.*, 2012). This result raises multiple intriguing possibilities. First, the molecular milieu of transcription factors downstream of β-catenin and LEF1 (e.g. Sox17, Zic3, Foxq1) and their expression changes may differ between ECs in

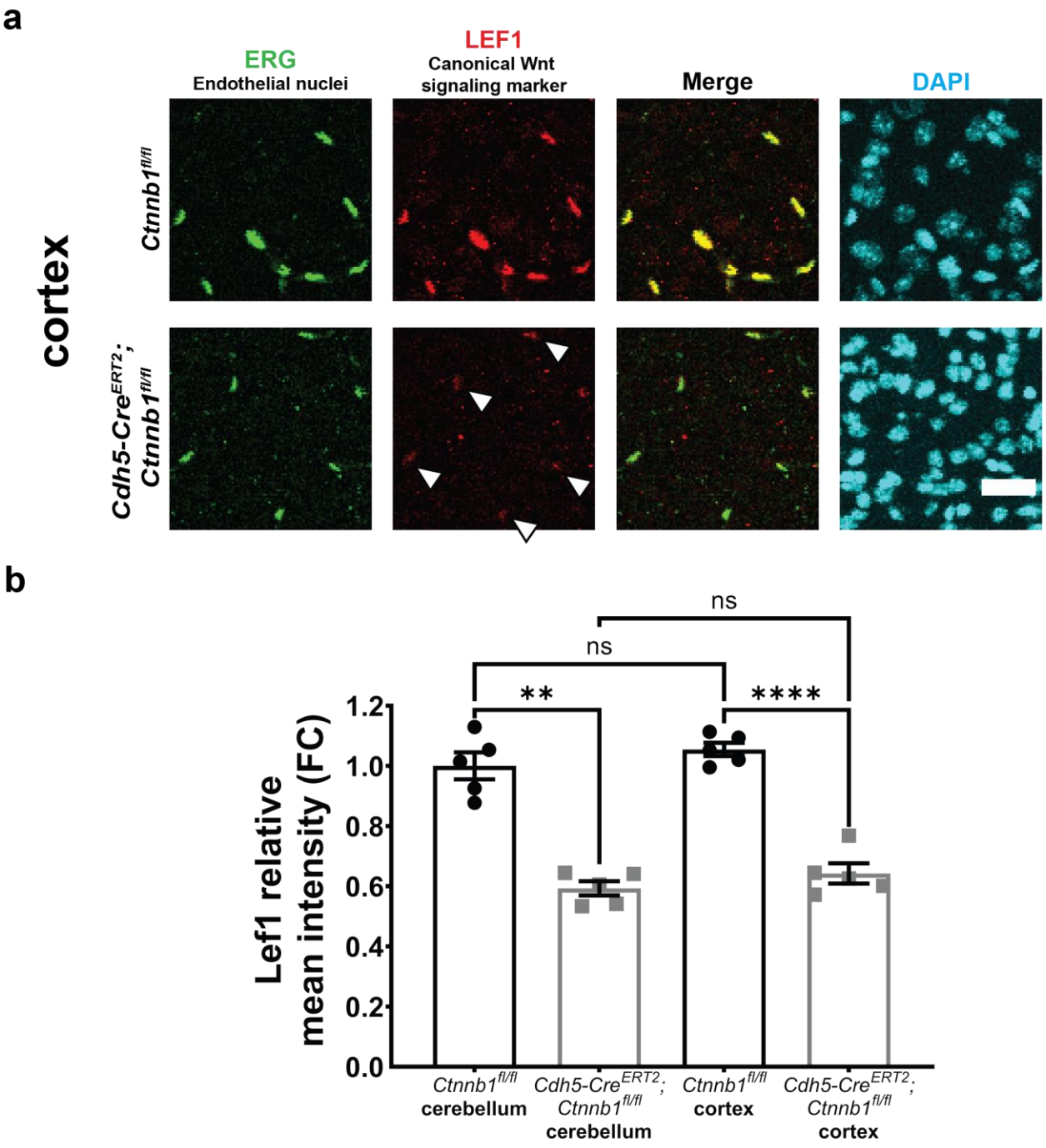

Figure 3.2. Endothelial-specific knockout of β-catenin results in widespread attenuation of canonical Wnt signaling in the adult brain vasculature. (a) Immunofluorescence images of endothelial nuclei (ERG), canonical Wnt signaling marker LEF1, and all nuclei (DAPI) in the cortex of control (*Ctnnb1*$^{fl/fl}$) and mutant (*Cdh5-Cre*^{ERT2}*;Ctnnb1*$^{fl/fl}$) mice. (Scale bar: 10 μm) **(b)**

Figure 3.2 (Continued)

Quantification of the LEF1 mean fluorescence intensity across ERG^+ endothelial nuclei in cerebellar molecular layer and cortical endothelial cells (data are mean ± SEM, n=5 animals per genotype). Note that cerebellar and cortical endothelial nuclei in control mice have comparable levels of LEF1 and that mutant mice have the same level of LEF1 reduction in endothelial nuclei in the cerebellum and cortex. Cerebellar molecular layer LEF1 data are from **Figure 3.1**. **p<0.01, ****p<0.0001, ns = not significant, Brown-Forsythe ANOVA with Dunnett's T3 multiple comparisons test.

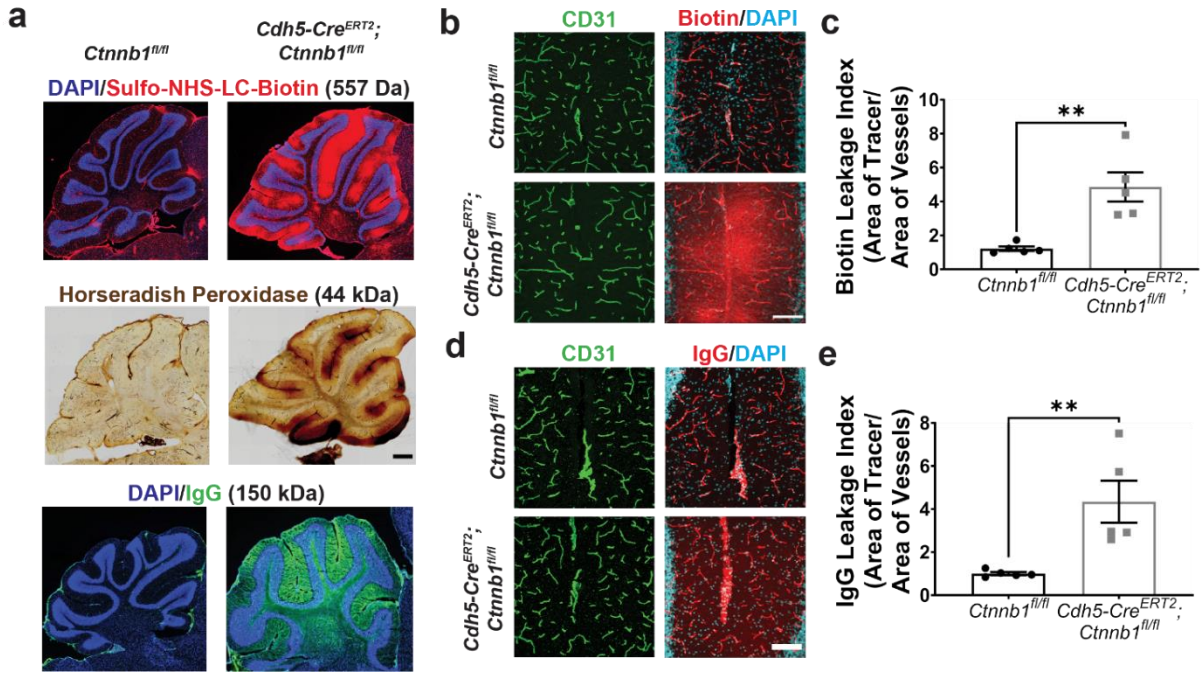

Figure 3.3. An acute, EC-specific attenuation of canonical Wnt signaling in adult mice alters BBB permeability. (a) Immunofluorescence images of sulfo-NHS-LC-biotin (top) and IgG (bottom) BBB leakage in the cerebellum with nuclear (DAPI) counterstain. Brightfield image of horseradish peroxidase (middle) leakage in the cerebellum. Confocal images of sulfo-NHS-LC-biotin **(b)** and IgG **(d)** leakage in the cerebellar molecular layer with vessel (CD31) counterstain. (Scale bar: 100 µm) Quantification of the biotin **(c)** and IgG **(e)** leakage indices: area of tracer/area of $CD31^+$ vessels (data are mean ± SEM, n=5 animals per genotype). **p<0.01, Mann-Whitney test.

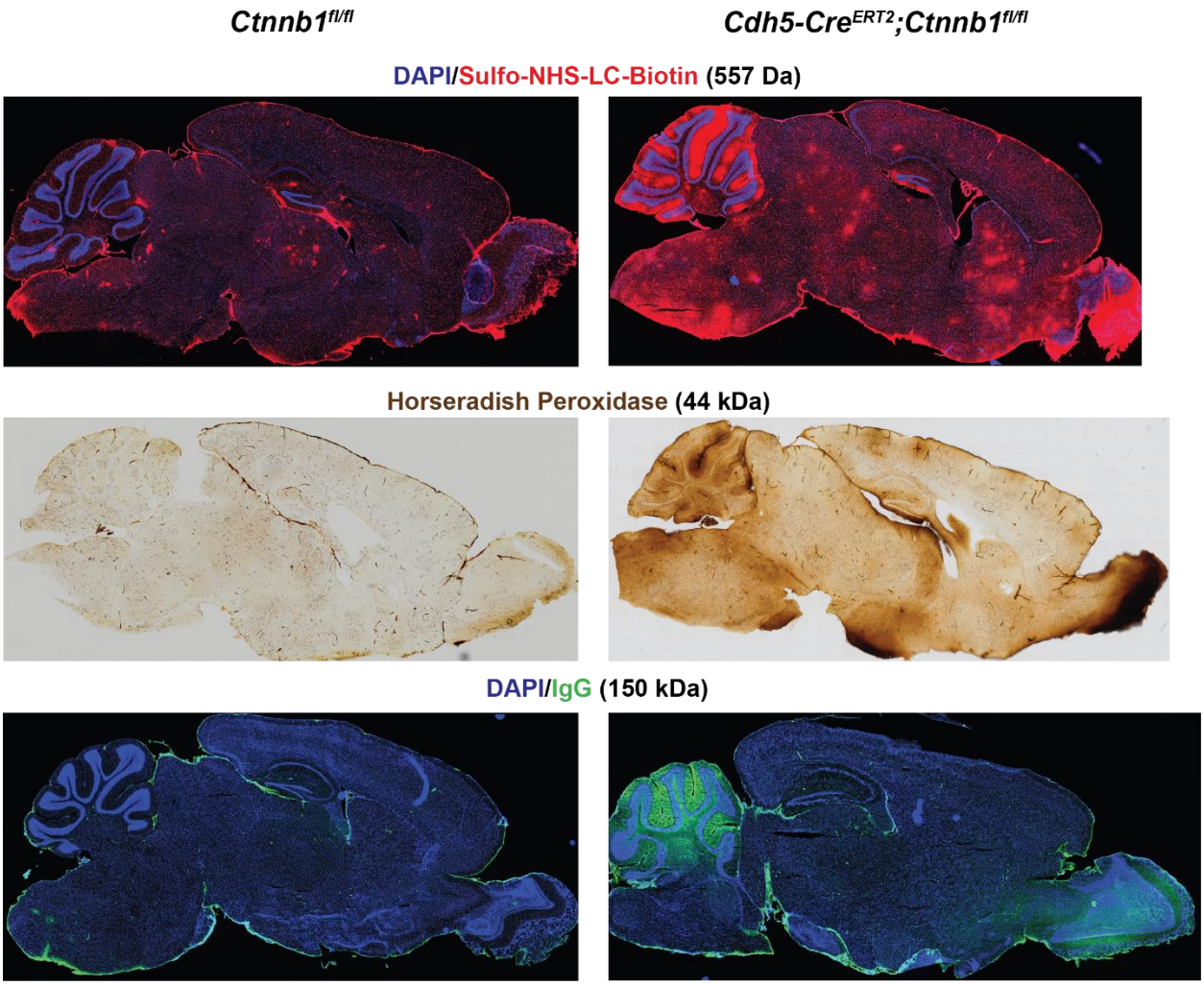

Figure 3.4. An acute, EC-specific attenuation of canonical Wnt signaling in adult mice results in widespread but heterogeneous BBB leakage. Immunofluorescence images of BBB leakage in control (*Ctnnb1*$^{fl/fl}$) and mutant (*Cdh5-Cre*^{ERT2}*;Ctnnb1*$^{fl/fl}$) mice: sulfo-NHS-LC-biotin (top) and IgG (bottom) with nuclear (DAPI) counterstain and brightfield image of horseradish peroxidase (middle). Low magnification images illustrate interregional heterogeneity in BBB leakage.

different brain regions. Second, ECs with less severe leakage may possess β-catenin-independent pathways for maintaining BBB integrity in adulthood.

Due to the consistent and anatomically stereotyped nature of BBB leakage across multiple tracers in the cerebellum, and in particular the cerebellar molecular layer, we focused all subsequent analyses on this subregion.

3.3.2. Suppression of transcytosis by canonical Wnt signaling is required for BBB integrity

Having established increased BBB permeability, we next evaluated transcytosis using electron microscopy (EM) in HRP-injected mice. HRP has an electron-dense reaction product that appears as black in electron micrographs, enabling its subcellular visualization in ECs. To best capture the vesicular landscape, we employed low-pressure gravity perfusion, which clears the blood circulation and introduces fixative at a low flow rate equivalent to the cardiac output of adult mice. This technique better preserves a snapshot of vesicular structures by preventing artifact introduced by high pressure perfusion. In mutant mice, there was a 40% increase in the density of HRP-filled vesicles in ECs (**Figure 3.5**). A close observation of HRP-filled vesicles revealed a diversity of vesicular morphologies, including large spherical vesicles and tubular vesicles (**Figure 3.5**). In addition, we observed HRP accumulation in the basement membrane, a clear indication that tracer was able to leak out of brain ECs (**Figure 3.5**). Notably, 100% of TJs observed were impermeable to HRP (**Figure 3.5**). Taken together, these data demonstrate that HRP leakage in mutant mice is due to increased transcytosis and that canonical Wnt signaling suppresses transcytosis to maintain BBB integrity. Moreover, given that mutant TJs are impermeable to HRP (44 kDa), our observation of leakage of the much larger serum protein IgG (150 kDa) is likely also due to increased transcytosis.

Figure 3.5. Suppression of transcytosis by canonical Wnt signaling is required for blood-brain barrier integrity. **(a)** Representative electron microscopy (EM) high magnification images of cerebellar molecular layer ECs following HRP (black) injection and low-pressure gravity perfusion. Yellow arrowheads show HRP-filled vesicles, red dashed lines denote the abluminal membrane of ECs; EC = endothelial cell, L = lumen (Scale bar: 200 nm) **(b)** Quantification of mean vesicular density (number of HRP-filled vesicles per μm^2 of EC cytoplasm): data are mean ± SEM, n=5 animals per genotype, *p<0.05, nested t-test. **(c)** Representative high magnification images of HRP-filled large spherical and tubular vesicles in mutant mice. (Scale bar: 200 nm) **(d)** Representative EM images of cerebellar molecular layer EC cross sections following HRP (black) injection and low-pressure gravity perfusion (Scale bar: 500 nm). Insets show high magnification of areas within yellow dashed lines (Scale bar: 200 nm). Yellow arrowheads indicate HRP in basement membrane (BM) of mutants or absence in controls. EC = endothelial cell, L = lumen, P = pericyte. **(e)** Quantification of % of vessels with HRP in BM (data are mean ± SEM, n=5 animals per genotype, *p<0.05, Mann-Whitney test). **(f)** Representative EM high magnification images of cerebellar molecular layer ECs following HRP (black) injection and immersion fixation. Yellow arrowheads indicate where HRP in the lumen (L) is halted by tight junctions (TJs) between adjacent ECs, red dashed lines denote the abluminal membrane of ECs (Scale bar: 200 nm) **(g)** Quantification of HRP-impermeable TJs (n=5 animals per genotype, total number of TJs analyzed per genotype are in parentheses).

Figure 3.5 (Continued)

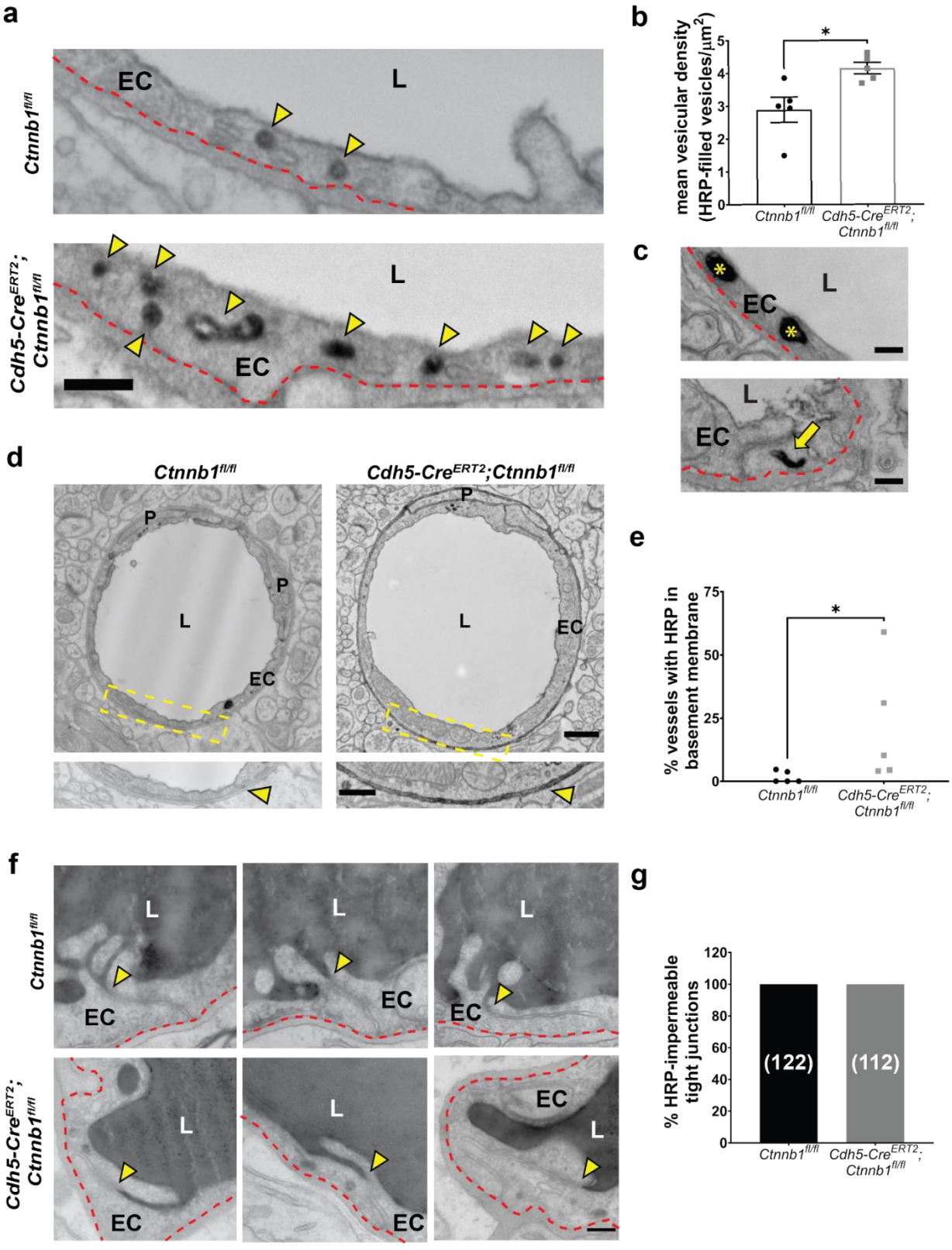

To evaluate the molecular mechanism underlying the increased transcytosis phenotype, we examined MFSD2A levels in control and mutant mice by immunohistochemistry (**Figure 3.6**). In mutant mice, there was a robust 90% decrease in MFSD2A levels, with levels first decreasing as early as 3 days after initial Cre activation (**Figure 3.6**). Given this phenotype, we hypothesized that increased transcytosis in mutant mice is mediated by MFSD2A loss. To test this hypothesis, we employed a genetic rescue strategy to overexpress MFSD2A in mutant ECs, crossing Cre^{+} mutants with a novel mouse line that enables Cre-dependent expression of an MFSD2A cassette from the ROSA26 locus (*R26:LSL-Mfsd2a*) (**Figure 3.7**). In these mice, following tamoxifen injections, there is a rapid overexpression of MFSD2A in brain ECs (**Figure 3.7**), which we have previously shown leads to a robust downregulation of caveolae (Chow *et al.*, 2020). Strikingly, MFSD2A overexpression in mutant ECs was not sufficient to rescue IgG (**Figure 3.7**) or HRP (**Figure 3.7**) leakage. Accordingly, it also did not rescue increased transcytosis, as we observed abundant HRP-filled vesicles (**Figure 3.8**).

These data raise the exciting possibility that multiple transcytotic pathways are regulated by canonical Wnt signaling in brain ECs. Moreover, they expand our understanding of the complex landscape of brain EC transcytosis and open up an exciting new avenue of research. In addition, while our study focused on transcytosis, TJs likely also play a major role in canonical Wnt signaling regulation of BBB integrity due to the pathway's regulation of CLDN5 expression. While we found that mutant TJs were impermeable to HRP, it is possible that they are permeable to smaller molecules like sulfo-NHS-LC-biotin. The development and optimization of EM-compatible tracers to evaluate TJ permeability will enable these mechanistic investigations (see **Chapter 4**).

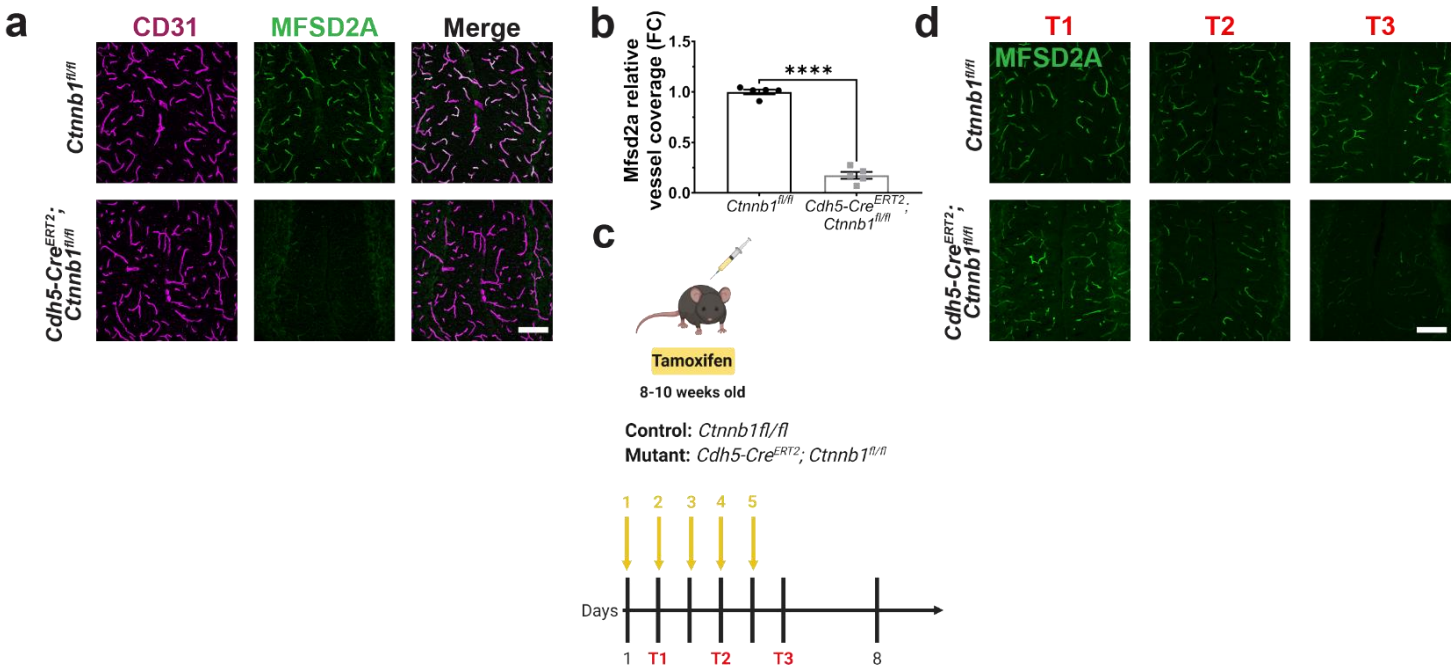

Figure 3.6. Acute attenuation of canonical Wnt signaling in adult brain ECs leads to a rapid loss of MFSD2A.

(a) Immunofluorescence images of MFSD2A in the cerebellar molecular layer with vessel (CD31) counterstain. (Scale bar: 100 µm) **(b)** Quantification of relative MFSD2A levels as fold change relative to control (data are mean ± SEM, n=5 animals per genotype). ****p<0.0001, unpaired t test. **(c)** Schematic of MFSD2A expression time course. control (*Ctnnb1*$^{fl/fl}$) and mutant (*Cdh5-Cre*^{ERT2}*;Ctnnb1*$^{fl/fl}$) mice received 1, 3, or 5 consecutive days of tamoxifen injections and were sacrificed 24 hours after their last injection. T1, T2, and T3 correspond to the time points shown in the next panel. Created with BioRender.com

(d) Immunofluorescence images of MFSD2A in the cerebellar molecular layer displaying stable levels of MFSD2A in control animals but rapidly decreasing levels in mutant animals. (Scale bar: 100 µm)

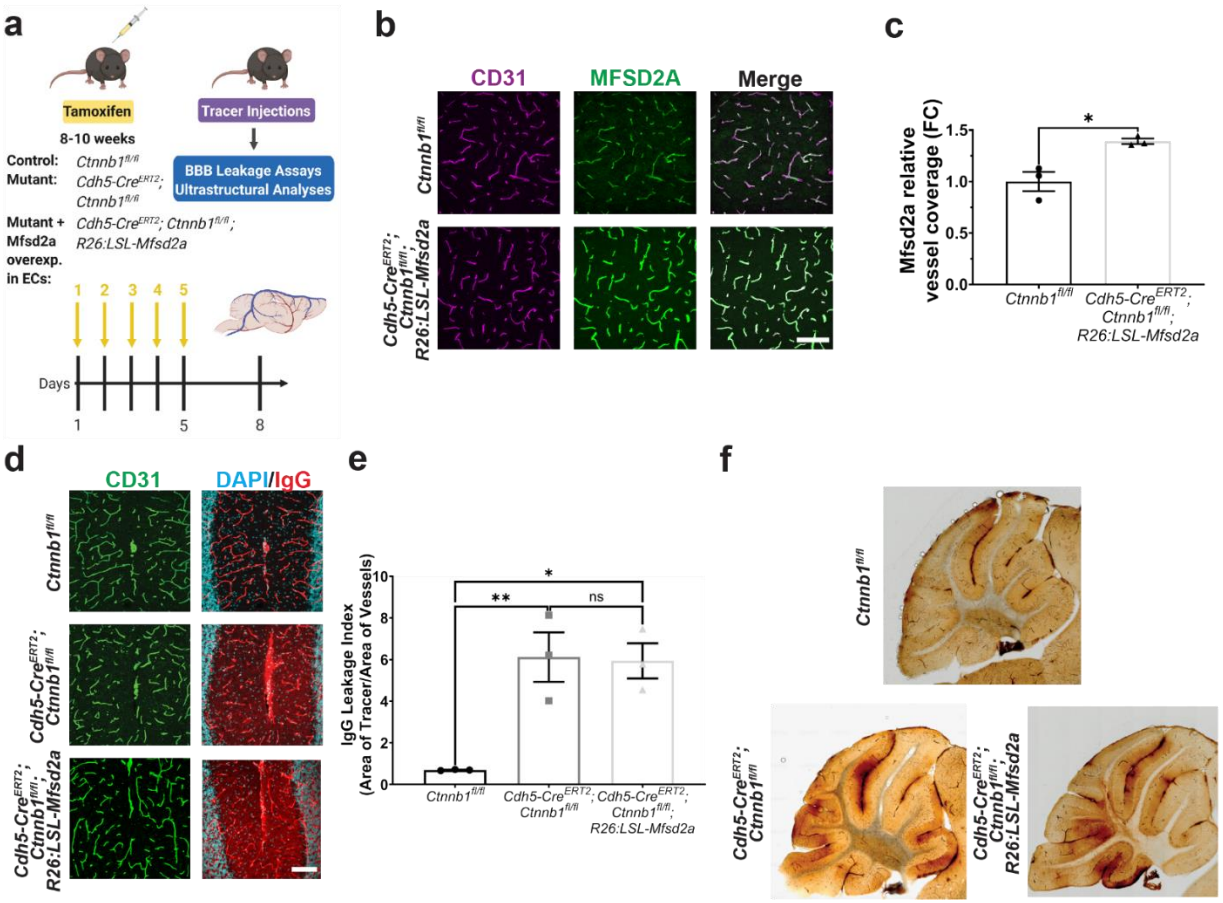

Figure 3.7. Overexpression of MFSD2A in Wnt signaling-deficient adult brain ECs is not sufficient to rescue BBB leakage. (a) Schematic of genetic strategy to overexpress MFSD2A in mutant brain ECs. Created with BioRender.com **(b)** Immunofluorescence images of MFSD2A displaying robust overexpression of MFSD2A in *Cdh5-Cre^{ERT2};Ctnnb1$^{fl/fl}$;R26:LSL-Mfsd2a* animals. (Scale bar: 100 µm) **(c)** Quantification of relative MFSD2A levels as fold change relative to control (data are mean ± SEM, n=3 animals per genotype). *p<0.05, unpaired t test with Welch's correction. **(d)** Immunofluorescence images of IgG leakage in control (*Ctnnb1$^{fl/fl}$*), mutant (*Cdh5-Cre^{ERT2};Ctnnb1$^{fl/fl}$*), and *Cdh5-Cre^{ERT2};Ctnnb1$^{fl/fl}$;R26:LSL-Mfsd2a* cerebellar molecular layer with vessel (CD31) counterstain. (Scale bar: 100 µm) **(e)** Quantification of IgG leakage indices as area of tracer / area of vessels (data are mean ± SEM, n=3 animals per

Figure 3.7 (Continued)

genotype). *p<0.05, **p<0.01, ns = not significant, one-way ANOVA with Tukey's multiple comparisons test. **(f)** Brightfield images of HRP leakage in control (*Ctnnb1*$^{fl/fl}$), mutant (*Cdh5-Cre*^{ERT2}*;Ctnnb1*$^{fl/fl}$), and *Cdh5-Cre*^{ERT2}*;Ctnnb1*$^{fl/fl}$*;R26:LSL-Mfsd2a* cerebellum.

Figure 3.8. Overexpression of MFSD2A in Wnt signaling-deficient adult brain ECs is not sufficient to rescue increased transcytosis. **(a)** Representative electron microscopy (EM) high magnification images of cerebellar molecular layer ECs following HRP (black) injection and low-pressure gravity perfusion. Yellow arrowheads show HRP-filled vesicles, red dashed lines denote the abluminal membrane of ECs; EC = endothelial cell, L = lumen (Scale bar: 200 nm) **(b)** Quantification of mean vesicular density (number of HRP-filled vesicles per μm^2 of EC cytoplasm): data are mean ± SEM, n=4 animals per genotype, *$p<0.05$, ns = not significant, nested one-way ANOVA.

Figure 3.8 (Continued)

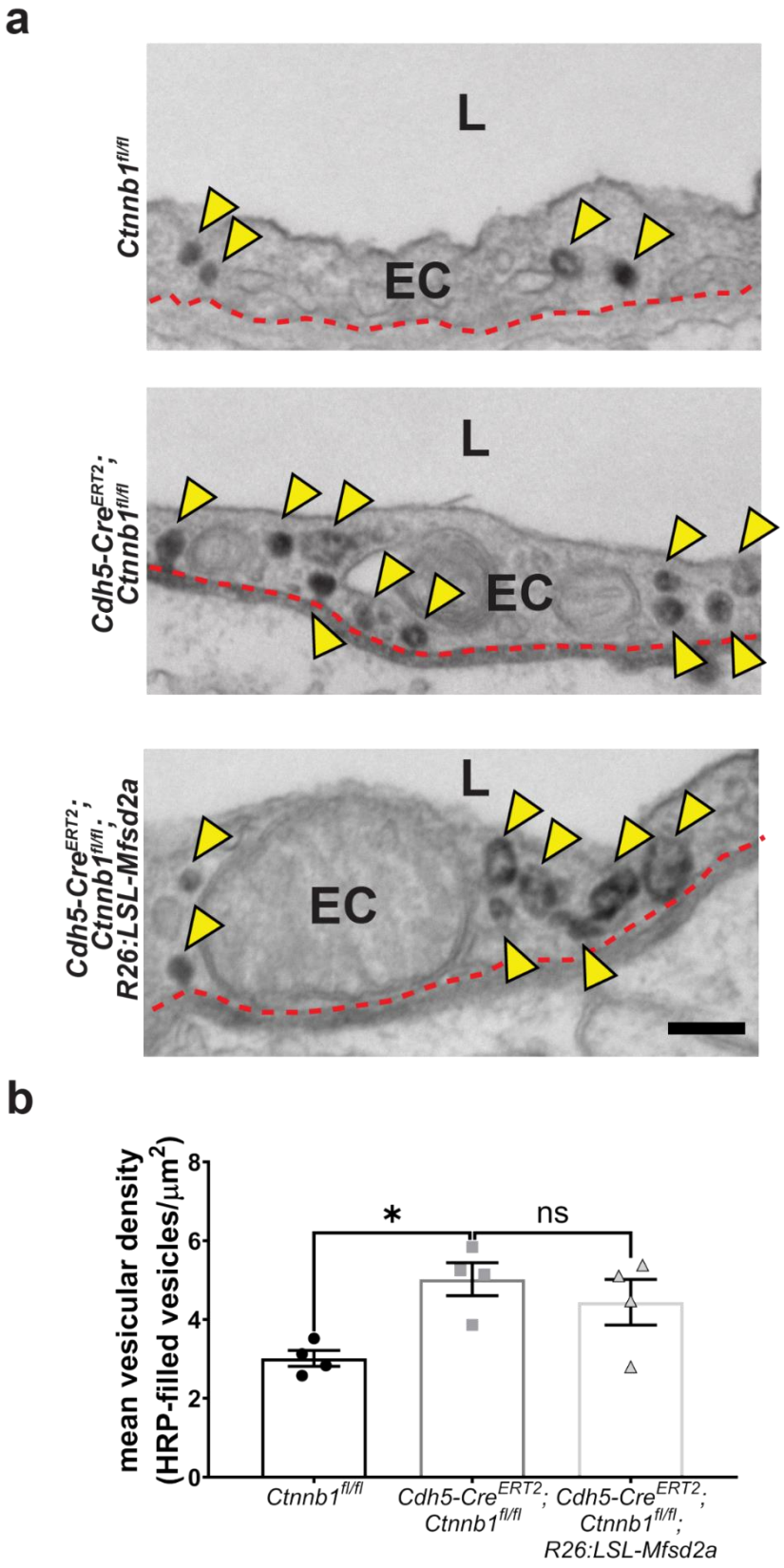

Overall, these findings add to a growing body of research that demonstrates the critical importance of transcytosis for the development, maintenance, regulation, and function of the BBB in health and disease (Ben-Zvi *et al.*, 2014; Chow and Gu, 2017; Knowland et al., 2014; O'Brown et al., 2019; Sadeghian et al., 2018). These and future mechanistic insights into the maintenance of the BBB in adulthood will continue to drive the advancement of drug and therapeutic delivery to the CNS, a critical need in 21st century healthcare.

CHAPTER 4

Molecular and Cellular Mechanisms Governing Canonical Wnt Signaling

Regulation of Adult BBB Maintenance: Tight Junctions

4.1. Assessing Tight Junction Permeability

While the tight junction (TJ) protein CLDN5 is a well-established target of canonical Wnt signaling in brain ECs, it is not known if canonical Wnt signaling maintains adult BBB integrity through regulation of TJ permeability. A major bottleneck in addressing this question has been the limited availability of assays that can clearly show alterations in TJ permeability.

In vitro evaluation of TJs often relies on transendothelial electrical resistance (TEER), which is a measurement of electric resistance across a cellular monolayer that corresponds to the ionic conductance of the paracellular barrier, and thus is thought to correlate with the tightness of paracellular barriers (Srinivasan et al., 2015). However, it is unclear how specific TEER values *in vitro* translate to the physical apposition of EC-EC membranes at junctions. Moreover, since brain ECs quickly lose their barrier properties *in vitro* (including the expression of specific TJ proteins) (Sabbagh and Nathans, 2020), *in vitro* TEER values do not translate well to *in vivo* TEER values. Thus, while TEER may be a useful proof of principle tool for forming hypotheses about molecular mechanisms, it cannot be extrapolated to infer causal mechanisms *in vivo*.

An additional tool used in the field to indirectly assess TJ permeability is leakage assays. Specifically, some studies have argued that the leakage of small molecular weight tracers implies de facto that TJ defects are present. However, there is no evidence to prove that this is the case. Comparing the phenotypes of *Cldn5*$^{-/-}$ and *Mfsd2a*$^{-/-}$ mice demonstrates this point.

Cldn5$^{-/-}$ mice – which have an increase in TJ permeability while transcytosis is unaffected – have size-selective leakage of small molecular weight tracers, while larger tracers are confined to the brain vasculature (Nitta *et al.*, 2003). In contrast, *Mfsd2a*$^{-/-}$ mice – which have an increase in transcytosis while TJs are unaffected – present with leakage of both small and large molecular weight tracers (Andreone *et al.*, 2017; Ben-Zvi *et al.*, 2014; Chow and Gu, 2017). These data

show that the leakage of small molecular weight tracers across the BBB is not by itself sufficient evidence for TJ defects. Similarly, leakage of larger molecular weight tracers does not prove that there is increased transcytosis since this may be due to severe junctional defects. Overall, it is important to use a variety of tracers to make informed hypotheses about whether leakage may be due to paracellular and/or transcellular aberrations.

While electron microscopy (EM) provides an avenue to assay TJ permeability more directly, it presents its own set of limitations. Specifically, most studies that assess TJ function *in vivo* do so by analyzing various aspects of TJ ultrastructure, which may include TJ length, TJ width, and the presence of 'kissing points' where organized strands of TJ proteins from adjacent ECs come together to induce close apposition of the EC membranes. While these hallmarks of TJ ultrastructure may be helpful at distinguishing vascular beds with extremely different permeability properties, such as brain vs. cardiac ECs, they are an unreliable predictor of changes in TJ permeability within a given tissue-specific vascular bed. Most notably, *Cldn5*$^{-/-}$ mice display a size-selective BBB leakage phenotype attributed to altered TJ permeability despite displaying normal TJ ultrastructure (as determined by EM), as well as normal localization of other TJ proteins to junctional structures (as determined by immunostaining) (Nitta *et al.*, 2003).

The most direct way to assay TJ permeability *in vivo* is by coupling EM with the injection of electron-dense tracers that can be visualized in electron micrographs. One of the most common tracers used for this purpose, which was first introduced in the pioneering studies of Reese and Karnovsky, is horseradish peroxidase (HRP) (Reese and Karnovsky, 1967). This 44 kDa tracer forms an electron-dense reaction product that appears as black in electron micrographs when it is exposed to its substrate 3,3'-diaminobenzidine (DAB). This tracer has

been especially useful in evaluating transcytosis, as it is taken up into luminal and abluminal vesicles and can also be visualized in cytoplasmic vesicles.

However, due to its molecular weight, HRP is not a very sensitive at detecting subtle alterations in TJ permeability. While there are clear differences in HRP permeability through TJs of brain and cardiac ECs – which are both continuous non-fenestrated ECs – these two tissues have dramatically different permeability properties overall. HRP is too large to be able to detect subtler alterations in TJ permeability that may result in a size-selective leakage phenotype. This limitation of HRP necessitates the utilization of smaller molecular weight tracers that are also compatible with EM.

One such tracer is microperoxidase, which also forms an electron-dense reaction product in the presence of DAB. Despite a clear demonstration in an early study of its ability to be taken up into vesicles and to be halted at functional TJs (Westergaard, 1980), there have been very few publications utilizing microperoxidase to evaluate TJ permeability since this time. Another potentially useful tracer for evaluating TJ permeability is biotin ethylenediamine, which was used in a 2006 study to evaluate the permeability of developing cerebral vessels in opossum to small, water-soluble molecules (Ek et al., 2006). These and additional tracers are discussed below in the context of evaluating TJ permeability in brain ECs with attenuated canonical Wnt signaling, as well as developing and optimizing novel EM-compatible tracers to evaluate TJ permeability.

4.2. The Development and Optimization of Tools to Assess the Permeability of Tight Junctions at the Ultrastructural Level

In order to establish an assay sensitive enough to detect subtle alterations in TJ permeability, we opted to develop and/or optimize a series of tracers that all have a molecular

weight substantially smaller than HRP (44 kDa): microperoxidase (1.9 kDa), gadodiamide (592 Da), sulfo-NHS-LC-biotin (557 Da), Neurobiotin (323 Da), and biotin ethylenediamine (286 Da).

Microperoxidase (1.9 kDa)

Having a previously established protocol for using peroxidase tracers for EM ultrastructural analyses, we first evaluated microperoxidase a potential tracer for use with EM (**Figure 4.1**). The biggest technical hurdle was getting microperoxidase into solution, which limited the concentration and total amount of tracer that we were able to inject into mice. Once injected, we also optimized the tracer circulation time since it was cleared from the cerebral blood circulation more rapidly than HRP, as evidenced by its absence from the lumen in electron micrographs at longer circulation time points. We determined empirically that circulation for 10 minutes rather than 30 minutes would allow for optimal tracer perfusion of the blood circulation. Lastly, the generation of the reaction product was not as robust with microperoxidase, which may be due to a lower sensitivity to DAB compared to HRP, or an overall lower concentration in the circulation. To mitigate this, we optimized the DAB incubation conditions through empirical analysis, eventually increasing the incubation time from 35 min to 2 hrs. Further details are available in Chapter 2 (Experimental Methods).

Gadodiamide (592 Da)

Gadolinium (Gd) is chemical element that is commonly used as a contrast agent for magnetic resonance imaging (MRI) in human patients. It has also been used in rodent studies as a clinically relevant readout of BBB permeability, as it can be detected in the brain parenchyma via MRI following intravenous injection (Menard et al., 2017; Nitta *et al.*, 2003). Studies in rat have shown that it forms electron-dense deposits in and around cerebellar blood vessels that are

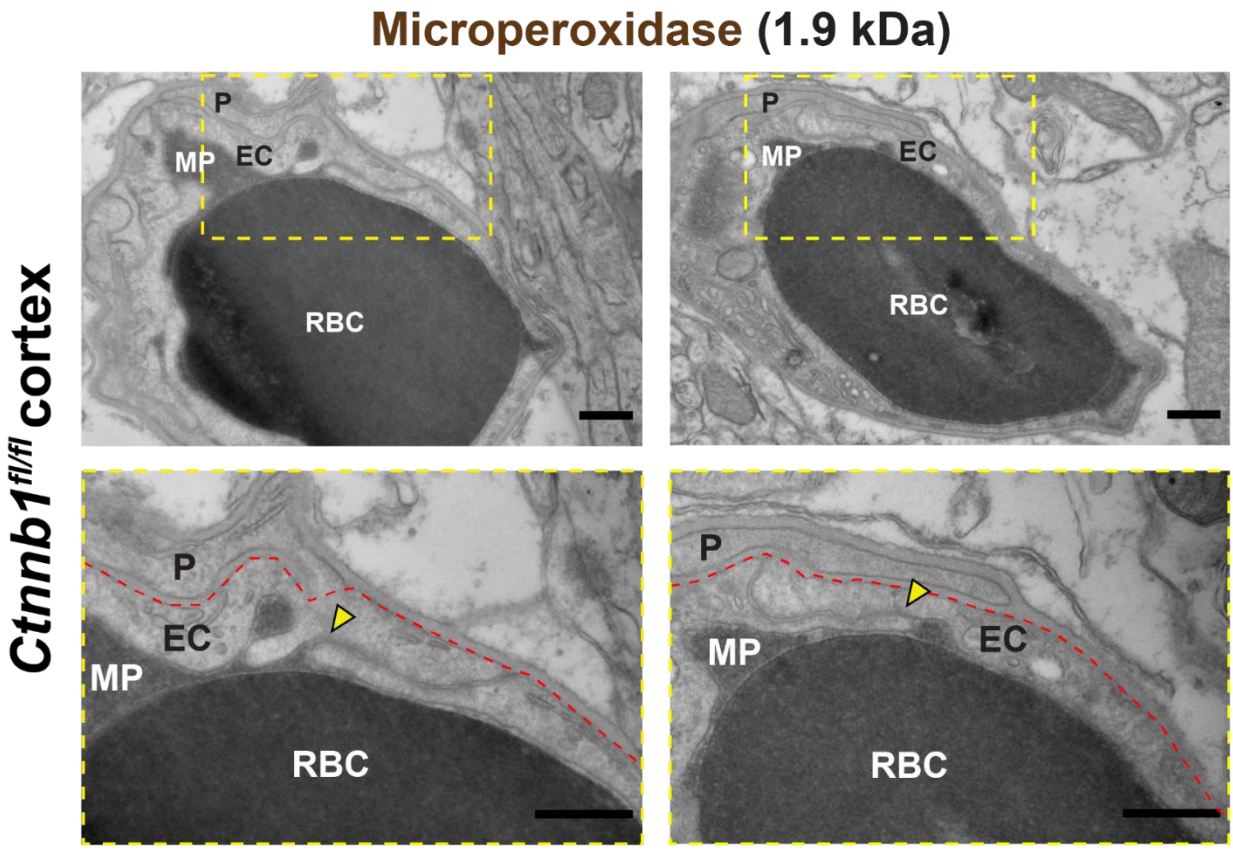

Figure 4.1. Development and optimization of tracers for the evaluation of tight junction permeability: microperoxidase. Following 10 minutes of circulation in the blood, microperoxidase was visualized in cerebral vessels via incubation with its substrate 3,3'-diaminobenzidine, producing an electron-dense reaction product. Top: Electron micrographs of cortical vessel cross sections shows red blood cells and microperoxidase tracer in the lumen. Bottom: Insets (yellow dashed line boxes from top images) show microperoxidase sharply halted at tight junctions (yellow arrowheads). Red dashed lines outline the abluminal membrane of ECs. RBC = red blood cell, MP = microperoxidase, EC = endothelial cell, P = pericyte. All scale bars: 500 nm.

visible in electron micrographs (Lohrke et al., 2017; Rasschaert et al., 2018b). Among the commonly used Gd-based contrast agents, gadodiamide (which is commercially available as Omniscan) is detectable at the highest levels in the brain following intravascular injection (Lohrke *et al.*, 2017; Rasschaert et al., 2018a). For these reasons, we decided to utilize gadodiamide as a potentially EM-compatible tracer to evaluate brain EC TJ permeability. While we were able to detect gadodiamide in cerebellar EC lumens following injection, it was not electron-dense enough to contrast with TJs (**Figure 4.2**). Thus, we determined that it was unsuitable for use as a TJ permeability tracer.

Sulfo-NHS-LC-Biotin (557 Da)

Sulfo-NHS-LC-Biotin was a clear candidate to assay for evaluation of TJ permeability since our group and others have extensively used it for BBB leakage assays and it produces a robust signal in histological analyses. In order to detect sulfo-NHS-LC-biotin at the ultrastructural level, we employed the biotin-streptavidin system but rather than using a fluorophore-conjugated streptavidin – which we use for BBB leakage assays – we used an HRP-conjugated streptavidin, followed by incubation with DAB. While sulfo-NHS-LC-biotin was detectable in the lumen of electron micrographs, it was so electron-light relative to the TJs themselves that it was impossible to determine if it was able to permeate TJs (**Figure 4.3**). We hypothesized that this was due to a very low concentration in the lumen, which was likely due to it being "washed out" of the circulation during the various tissue processing steps.

Neurobiotin (323 Da)

To mitigate the limited utility of sulfo-NHS-LC-biotin, we used Neurobiotin and biotin ethylenediamine, two biotin derivatives with similar molecular composition that are glutaraldehyde-fixable. We hypothesized that this important chemical property would lead to a

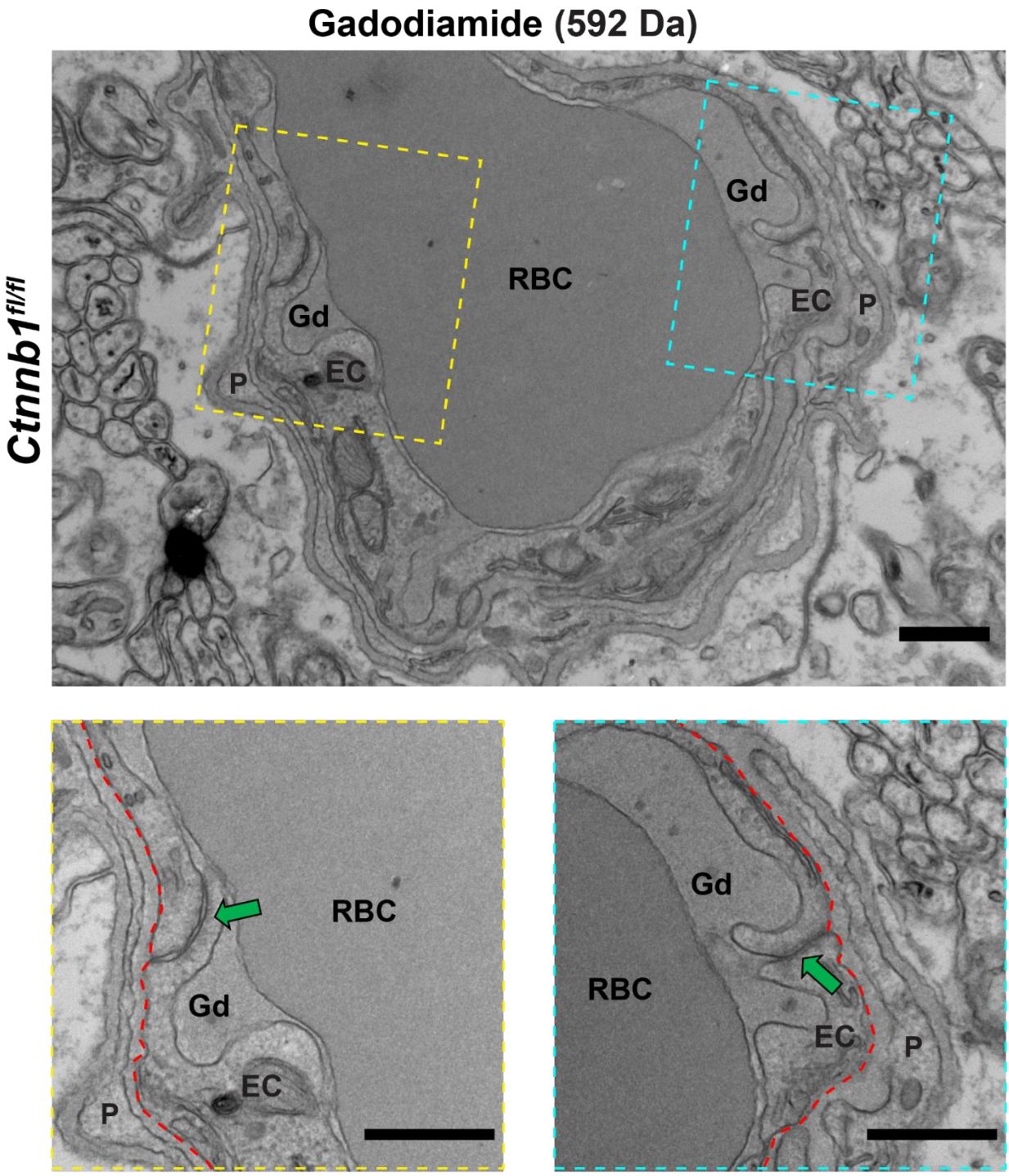

Figure 4.2. Development and optimization of tracers for the evaluation of tight junction permeability: gadodiamide. Following 10 minutes of circulation in the blood, gadodiamide (Omniscan) was visualized in cerebellar vessel cross sections. Top: Electron micrographs of cortical vessel cross sections show red blood cells and gadodiamide in the lumen. Bottom: Insets

Figure 4.2 (Continued)

(yellow and blue dashed line boxes from top image) show gadodiamide in the lumen adjacent to tight junctions (green arrows), which are more electron-dense. Red dashed lines outline the abluminal membrane of ECs. RBC = red blood cell, Gad = gadodiamide, EC = endothelial cell, P = pericyte. All scale bars: 500 nm.

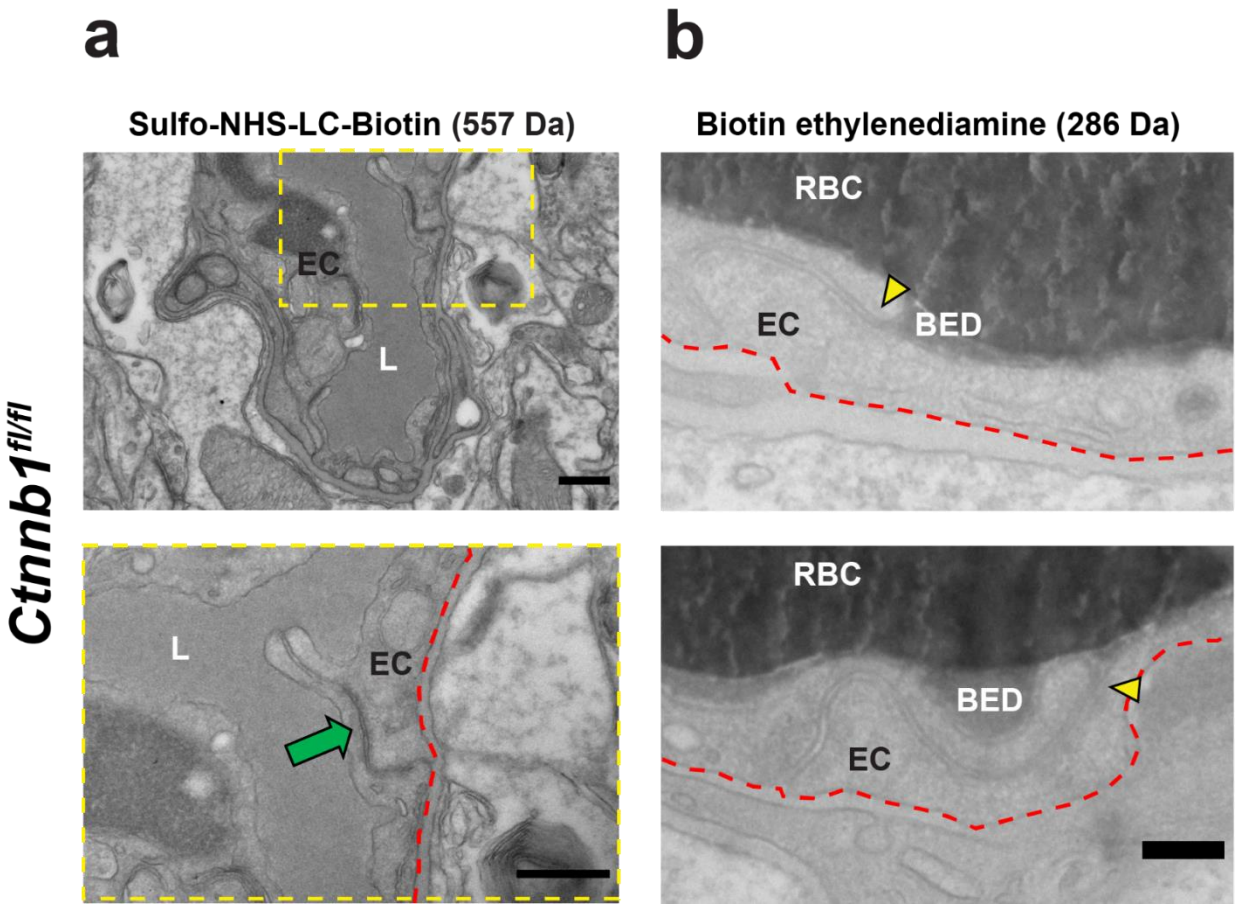

Figure 4.3. Development and optimization of tracers for the evaluation of tight junction permeability: biotin derivatives. Following 10 minutes of circulation in the blood, sulfo-NHS-LC-biotin and biotin ethylenediamine were visualized in cerebellar vessel cross sections via coupling to horseradish peroxidase–conjugated streptavidin and subsequent incubation with 3,3'-diaminobenzidine. **(a)** Top: Electron micrograph of a cerebellar vessel cross section shows sulfo-NHS-LC-biotin in the lumen (L). Bottom: Inset (yellow dashed line box from top image) shows sulfo-NHS-LC-biotin in the lumen adjacent to a tight junction (green arrow), which is more electron-dense than the tracer. (Scale bars: 500 nm) **(b)** Top and Bottom: High magnification images show electron-dense biotin ethylenediamine sharply halted at tight junctions (yellow

Figure 4.3 (Continued)

arrowheads). Red dashed lines outline the abluminal membrane. L = lumen, RBC = red blood cell, BED = biotin ethylenediamine, EC = endothelial cell, P = pericyte. (Scale bar: 200 nm)

higher stability and containment of the tracer within the lumen, which would make subsequent streptavidin-HRP- and DAB-mediated detection more robust and increase the signal-to-noise ratio. Unfortunately, retroorbital injection of Neurobiotin at a concentration of 0.5 mg/g body weight led to acute lethality, which prevented proceeding with the subsequent steps.

Biotin ethylenediamine (286 Da)

While biotin ethylenediamine had similar outcomes at higher concentrations (0.5 mg/g body weight), we were able to empirically determine a safe dosage: 0.2 mg/g body weight. With these optimizations, which increased the signal-to-noise of biotin ethylenediamine, we were able to detect it in the lumen of cerebral ECs with a high enough contrast to distinguish it from TJs (**Figure 4.3**). While there were issues with achieving consistently robust detection of biotin ethylene diamine, further optimization will help establish conditions under which it can be used as a reliable tracer.

4.3. Canonical Wnt Signaling Regulation of Tight Junction Permeability

Having established the necessity of canonical Wnt signaling for the suppression of transcytosis to maintain adult BBB integrity (see **Chapter 3**), we next sought to investigate if TJ permeability is altered in Wnt signaling-deficient ECs. We first pursued this line of investigation using electron microscopy in HRP-injected mice. As presented in Chapter 3, in 100% of control and mutant ECs, we observed that HRP was sharply halted at areas of close membrane apposition between adjacent ECs (‘kissing points’) where TJs occur, indicating that TJs were impermeable to HRP (**Figure 4.4**). To detect more subtle changes in TJ permeability, we employed microperoxidase (1.9 kDa). Like HRP, microperoxidase was also sharply halted at ‘kissing points’, with nearly 100% of TJs in control and mutant ECs impermeable to this tracer (**Figure 4.4**).

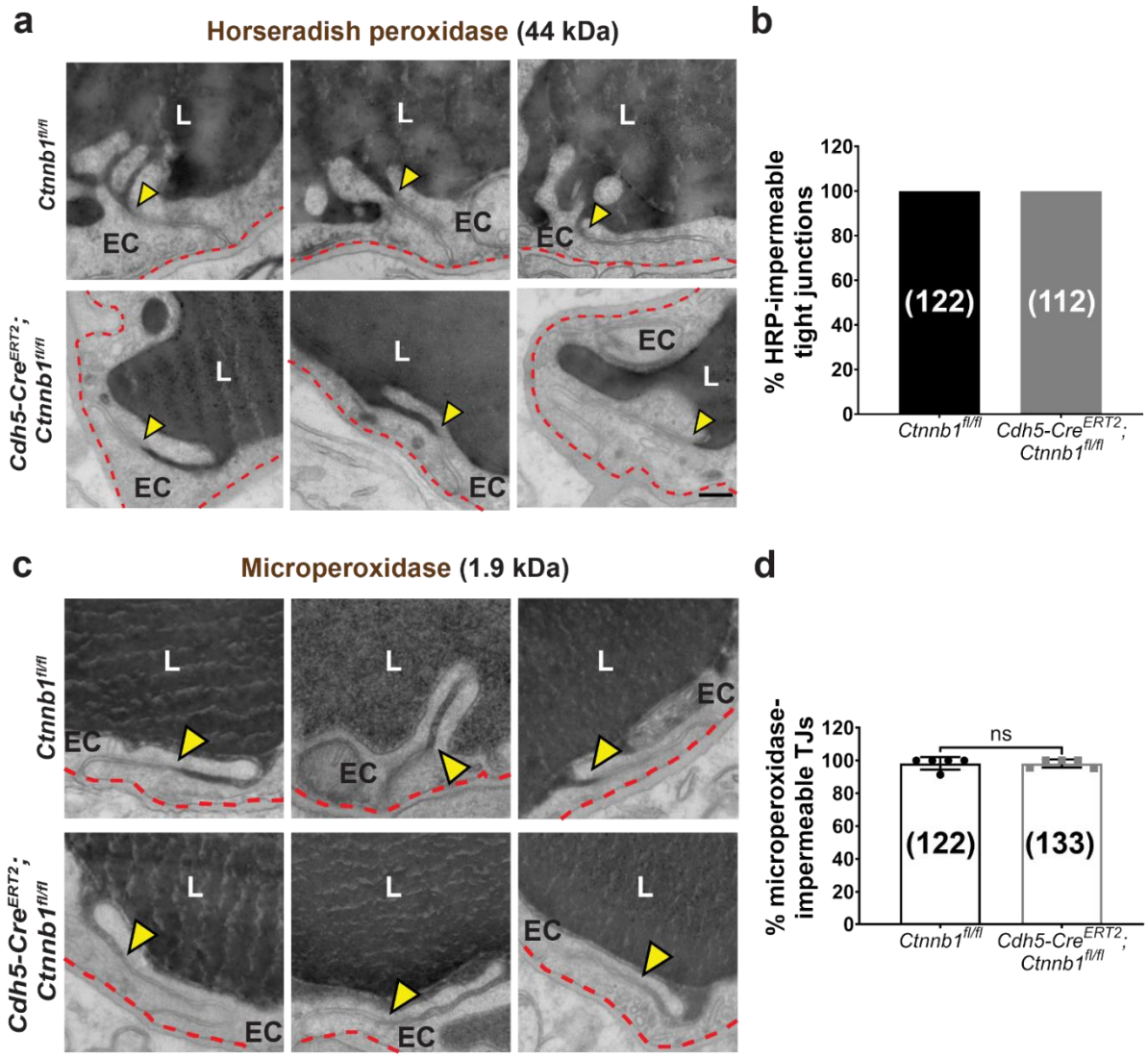

Figure 4.4. Acute attenuation of canonical Wnt signaling in adult brain vasculature does not alter TJ permeability to tracers as small as 1.9 kDa. Electron micrographs showing cross sections of cerebellar ECs demonstrate that both HRP **(a)** and microperoxidase **(c)** are halted at TJs (yellow arrowheads) in both control (*Ctnnb1*$^{fl/fl}$) and mutant (*Cdh5-Cre*^{ERT2}*;Ctnnb1*$^{fl/fl}$) mice. Scale bar: 200 nm. **(b)** Quantification of data in (a) showing that 100% of TJs observed were impermeable to HRP (n=5 animals per genotype, total number of TJs observed per genotype in

Figure 4.4 (Continued)

parentheses). Data in (a) and (b) also shown in Chapter 3 (**Figure 3.5**). **(d)** Quantification of data in (c), showing that the vast majority of TJs observed in control (*Ctnnb1*$^{fl/fl}$) and mutant (*Cdh5-Cre*^{ERT2}*;Ctnnb1*$^{fl/fl}$) mice were impermeable to microperoxidase (data are mean ± SEM, n=5 animals per genotype, total number of TJs per genotype in parentheses, ns = not significant, unpaired t test). L = lumen, EC = endothelial cell. Red dashed lines outline abluminal membranes of ECs.

As an internal control, we also evaluated TJ permeability to HRP and microperoxidase in the choroid plexus (CP), a non-BBB-containing brain vasculature which is known to have very low levels of canonical Wnt signaling in ECs (Wang *et al.*, 2019). In contrast to control and mutant TJs, nearly all choroid plexus TJs observed were permeable to HRP (**Figure 4.5**) and all choroid plexus TJs observed were permeable to microperoxidase (**Figure 4.6**).

To evaluate the molecular composition of TJs in mutant mice, we stained for CLDN5, the predominant component of brain EC TJs and a known transcriptional target of the pathway, as well as its cytoplasmic partner ZO-1. In mutant ECs, we observed a significant decrease in the levels of CLDN5, with a 40% reduction in CLDN5 coverage of $CD31^+$ blood vessels (**Figure 4.7**). In addition, we observed a very small but significant 10% reduction in ZO-1 coverage of $CD31^+$ blood vessels (**Figure 4.7**). Overall, these data demonstrate that although acute attenuation of canonical Wnt signaling in adult brain ECs alters the molecular composition of TJs, it does not alter TJ permeability to macromolecules as small as 1.9 kDa. Notably, these results are in accordance with the previously reported size-selective leakage of *Cldn5*$^{-/-}$ mice, which display leakage of smaller molecular weight tracers like sulfo-NHS-biotin (443 Da) but not larger tracers like microperoxidase (Nitta *et al.*, 2003). Optimization of smaller molecules like biotin ethylenediamine will enable us to evaluate subtler alternations in TJ permeability in future studies.

4.4. Heterogeneous Expression of Canonical Wnt Target Genes in Wnt Signaling-Deficient Brain ECs

In addition to assessing the molecular composition of TJs, we also determined the expression of other genes that are known to be regulated by canonical Wnt signaling in brain ECs: the glucose transporter GLUT1 and the fenestral diaphragm–associated protein PLVAP.

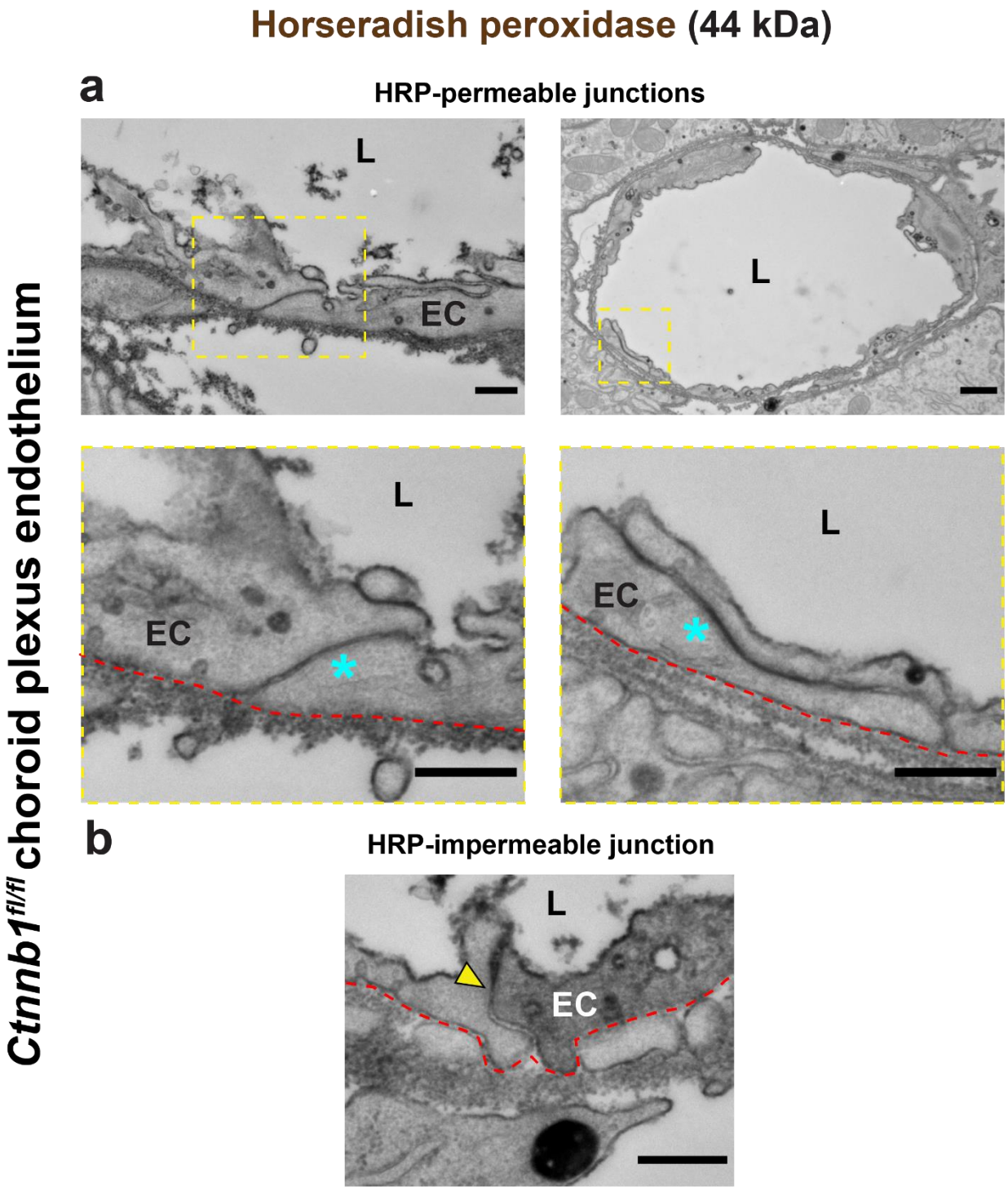

Figure 4.5. Choroid plexus endothelial tight junctions are mostly permeable to horseradish peroxidase. (a) Top: Electron micrographs of choroid plexus vessel cross sections. Bottom: High magnification insets (yellow dotted line boxes from overview images) show HRP

Figure 4.5 (Continued)

permeation through EC TJs (blue asterisk). **(b)** Electron micrograph showing a rare instance of luminal HRP sharply halted at a choroid plexus EC TJ (yellow arrowhead). L = lumen, EC = endothelial cell. Red dashed lines outline abluminal membranes of ECs. Scale bars: 500 nm.

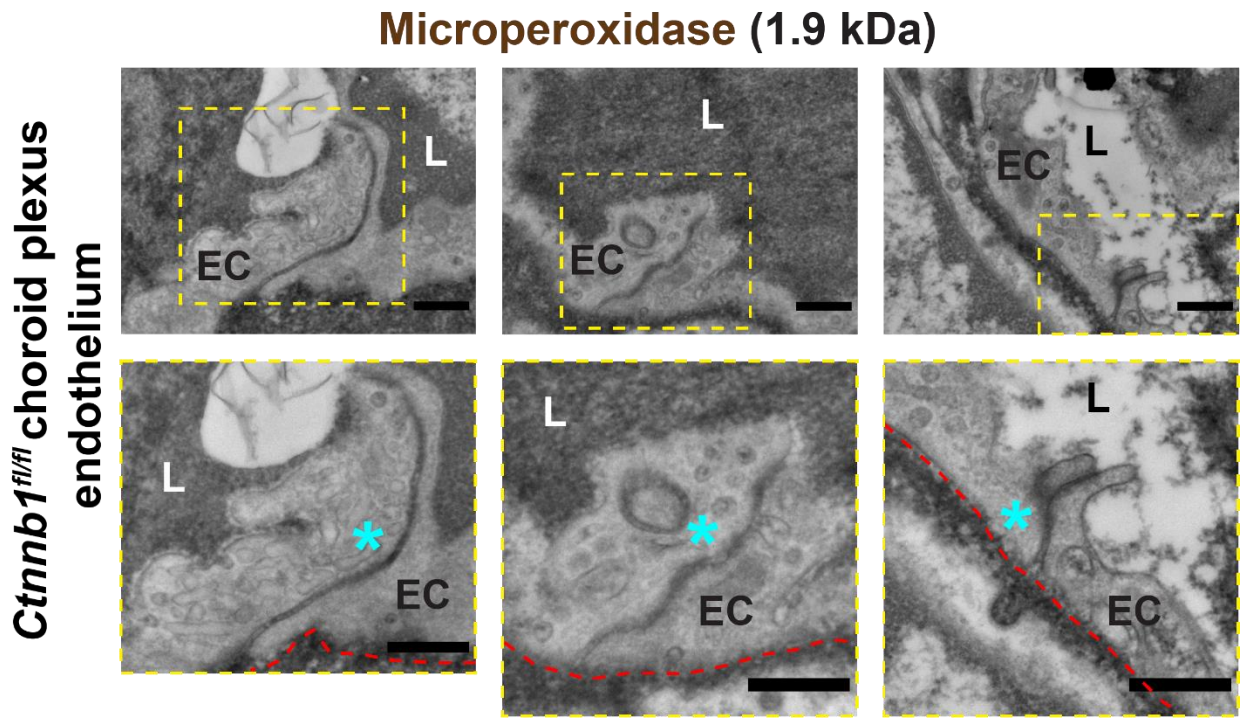

Figure 4.6. Choroid plexus endothelial tight junctions are permeable to microperoxidase. Top: Electron micrographs of choroid plexus EC cross sections. Bottom: High magnification insets (yellow dotted line boxes from overview images) show microperoxidase permeation through EC TJs (blue asterisk). L = lumen, EC = endothelial cell. Red dashed lines outline abluminal membranes of ECs. All scale bars: 500 nm.

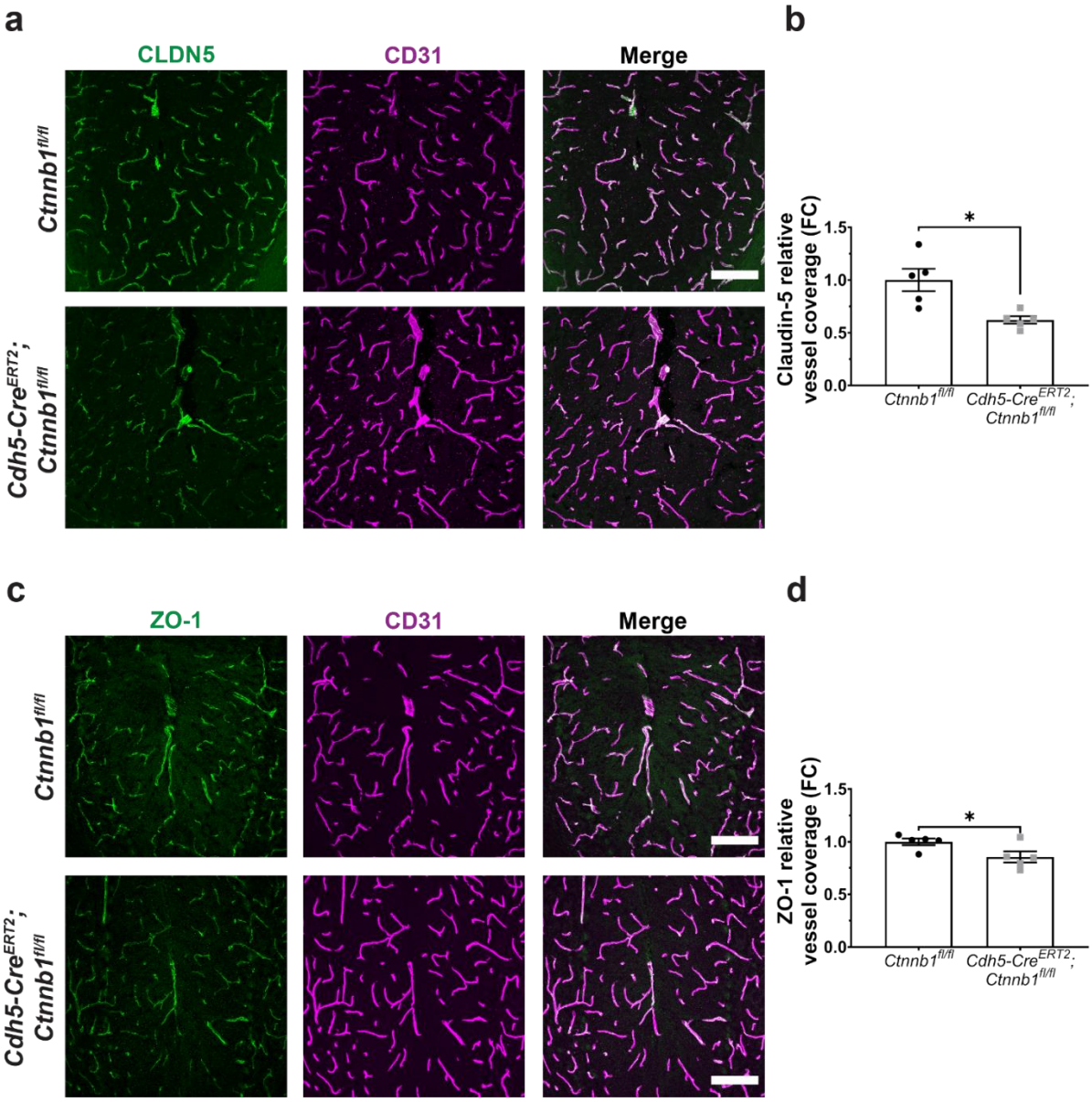

Figure 4.7. Acute attenuation of canonical Wnt signaling in the adult brain vasculature alters the molecular composition of tight junctions. (a) CLDN5 immunofluorescence staining in the cerebellar vasculature with CD31 (EC) co-stain. Scale bar: 100 µm. **(b)** Quantification of CLDN5 relative levels normalized to controls (data are mean ± SEM, n=5 animals per genotype, *p<0.05, unpaired t test with Welch's correction). **(c)** ZO-1 immunofluorescence staining in the cerebellar vasculature with CD31 (EC) co-stain. Scale bar: 100 µm. **(d)** Quantification of ZO-1

Figure 4.7 (Continued)

relative levels normalized to controls (data are mean ± SEM, n=5 animals per genotype, *p<0.05, unpaired t test).

First, we found that GLUT1 levels were not altered in mutant brain ECs relative to controls (**Figure 4.8**). In addition to showing that GLUT1 expression is stable within this timeframe, this result also demonstrates that the observed subcellular phenotypes cannot be attributed to altered GLUT1 levels. Second, we found that there was very sparse upregulation of PLVAP (**Figure 4.8**). Within the cerebellum, this was restricted to the central axis of the molecular layer, which contained segments of $CLDN5^{+}PLVAP^{+}$ vessels. These results contrast with previous studies in which the expression GLUT1 was reduced in canonical Wnt pathway mutants (Cullen *et al.*, 2011; Daneman *et al.*, 2009; Kuhnert *et al.*, 2010; Stenman *et al.*, 2008). In addition, they contrast with previous studies in which the expression of CLDN5 and PLVAP was anticorrelated in canonical Wnt pathway mutants following acute genetic manipulations in sexually mature adult mice (Wang *et al.*, 2012; Zhou *et al.*, 2014).

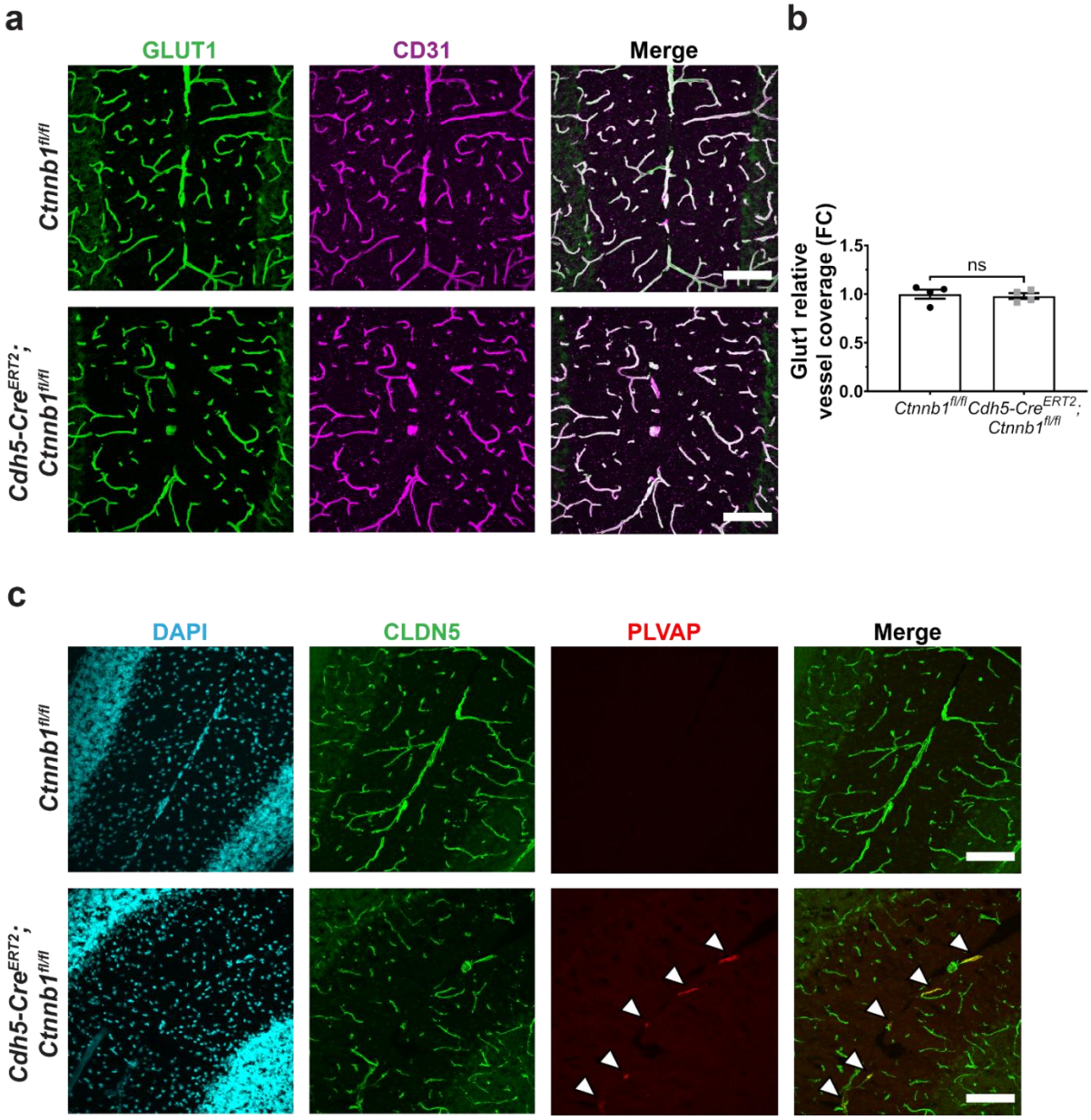

Figure 4.8. Differential expression of Wnt target genes in the adult brain vasculature following acute attenuation of canonical Wnt signaling. (a) GLUT1 staining in the cerebellar vasculature with CD31 (EC) co-stain. Scale bar: 100 µm. **(b)** Quantification of area of GLUT1 / area of CD31 (data are mean ± SEM, n=4 animals per genotype, ns = not significant, unpaired t-test). **(c)** PLVAP staining in the cerebellar vasculature with CLDN5 and DAPI co-stain. White

Figure 4.8 (Continued)

arrowheads indicate vessel segments along the central axis of the cerebellar molecular layer with sparse PLVAP expression. Scale bar: 100 μm.

CHAPTER 5

Nutrient Transporters: Candidate Novel Regulators of BBB Integrity

5.1. Utilizing Transcriptomic Studies to Identify Novel Regulators of BBB Integrity

To confer specialized barrier properties, brain ECs express a unique set of genes. Several studies have generated "BBB transcriptomes" by comparing relative gene expression between brain ECs and non-BBB peripheral (e.g. lung, liver) ECs (Daneman et al., 2010a; Tam et al., 2012). These microarray studies have served as useful tools for identifying novel candidate barrier-promoting genes. Later studies have used RNA-seq to generate a more precise quantitative picture of transcript abundance (Sabbagh *et al.*, 2018; Wang *et al.*, 2019; Zhang *et al.*, 2014). With the latest technological advancements, recent studies have also begun to use single-cell RNA-seq and ATAC-seq to uncover the molecular heterogeneity of ECs across different brain regions and organs at the level of transcript abundance and chromatin accessibility (He et al., 2018; Sabbagh *et al.*, 2018; Vanlandewijck and Betsholtz, 2018; Wang *et al.*, 2019).

Using a subset of these transcriptomic data sets to cross reference hits, we sought to identity novel candidate regulators of BBB integrity. Our initial analyses showed that there were a variety of genes in the solute carrier family enriched in brain vs. peripheral ECs, reflecting an established feature of the BBB, the expression of influx transporters (**Table 5.1**). Given recent work on the important roles of the glucose transporter GLUT1 and the DHA-containing lipid species transporter MFSD2A in regulating BBB function (Andreone *et al.*, 2017; Ben-Zvi *et al.*, 2014; Chow and Gu, 2017; Winkler *et al.*, 2015), we were particularly intrigued by the nutrient transporters enriched in brain ECs.

From this initial list of 50 genes, we were able to narrow down candidates of interest with the following selection criteria: (1) highly expressed in brain ECs (according to RNA-seq data), (2) highly enriched in brain ECs vs. peripheral ECs (according to microarray data), (3)

Table 5.1. Comparison of Nutrient Transporter Relative RNA Levels in CNS and Peripheral Endothelial Cells. These compiled data show that nutrient transporters are some of the most highly expressed genes in brain ECs and are highly enriched in brain ECs relative to peripheral ECs. "RNA-seq pct." – this column displays the fragments per kilobase million (FPKM) percentile among all mouse genes in this RNA-seq database (Zhang *et al.*, 2014) (e.g. *Slc16a1* is expressed more than 99% of all other genes in the P7 mouse cerebral cortex according to its FPKM value). The remaining columns display the relative expression or fold change of genes in mouse brain ECs compared to lung and/or liver ECs at various ages.

Gene (Protein)	**Substrates**	**RNA-seq pct. (adult)**	**brain vs. lung (E13.5)**	**brain vs. lung/ liver (E14.5)**	**brain vs. lung/ liver (P7.5)**	**brain vs. lung/ liver (adult)**	**brain vs. liver (adult)**	**brain vs. lung (adult)**
Source	---	(Zhang *et al.*, 2014)	(Ben-Zvi *et al.*, 2014)	(Tam *et al.*, 2012)	(Tam *et al.*, 2012)	(Tam *et al.*, 2012)	(Daneman *et al.*, 2010a)	(Daneman *et al.*, 2010a)
Slc16a1 (MCT1)	short-chain mono-carboxylic acids	99	0.9	---	128.0	98.2	59.3	148.3
Slc7a5 (LAT1)	large neutral amino acids	98	5.6	25.2	56.4	30.3	15.8	734.2
Slc38a5 (SNAT5)	glutamine	96	24.1	---	2.1	9.5	237.6	13.5
Slc22a8 (OAT3)	organic anions	91	22.5	19.0	71.6	216.4	774.6	764.3
Slc16a4 (MCT5)	mono-carboxylic acids (predicted)	85	1	32.3	882.9	1509.9	94.0	34.0
Slco1c1 (OATP1C1)	thyroxine	99	56.4	56.0	102.9	123.4	1745.2	310.2
Slc7a1 (CAT1)	cationic L-amino acids	93	1.9	17.0	58.6	29.7	31.2	9.1
Slco1a4 (OATP1A4)	organic anions	---	---	---	26.6	65.4	847.4	450.2
Slc40a1 (FPN1)	iron	91	4.0	8.2	10.6	7.3	1.1	59.2
Slc35f2 (SLC35F2)	lipophilic drugs	83	1.8	7.7	29.0	171.5	552.5	69.2

expression validated across multiple studies, (4) general brain expression pattern similar in mouse and human, (5) known substrates, and (6) available genetic tools to manipulate gene expression. This iterative process of narrowing down the candidates left us with 9 in total, most of which are displayed in **Table 5.1**. Two of these nutrient transporters – *Slc16a1* (MCT1) and *Slc7a5* (LAT1) – are the subject of this chapter.

5.2. *Slc16a1* (MCT1) and *Slc7a5* (LAT1) are not required for blood-brain barrier integrity.

Monocarboxylate transporter 1 (MCT1) – encoded by the gene *Slc16a1* – transports lactate, pyruvate, and ketone bodies and is expressed in brain ECs of early postnatal and adult mice (Daneman *et al.*, 2010a; Halestrap and Wilson, 2012; Tam *et al.*, 2012), whereas the large neutral amino acid transporter (LAT1) – encoded by the gene *Slc7a5* – transports large neutral and branched-chain amino acids and is expressed in brain ECs of embryonic, early postnatal, and adult mice (Ben-Zvi *et al.*, 2014; Daneman *et al.*, 2010a; Mastroberardino et al., 1998; Napolitano et al., 2015; Tam *et al.*, 2012; Tarlungeanu et al., 2016). The temporal expression of these transporters suggests possible roles in diverse aspects of brain EC function, including BBB formation (E13.5-E15.5), BBB maintenance (after E15.5), and postnatal cerebrovascular patterning (P0-P28).

To interrogate the role of MCT1 and LAT1 in BBB integrity, we employed the Cre-Lox system to achieve endothelial-specific loss of each gene, separately crossing floxed mice for each of the genes to a hematopoietic lineage–targeting Cre line, *Tie2-Cre* (Kisanuki et al., 2001), which is predominantly expressed in ECs. This allowed us to generate endothelial-specific MCT1 KO mice (MCT1 cKO) and endothelial-specific LAT1 KO mice (LAT1 cKO).

MCT1 is highly expressed in brain ECs of early postnatal and adult mice (**Table 5.1**) (Daneman *et al.*, 2010a; Tam *et al.*, 2012; Zhang *et al.*, 2014), suggesting possible roles in

postnatal cerebrovascular patterning (P0-P28) or BBB maintenance (after E15.5). To determine the necessity of MCT1 for BBB maintenance, we first performed BBB leakage assays in control and MCT1 cKO P5 animals. To appreciate the full spectrum of BBB permeability in these animals, we used tracers representing a variety of molecular weights and chemical properties: the small molecule sulfo-NHS-LC-biotin (557 Da), the carbohydrate 10 kDa dextran, and the protein bovine serum albumin (67 kDa). We found that for all three tracers, there was no sign of BBB leakage in MCT1 cKO mice (**Figure 5.1**). We also assessed endogenous serum protein leakage by staining for IgG and fibrinogen and found that there was also no IgG or fibrinogen leakage (**Figure 5.1**).

These findings were corroborated by ultrastructural analyses of cortical ECs in control (*Slc16a1*$^{fl/fl}$) and MCT1 cKO mice. Specifically, the density of luminal and abluminal non-clathrin-coated vesicles was unaltered between control and MCT1 cKO mice, indicative of normal levels of vesicle formation (**Figure 5.2**). In addition, both control and MCT1 cKO mice displayed TJs with no gross abnormalities and normal ultrastructure, including the hallmark 'kissing points' (**Figure 5.2**). While neither of these ultrastructural phenotypes are sufficient evidence on their own to definitively prove that transcytosis and TJs are unaltered in MCT cKO mice, taken together with the clear lack of BBB leakage, these results collectively indicate that MCT1 is not required for BBB integrity.

LAT1 is expressed from embryonic stages through adulthood (**Table 5.1**) (Daneman *et al.*, 2010a; Tam *et al.*, 2012; Tarlungeanu *et al.*, 2016; Zhang *et al.*, 2014), suggesting possible roles in BBB formation and maintenance. To determine the necessity of LAT1 for BBB integrity, we performed BBB leakage assays using sulfo-NHS-LC-biotin and 10 kDa dextran. We found that in early postnatal and adult LAT cKO mice, there was no biotin or dextran leakage (**Figure**

5.3). Given the clear lack of a BBB leakage phenotype, we decided not to pursue further studies in LAT cKO mice.

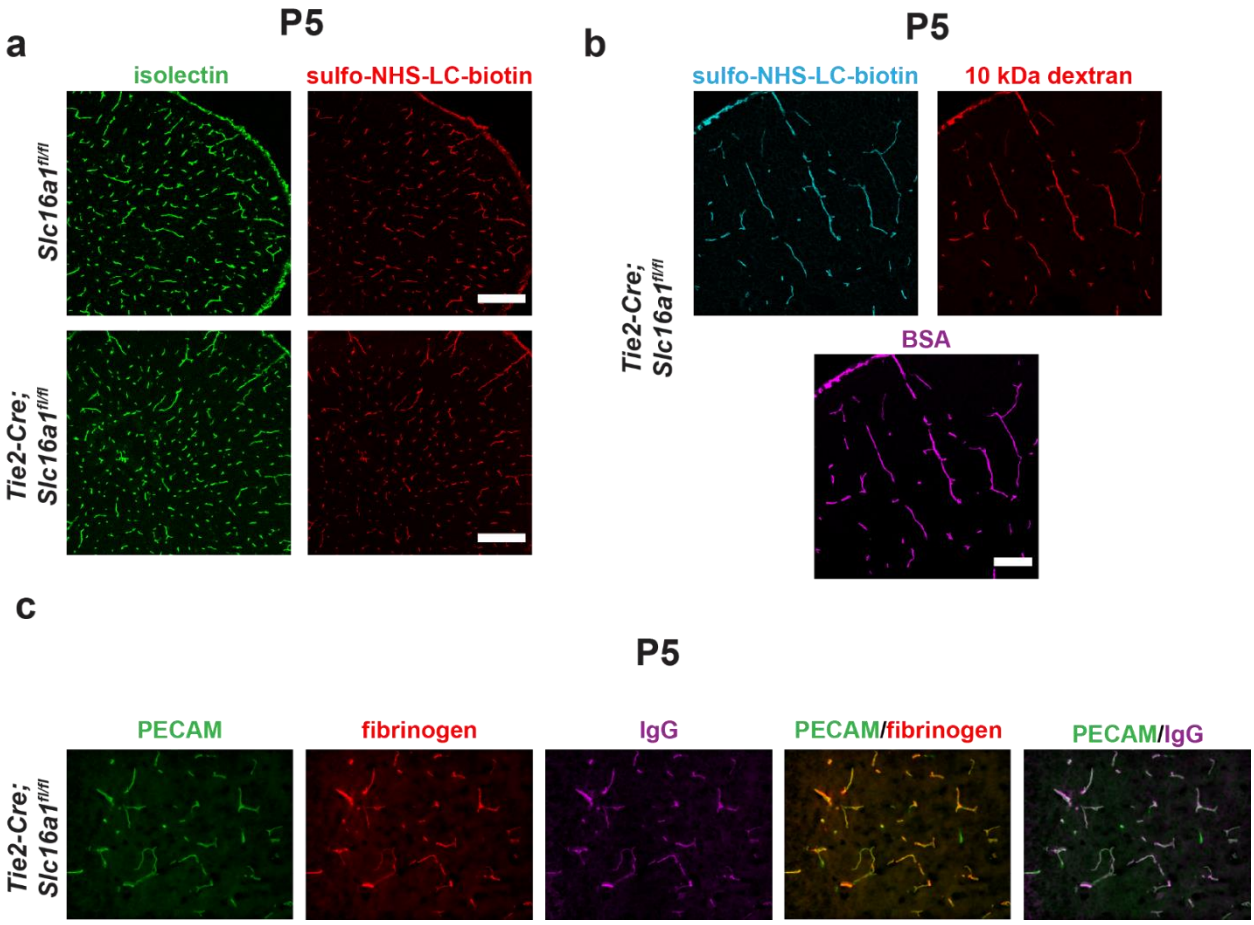

Figure 5.1. Endothelial-specific deletion of MCT1 (*Slc16a1*) does not alter BBB integrity. Immunofluorescence images of cortical brain sections in P5 control and LAT1 cKO animals demonstrating that BBB permeability to sulfo-NHS-LC-biotin (557 Da) **(a)**, 10 kDa dextran **(b)**, bovine serum albumin (BSA, 67 kDa, **b**), IgG (150 kDa) **(c)**, and fibrinogen (340 kDa) **(c)** are unaltered in mutant animals. Isolectin and PECAM are used as vessel counterstains. Scale bars: 100 µm.

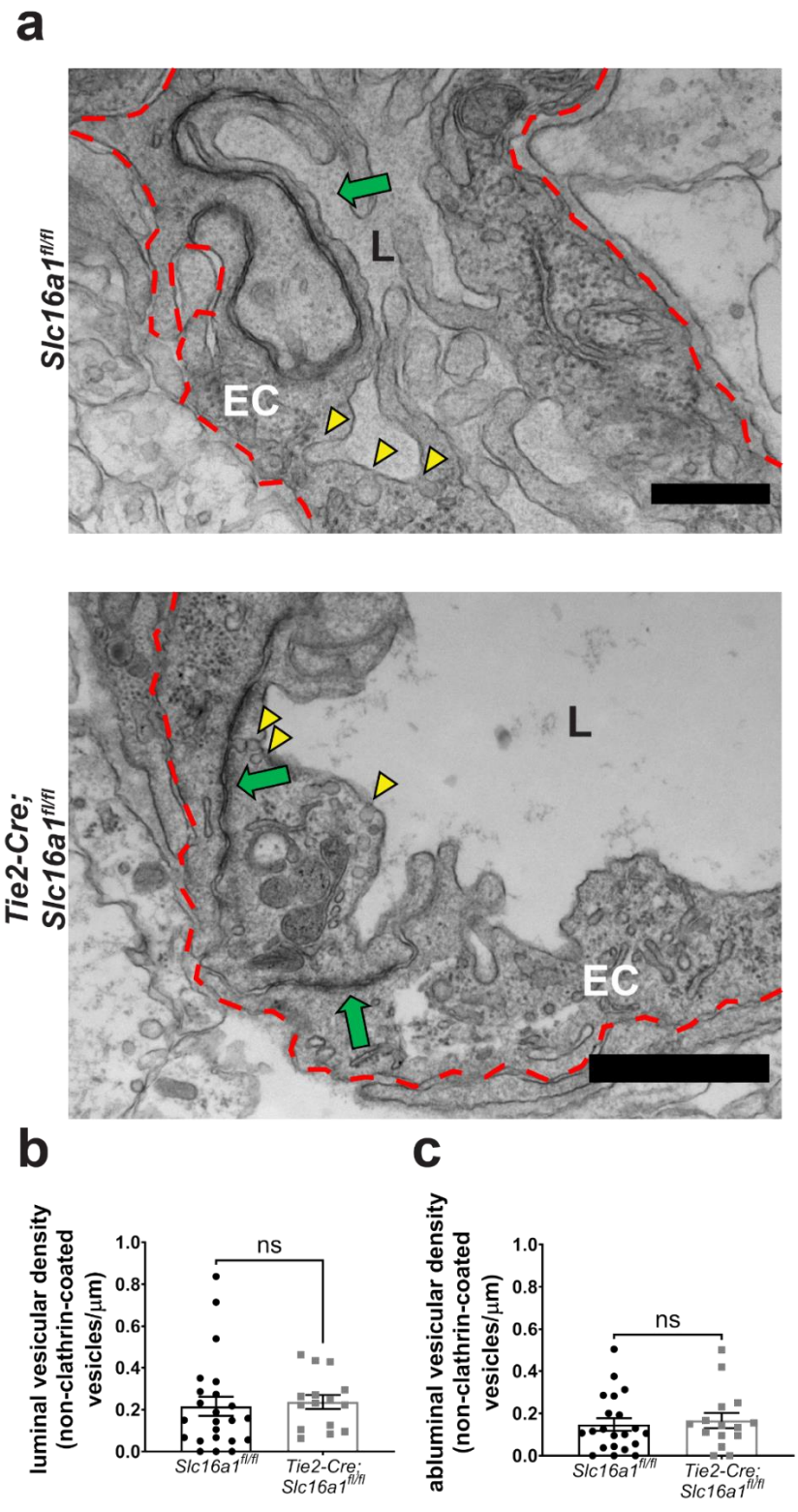

Figure 5.2. Endothelial-specific deletion of MCT1 (*Slc16a1*) does not alter brain endothelial cell ultrastructural properties. (a) Representative electron micrographs of cortical ECs in

Figure 5.2 (Continued)

control and MCT1 cKO P5 animals displaying non-clathrin-coated vesicles (yellow arrowheads) and TJs with normal ultrastructure and 'kissing points' (green arrows). Red dashed line outlines the endothelial abluminal membrane. EC = endothelial cell, L = lumen. (Scale bars: 500 nm) Quantification of luminal **(b)** and abluminal **(c)** non-clathrin-coated vesicular density between control and MCT1 cKO animals shows no significant difference (data are mean ± SEM, n=2 animals per genotype, individual data points are vesicular density values for individual blood vessels). ns = not significant, unpaired t-test

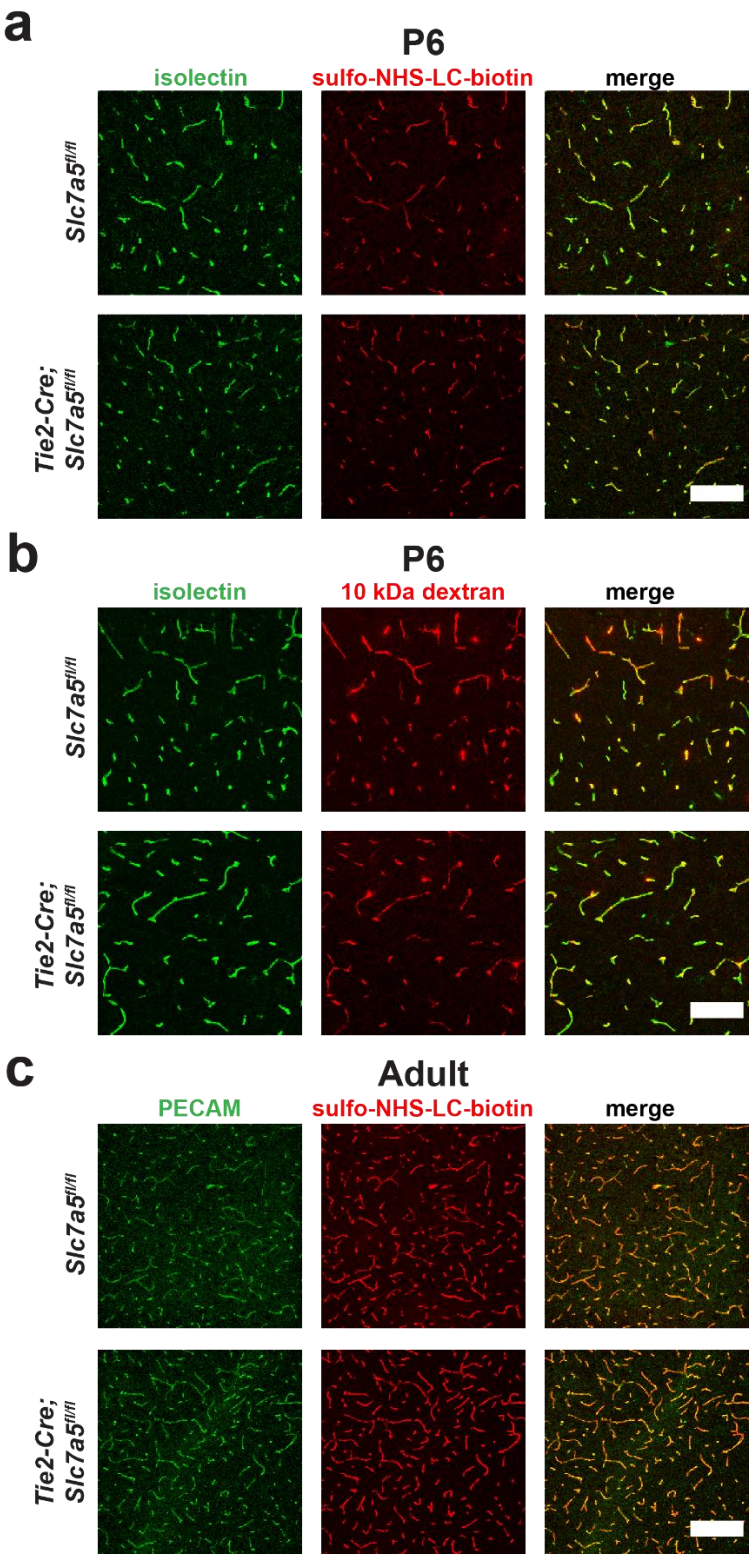

Figure 5.3. Endothelial-specific loss of LAT1 (*Slc7a5*) does not alter BBB integrity.

Immunofluorescence images of sulfo-NHS-LC-biotin **(a** and **c)** and 10 kDa dextran **(b)** confined

Figure 5.3 (Continued)

within the brain vasculature (isolectin or PECAM) of P6 **(a** and **b)** or adult **(c)** control and LAT1 cKO animals, demonstrating that *Slc7a5* (LAT1) is not required for BBB integrity. Scale bars: 100 μm.

CHAPTER 6

Conclusions and Outlook

The goal of my thesis work is to identify novel mechanisms of adult BBB maintenance. In my work, we provide novel insights into the role of the canonical Wnt signaling pathway in maintaining adult BBB integrity. First, we show that canonical Wnt signaling in the adult brain vasculature maintains BBB integrity by suppressing transcytosis. Second, we develop and optimize tools for evaluating TJ permeability, showing that acute attenuation of canonical Wnt signaling in the adult brain vasculature does not affect TJ permeability to molecules as small as 1.9 kDa. Lastly, we investigate the roles of two highly expressed endothelial nutrient transporters – MCT1 (*Slc16a1*) and LAT1 (*Slc7a5*) – in regulating BBB integrity and find that both are dispensable under physiological conditions.

6.1. Spatiotemporal Heterogeneity in Canonical Wnt Signaling Regulation of the Adult Blood-Brain Barrier

One striking phenotype we observed in mutant animals – with an acute attenuation of canonical Wnt signaling in adult brain ECs – was a marked heterogeneity in canonical Wnt target gene expression. Whereas mutants (*Cdh5-Cre^{ERT2};Ctnnb1$^{fl/fl}$*) displayed a moderate decrease in CLDN5 levels (**Figure 4.7**) and a severe reduction in MFSD2A levels (**Figure 3.6**), there was only sparse expression of the fenestral diaphragm-associated protein PLVAP, while GLUT1 levels were unaltered (**Figure 4.8**). In addition to differences in the magnitude of expression changes, there were also differences in the spatial distribution of Wnt target gene expression. Whereas MFSD2A downregulation was present throughout the brain vasculature, expression of PLVAP was limited to specific regions, including the molecular layer of the cerebellum (**Figure 4.8**) and subsets of the olfactory bulb and hippocampal vasculature (data not shown).

There are multiple potential explanations for these results. One, these differences may reflect a variable kinetic response to canonical Wnt signaling. For example, in contrast to previous studies (Cullen *et al.*, 2011; Daneman *et al.*, 2009; Kuhnert *et al.*, 2010; Stenman *et al.*, 2008; Wang *et al.*, 2018; Wang *et al.*, 2012; Wang *et al.*, 2019), GLUT1 expression was unaltered by attenuated canonical Wnt signaling in our mutant mice. This may reflect a slow turnover rate of GLUT1, in which case it would take longer to observe a decrease in GLUT1 levels. In contrast, proteins encoded by other Wnt target genes, like CLDN5, may have a faster turnover rate, facilitating an appreciable and measurable decrease in CLDN5 levels within the experimental time frame.

It is also worth noting that most of the previous studies observing changes in GLUT1 levels utilized null mutants of canonical Wnt pathway components, which may explain the dramatic loss of GLUT1. Even for the study that performed an acute, EC-specific genetic manipulation and observed altered GLUT1 expression, mice were observed 3 or more weeks after tamoxifen administration at P8-11. In contrast, we administer tamoxifen for five consecutive days in sexually mature adult mice (P56-70) and observe them 1 week after the first injection. Conditional, EC-specific deletion of the genes encoding GLUT1 and CLDN5 in adult mice would help resolve this conundrum by establishing the turnover rates of these proteins in the adult brain vasculature.

Another possible explanation of differences in canonical Wnt target gene expression is a region-dependent differential sensitivity to canonical Wnt signaling. This hypothesis is supported by the fact that although cortical and cerebellar endothelial nuclei had virtually identical decreases in LEF1 levels in mutant mice (**Figure 3.2**), they had drastically different levels of BBB leakage (**Figure 3.4**). Interestingly, this phenotype, with the strongest BBB leakage in the

cerebellum and olfactory bulbs, mirrors earlier studies of global or EC-specific KO of the Wnt receptor FZD4, which resulted in selective BBB leakage in these regions (Wang *et al.*, 2012; Zhou *et al.*, 2014).

While BBB leakage in our mutant mice was strongest in but not selective to these regions (**Figure 3.4**), the general pattern of severity is similar. In the case of *Fzd4* mutants, one potential explanation of the regional selectivity is that other Frizzled receptors expressed in brain ECs (e.g. *Fzd6*), are able to compensate for the loss of FZD4, thereby preserving canonical Wnt signaling and preventing BBB leakage in these regions (e.g. cortex). However, in our studies, we directly target the central transcriptional mediator β-catenin, preventing compensation from any upstream components of the pathway. Therefore, likely explanations of the differential sensitivity observed in our mutants include differences in transcription factor networks downstream of β-catenin/LEF1 (e.g. SOX17, ZIC3, FOXQ1) between different brain regions or β-catenin-independent pathways of BBB gene regulation in different brain regions. Lending credence to this latter hypothesis, a recent study demonstrated a role of Notch in regulating GLUT1 expression (Veys *et al.*, 2020). Thus, vascular GLUT1 expression may be regulated by β-catenin-independent mechanisms once mice reach adulthood.

Another potential explanation of the inter- and intraregional heterogeneity in canonical Wnt target gene expression is different regulatory modes for different genes (e.g. transcriptional vs. post-translational). This is particularly relevant for MFSD2A, which was robustly downregulated across the brain vasculature in mutant mice (**Figure 3.6**). While there is very strong evidence for canonical Wnt signaling regulation of MFSD2A at the genetic and transcriptional level (Chen *et al.*, 2012; Schafer *et al.*, 2009; Wang *et al.*, 2019), a recent study has uncovered a post-translational mode of regulation involving degradation of MFSD2A by the

E3 ubiquitin ligase NEDD-4 (Cui et al., 2021). This mode of regulation may explain the rapid loss of MFSD2A in mutant mice beginning as early as 3 days after initial Cre induction (**Figure 3.6**). To distinguish between these modes of regulation, we could perform quantitative PCR to determine if *Mfsd2a* mRNA is reduced in mutant mice and if this reduction precedes loss of MFSD2A protein. We could also determine if NEDD-4 expression is increased in mutant mice and if this precedes loss of MFSD2A protein or *Mfsd2a* mRNA.

6.2. Canonical Wnt Signaling Regulation of Transcytosis

In our investigations of canonical Wnt signaling regulation of brain EC subcellular properties, we provide strong evidence that the pathway suppresses transcytosis in adulthood. Using mutant mice in which canonical Wnt signaling is acutely attenuated in adult brain ECs, we first show that there is a significant upregulation of HRP-filled vesicles (**Figure 3.5**), which is indicative of increased vesicle formation and endocytosis. Second, we show that there is accumulation of HRP in the basement membrane in mutant mice (**Figure 3.5**), which indicates that HRP does not just accumulate within brain ECs but is able to traverse the endothelium. While this finding provided further evidence of increased transcytosis, it did not rule out a potential contribution of TJs to HRP accumulation in the basement membrane.

Importantly, we also showed that 100% of TJs observed in mutant brain ECs were impermeable to HRP (**Figure 3.5**). This final result ruled out a contribution of TJs and definitively showed that transcytosis was the sole driver of HRP leakage across the BBB in mutant mice. Given the significantly larger molecular weight of the endogenous serum protein IgG, which was also demonstrated to leak across the BBB (**Figure 3.3** and **Figure 3.4**), these results also provided indirect evidence that IgG leakage in mutant mice was also due to increased

transcytosis. Interestingly, a recent study of endogenous IgG trafficking at the BBB linked brain EC IgG to endosomes (Villasenor et al., 2016).

In mutant mice (*Cdh5-Cre^{ERT2};Ctnnb1$^{fl/fl}$*), we observed HRP-filled vesicles with a variety of morphologies, including those with the classical omega-shaped morphology of caveolae, larger vesicles reminiscent of clathrin-coated vesicles, and tubular vesicles (**Figure 3.5**). While the molecular markers of the HRP-filled vesicles are not clear, we can nonetheless form hypotheses about their identities and functions.

First, we observed HRP-filled vesicles that are reminiscent of caveolae. This finding is not unexpected given the robust loss of MFSD2A in mutant mice (**Figure 3.6**) and the established role of MFSD2A in mediating suppression of caveolae-dependent transcytosis (Andreone *et al.*, 2017). To determine the molecular identity of these vesicles, we can perform immuno-electron microscopy (immuno-EM) to detect caveolin-1 (CAV1), a protein that coats caveolae and serves as a molecular marker for these vesicles. One of the challenges of immuno-EM is that antigen labeling can be inefficient (Skepper, 2000), which would result in an undercount of caveolae vesicles. However, an advantage of this method is that luminal, abluminal, and cytoplasmic vesicles can all be readily identified as CAV1^{+} and bona fide caveolae. Alternatively, luminal and abluminal membrane-bound caveolae may be quantified, relying solely on the stereotyped morphology of caveolae for identification. While this method has the disadvantage of not capturing cytoplasmic caveolae – due the difficulties of disambiguating cytoplasmic caveolae from other types of cytoplasmic vesicles – it has the advantage of not undercounting membrane-bound caveolae.

Because CAV1 is required for caveolae formation and MFSD2A is a known suppressor of caveolae formation, we have a good genetic handle on testing the hypothesis that caveolae

vesicles functionally contribute to BBB leakage in canonical Wnt signaling-deficient brain ECs. In our studies, we opted to selectively and acutely overexpress MFSD2A in mutant ECs to prevent the loss of MFSD2A observed in mutant mice. Strikingly, this approach was not sufficient to rescue HRP or IgG leakage (**Figure 3.7**), which raises multiple non-mutually exclusive possibilities.

One, the non-caveolae HRP-filled vesicles observed in mutant mice (**Figure 3.5**) contribute functionally to BBB leakage to such a degree that reducing caveolae vesicles does not affect BBB leakage. Second, a more technical explanation would be that despite the rapid Cre-dependent overexpression of MFSD2A as soon as 24 hours following initial Cre induction (data not shown), MFSD2A was not able to robustly suppress caveolae within the time frame observed. To evaluate the first possibility, we can quantify the proportion of HRP-filled vesicles that did not display the stereotyped omega-shaped flask morphology of caveolae. This would give us an idea of the abundance and potential functional contribution of non-caveolae vesicles to HRP leakage. To evaluate the second possibility, we can quantify membrane-bound luminal and abluminal caveolae across control, mutant, and MFSD2A-overexpressing mutant cerebellar ECs.

Alternative approaches for directly testing the contribution of caveolae to BBB leakage in mutant mice is to alter caveolae abundance. One way to do this is to cross mutant mice (*Cdh5-Cre^{ERT2};Ctnnb1$^{fl/fl}$*) to *Cav1$^{-/-}$* mice, the latter of which have a complete ablation of caveolae. This method has the advantage of completely removing the functional contribution of caveolae to BBB leakage in mutant mice. However, because it is a global knockout mouse, developmental abnormalities in the vasculature (Murata et al., 2007; Razani et al., 2001) may confound interpretations of leakage and ultrastructural phenotypes. Another method is to cross mutant

mice to *Cav1*$^{fl/fl}$ mice, which would result in an acute and EC-specific loss of CAV1 and resultant reduction in caveolae. This method has the advantage of avoiding developmental confounds but has the technical challenge of being able to achieve a sufficient loss of CAV1 and reduction in caveolae within the experimental time frame.

In addition to caveolae, we also observed larger HRP-filled vesicles in mutant mice that were reminiscent of clathrin-coated vesicles. To determine if these were indeed clathrin-coated vesicles, we could perform immuno-EM to detect clathrin. One disadvantage of this method is that the clathrin coat is removed from these vesicles upon dynamin-mediated pinching off. Thus, immuno-EM would only be able to label membrane-bound vesicles and likely would not be able to identify cytoplasmic vesicles that were clathrin-coated during their formation. Alternatively, due to their electron-dense clathrin coat, membrane-bound clathrin vesicles may also be identified by their stereotyped morphology. Overall, a disadvantage of these two methods, which don't employ electron-dense tracers, is that among the clathrin-coated vesicles, it is unclear which ones contribute functionally to BBB leakage by carrying HRP.

A third type of vesicle observed in mutant mice were tubular vesicles (**Figure 3.5**). These vesicles displayed a variety of morphologies, including different shapes and lengths, and also formed tubular networks with neighboring vesicles. Unlike caveolae and clathrin-coated vesicles, these vesicles could have a wide variety of molecular markers, including flotillin, CDC42, and ARF6 (Mayor et al., 2014). In addition, they could be associated with sorting or trafficking endosomes, which are distinguished by different Rab proteins and subcellular localizations (Villasenor *et al.*, 2016; Villasenor et al., 2017). Thus, testing the functional contribution of these vesicles to BBB leakage in mutant mice would be a lot more difficult than doing so for caveolae or clathrin-coated vesicles. Another open question is the relationship between these vesicles and

caveolae and clathrin vesicles (i.e. whether caveolae and clathrin vesicles serve as precursors for these vesicles).

6.3. Tool Development for Assessing Blood-Brain Barrier Subcellular Properties

Our work, in addition to highlighting the functional significance of transcytosis in regulating BBB integrity downstream of canonical Wnt signaling, also illuminates the need for tool development for assessing BBB subcellular properties. This is of particular importance with regard to evaluating TJ permeability, as discussed in Chapter 4. Existing methods, like the current standard of HRP injection in the blood circulation and subsequent observation at the ultrastructural level, are not sensitive enough to detect subtle alterations in TJ permeability due to the large molecular weight of tracers. Other tracers that possess the chemical properties to be more sensitive, such as lanthanum chloride (Li et al., 2021) or biotin ethylenediamine (**Figure 4.3**), are hampered by technical limitations or lack of robust, reproducible, and high throughout experimental conditions for tracer detection. Developing a robust EM-compatible tracer to evaluate TJ permeability will have an immense impact on the BBB field by enabling detailed mechanistic studies of the effects of established and novel BBB-regulating genes on TJs vs. transcytosis.

Another limitation of transmission EM is that the ultrathin sections used for imaging only capture a very small "2D" snapshot of ECs, which limits the amount of subcellular information that can be extracted from tissue sections. Recent developments in 3D reconstruction of electron micrographs (Phelps et al., 2021) present an opportunity to enhance our understanding of brain EC subcellular properties by enabling a 3D visualization of subcellular architecture, including the properties most relevant to barrier function, TJs and vesicular trafficking. For example, some studies (Daneman *et al.*, 2010b; Tao-Cheng *et al.*, 1987) have made claims about particular TJ

phenotypes (e.g. TJ length) whose measurement can be affected by the angle at which EC cross-sections are cut, and would be best studied and validated in 3D images as opposed to 2D sections. In addition, 3D reconstructions would enable a thorough characterization of vesicular trafficking by allowing for better visualization of vesicular networks, subcellular localization of vesicles, and identification of distinct vesicular morphologies. For example, in considering the variety of vesicular morphologies observed in Wnt signaling-deficient brain ECs (**Figure 3.5**), a 3D reconstruction would aid in a clear classification and quantification of tubular vesicles by length, volume, and shape.

Super-resolution microscopy – and notably STED microscopy and expansion microscopy (Chozinski et al., 2016) – also holds a lot of promise by facilitating the visualization of EC subcellular puncta that correspond to individual or neighboring vesicles (Villasenor *et al.*, 2017). These techniques are particularly powerful because they can be utilized to image fluorescent tracers and multiple vesicular markers within the same tissue specimen, enabling identification of molecular markers associated with the transport of specific tracers and cargoes within and across brain ECs. This technique could accelerate the identification of novel transcytosis pathways at the BBB by allowing for multiplexed screening of vesicular markers and compartments, circumventing some of the technical challenges of immuno EM.

6.4. Assessing the Functional Role of Nutrient Transporters at the Blood-Brain Barrier

Overall, we show that neither MCT1 nor LAT1 are required for BBB integrity, despite being highly expressed and highly enriched in brain ECs. While we have ruled out a role for these nutrient transporters in regulating BBB integrity, there are other properties of the BBB that they may regulate. Notably, we did not evaluate expression of brain EC leukocyte adhesion molecules in MCT1 cKO and LAT1 cKO animals. In addition, we did not rule out involvement

in brain angiogenesis, which has been reported for the nutrient transporter GLUT1 (Tang *et al.*, 2021; Veys *et al.*, 2020).

Other potential roles of these nutrient transporters could include regulation of brain EC, neuronal, or astrocyte metabolism. Specifically, loss of MCT1, which transports lactate, pyruvate, and ketone bodies, could alter the levels of these metabolites in ECs or the brain parenchyma, resulting in altered metabolism under baseline conditions or under conditions of altered nutrient availability, such as starvation (Gjedde and Crone, 1975; Pollay and Stevens, 1980). This could also be especially impactful under conditions in which the brain increases transport of these substrates, such as early postnatal development, when suckling pups upregulate MCT1 to accommodate energy accretion from ketone-rich milk (Baud et al., 2003; Leino et al., 1999; Leino et al., 2001; Vannucci and Simpson, 2003). While the metabolic constituents and environment of brain ECs *in vivo* remain largely unknown due to limitations of *in vitro* studies (Doddaballapur et al., 2015; Schoors et al., 2014; Veys *et al.*, 2020) – owing to the rapid de-differentiation of brain ECs in culture (Sabbagh and Nathans, 2020) – MCT1 cKO and LAT1 cKO could serve as useful tools for perturbing brain EC metabolism once it is characterized under baseline conditions.

Because many nutrient transporters are largely driven by diffusion gradients created by energy demands and consumption of the brain parenchyma, it is unclear to what degree their substrates pass through brain ECs to reach the parenchyma versus being incorporated into and consumed by brain ECs themselves. For LAT1, a previous study provides evidence for its importance in the brain parenchyma. Specifically, LAT1 cKO mice display motor delay and autism-related phenotypes, which is attributed to reduced levels of branched-chain amino acids in the brain and resultant abnormal mRNA translation (Tarlungeanu *et al.*, 2016). Whether brain

ECs also have these phenotypes is unclear. However, there is certainly precedent for nutrient transporters playing a dual role in delivering substrates to ECs in addition to the parenchyma.

This is well-demonstrated by MFSD2A, which is a transporter for long-chain fatty acid–containing lysophosphatidylcholine lipid species, notably those containing docosahexaenoic acid (DHA) (Nguyen *et al.*, 2014). *Mfsd2a*$^{-/-}$ mice have a BBB leakage phenotype due to the increased formation of caveolae vesicles, which results from a deficiency of DHA-containing lipid species in EC plasma membranes (Andreone *et al.*, 2017). In addition, *Mfsd2a*$^{-/-}$ mice display microcephaly, which results from a deficiency of DHA-containing lipid species in the brain parenchyma, affecting neuronal growth and development (Andreone *et al.*, 2017; Nguyen *et al.*, 2014). Thus, nutrient transporters may play an important role in not only the physiology and function of the parenchyma but also the brain ECs that express them. In the case of MFSD2A, its biological functions in brain ECs and the brain parenchyma differ. However, for other nutrient transporters, there may be shared biological functions of substrates between different cell types.

REFERENCES

Aird, W.C. (2007a). Phenotypic heterogeneity of the endothelium: I. Structure, function, and mechanisms. Circ Res *100*, 158-173. 10.1161/01.RES.0000255691.76142.4a.

Aird, W.C. (2007b). Phenotypic heterogeneity of the endothelium: II. Representative vascular beds. Circ Res *100*, 174-190. 10.1161/01.RES.0000255690.03436.ae.

Andreone, B.J., Chow, B.W., Tata, A., Lacoste, B., Ben-Zvi, A., Bullock, K., Deik, A.A., Ginty, D.D., Clish, C.B., and Gu, C. (2017). Blood-Brain Barrier Permeability Is Regulated by Lipid Transport-Dependent Suppression of Caveolae-Mediated Transcytosis. Neuron *94*, 581-594 e585. 10.1016/j.neuron.2017.03.043.

Andreone, B.J., Lacoste, B., and Gu, C. (2015). Neuronal and vascular interactions. Annu Rev Neurosci *38*, 25-46. 10.1146/annurev-neuro-071714-033835.

Armulik, A., Genove, G., Mae, M., Nisancioglu, M.H., Wallgard, E., Niaudet, C., He, L., Norlin, J., Lindblom, P., Strittmatter, K., et al. (2010). Pericytes regulate the blood-brain barrier. Nature *468*, 557-561. 10.1038/nature09522.

Banks, W.A., Reed, M.J., Logsdon, A.F., Rhea, E.M., and Erickson, M.A. (2021). Healthy aging and the blood-brain barrier. Nat Aging *1*, 243-254. 10.1038/s43587-021-00043-5.

Baud, O., Fayol, L., Gressens, P., Pellerin, L., Magistretti, P., Evrard, P., and Verney, C. (2003). Perinatal and early postnatal changes in the expression of monocarboxylate transporters MCT1 and MCT2 in the rat forebrain. J Comp Neurol *465*, 445-454. 10.1002/cne.10853.

Bell, R.D., Winkler, E.A., Sagare, A.P., Singh, I., LaRue, B., Deane, R., and Zlokovic, B.V. (2010). Pericytes control key neurovascular functions and neuronal phenotype in the adult brain and during brain aging. Neuron *68*, 409-427. 10.1016/j.neuron.2010.09.043.

Bell, R.D., Winkler, E.A., Singh, I., Sagare, A.P., Deane, R., Wu, Z., Holtzman, D.M., Betsholtz, C., Armulik, A., Sallstrom, J., et al. (2012). Apolipoprotein E controls cerebrovascular integrity via cyclophilin A. Nature *485*, 512-516. 10.1038/nature11087.

Ben-Zvi, A., Lacoste, B., Kur, E., Andreone, B.J., Mayshar, Y., Yan, H., and Gu, C. (2014). Mfsd2a is critical for the formation and function of the blood-brain barrier. Nature *509*, 507-511. 10.1038/nature13324.

Ben-Zvi, A., and Liebner, S. (2021). Developmental regulation of barrier- and non-barrier blood vessels in the CNS. J Intern Med. 10.1111/joim.13263.

Brault, V., Moore, R., Kutsch, S., Ishibashi, M., Rowitch, D.H., McMahon, A.P., Sommer, L., Boussadia, O., and Kemler, R. (2001). Inactivation of the beta-catenin gene by Wnt1-Cre-mediated deletion results in dramatic brain malformation and failure of craniofacial development. Development *128*, 1253-1264.

Campbell, M., Hanrahan, F., Gobbo, O.L., Kelly, M.E., Kiang, A.S., Humphries, M.M., Nguyen, A.T., Ozaki, E., Keaney, J., Blau, C.W., et al. (2012). Targeted suppression of claudin-5 decreases cerebral oedema and improves cognitive outcome following traumatic brain injury. Nat Commun *3*, 849. 10.1038/ncomms1852.

Campos-Bedolla, P., Walter, F.R., Veszelka, S., and Deli, M.A. (2014). Role of the blood-brain barrier in the nutrition of the central nervous system. Arch Med Res *45*, 610-638. 10.1016/j.arcmed.2014.11.018.

Castro Dias, M., Coisne, C., Baden, P., Enzmann, G., Garrett, L., Becker, L., Holter, S.M., German Mouse Clinic, C., Hrabe de Angelis, M., Deutsch, U., and Engelhardt, B. (2019a). Claudin-12 is not required for blood-brain barrier tight junction function. Fluids Barriers CNS *16*, 30. 10.1186/s12987-019-0150-9.

Castro Dias, M., Coisne, C., Lazarevic, I., Baden, P., Hata, M., Iwamoto, N., Francisco, D.M.F., Vanlandewijck, M., He, L., Baier, F.A., et al. (2019b). Claudin-3-deficient C57BL/6J mice display intact brain barriers. Sci Rep *9*, 203. 10.1038/s41598-018-36731-3.

Chang, J., Mancuso, M.R., Maier, C., Liang, X., Yuki, K., Yang, L., Kwong, J.W., Wang, J., Rao, V., Vallon, M., et al. (2017). Gpr124 is essential for blood-brain barrier integrity in central nervous system disease. Nat Med *23*, 450-460. 10.1038/nm.4309.

Chen, J., Stahl, A., Krah, N.M., Seaward, M.R., Joyal, J.S., Juan, A.M., Hatton, C.J., Aderman, C.M., Dennison, R.J., Willett, K.L., et al. (2012). Retinal expression of Wnt-pathway mediated genes in low-density lipoprotein receptor-related protein 5 (Lrp5) knockout mice. PLoS One *7*, e30203. 10.1371/journal.pone.0030203.

Cho, C., Smallwood, P.M., and Nathans, J. (2017). Reck and Gpr124 Are Essential Receptor Cofactors for Wnt7a/Wnt7b-Specific Signaling in Mammalian CNS Angiogenesis and Blood-Brain Barrier Regulation. Neuron *95*, 1221-1225. 10.1016/j.neuron.2017.08.032.

Chow, B.W., and Gu, C. (2015). The molecular constituents of the blood-brain barrier. Trends Neurosci *38*, 598-608. 10.1016/j.tins.2015.08.003.

Chow, B.W., and Gu, C. (2017). Gradual Suppression of Transcytosis Governs Functional Blood-Retinal Barrier Formation. Neuron *93*, 1325-1333 e1323. 10.1016/j.neuron.2017.02.043.

Chow, B.W., Nunez, V., Kaplan, L., Granger, A.J., Bistrong, K., Zucker, H.L., Kumar, P., Sabatini, B.L., and Gu, C. (2020). Caveolae in CNS arterioles mediate neurovascular coupling. Nature *579*, 106-110. 10.1038/s41586-020-2026-1.

Chozinski, T.J., Halpern, A.R., Okawa, H., Kim, H.J., Tremel, G.J., Wong, R.O., and Vaughan, J.C. (2016). Expansion microscopy with conventional antibodies and fluorescent proteins. Nat Methods *13*, 485-488. 10.1038/nmeth.3833.

Cui, Y., Wang, Y., Song, X., Ning, H., Zhang, Y., Teng, Y., Wang, J., and Yang, X. (2021). Brain endothelial PTEN/AKT/NEDD4-2/MFSD2A axis regulates blood-brain barrier permeability. Cell Rep *36*, 109327. 10.1016/j.celrep.2021.109327.

Cullen, M., Elzarrad, M.K., Seaman, S., Zudaire, E., Stevens, J., Yang, M.Y., Li, X., Chaudhary, A., Xu, L., Hilton, M.B., et al. (2011). GPR124, an orphan G protein-coupled receptor, is required for CNS-specific vascularization and establishment of the blood-brain barrier. Proc Natl Acad Sci U S A *108*, 5759-5764. 10.1073/pnas.1017192108.

Daneman, R., Agalliu, D., Zhou, L., Kuhnert, F., Kuo, C.J., and Barres, B.A. (2009). Wnt/beta-catenin signaling is required for CNS, but not non-CNS, angiogenesis. Proc Natl Acad Sci U S A *106*, 641-646. 10.1073/pnas.0805165106.

Daneman, R., Zhou, L., Agalliu, D., Cahoy, J.D., Kaushal, A., and Barres, B.A. (2010a). The mouse blood-brain barrier transcriptome: a new resource for understanding the development and function of brain endothelial cells. PLoS One *5*, e13741. 10.1371/journal.pone.0013741.

Daneman, R., Zhou, L., Kebede, A.A., and Barres, B.A. (2010b). Pericytes are required for blood-brain barrier integrity during embryogenesis. Nature *468*, 562-566. 10.1038/nature09513.

Deane, R., Du Yan, S., Submamaryan, R.K., LaRue, B., Jovanovic, S., Hogg, E., Welch, D., Manness, L., Lin, C., Yu, J., et al. (2003). RAGE mediates amyloid-beta peptide transport across the blood-brain barrier and accumulation in brain. Nat Med *9*, 907-913. 10.1038/nm890.

Doddaballapur, A., Michalik, K.M., Manavski, Y., Lucas, T., Houtkooper, R.H., You, X., Chen, W., Zeiher, A.M., Potente, M., Dimmeler, S., and Boon, R.A. (2015). Laminar shear stress inhibits endothelial cell metabolism via KLF2-mediated repression of PFKFB3. Arterioscler Thromb Vasc Biol *35*, 137-145. 10.1161/ATVBAHA.114.304277.

Ek, C.J., Dziegielewska, K.M., Stolp, H., and Saunders, N.R. (2006). Functional effectiveness of the blood-brain barrier to small water-soluble molecules in developing and adult opossum (Monodelphis domestica). J Comp Neurol *496*, 13-26. 10.1002/cne.20885.

Elahy, M., Jackaman, C., Mamo, J.C., Lam, V., Dhaliwal, S.S., Giles, C., Nelson, D., and Takechi, R. (2015). Blood-brain barrier dysfunction developed during normal aging is associated with inflammation and loss of tight junctions but not with leukocyte recruitment. Immun Ageing *12*, 2. 10.1186/s12979-015-0029-9.

Gautam, J., Zhang, X., and Yao, Y. (2016). The role of pericytic laminin in blood brain barrier integrity maintenance. Sci Rep *6*, 36450. 10.1038/srep36450.

Gjedde, A., and Crone, C. (1975). Induction processes in blood-brain transfer of ketone bodies during starvation. Am J Physiol *229*, 1165-1169. 10.1152/ajplegacy.1975.229.5.1165.

Greene, C., Kealy, J., Humphries, M.M., Gong, Y., Hou, J., Hudson, N., Cassidy, L.M., Martiniano, R., Shashi, V., Hooper, S.R., et al. (2018). Dose-dependent expression of claudin-5 is a modifying factor in schizophrenia. Mol Psychiatry *23*, 2156-2166. 10.1038/mp.2017.156.

Haj-Yasein, N.N., Vindedal, G.F., Eilert-Olsen, M., Gundersen, G.A., Skare, O., Laake, P., Klungland, A., Thoren, A.E., Burkhardt, J.M., Ottersen, O.P., and Nagelhus, E.A. (2011). Glial-conditional deletion of aquaporin-4 (Aqp4) reduces blood-brain water uptake and confers barrier function on perivascular astrocyte endfeet. Proc Natl Acad Sci U S A *108*, 17815-17820. 10.1073/pnas.1110655108.

Halestrap, A.P., and Wilson, M.C. (2012). The monocarboxylate transporter family--role and regulation. IUBMB Life *64*, 109-119. 10.1002/iub.572.

He, L., Vanlandewijck, M., Mae, M.A., Andrae, J., Ando, K., Del Gaudio, F., Nahar, K., Lebouvier, T., Lavina, B., Gouveia, L., et al. (2018). Single-cell RNA sequencing of mouse brain and lung vascular and vessel-associated cell types. Sci Data *5*, 180160. 10.1038/sdata.2018.160.

Heithoff, B.P., George, K.K., Phares, A.N., Zuidhoek, I.A., Munoz-Ballester, C., and Robel, S. (2021). Astrocytes are necessary for blood-brain barrier maintenance in the adult mouse brain. Glia *69*, 436-472. 10.1002/glia.23908.

Hellstrom, M., Kalen, M., Lindahl, P., Abramsson, A., and Betsholtz, C. (1999). Role of PDGF-B and PDGFR-beta in recruitment of vascular smooth muscle cells and pericytes during embryonic blood vessel formation in the mouse. Development *126*, 3047-3055.

Jha, M.K., Lee, Y., Russell, K.A., Yang, F., Dastgheyb, R.M., Deme, P., Ament, X.H., Chen, W., Liu, Y., Guan, Y., et al. (2020). Monocarboxylate transporter 1 in Schwann cells contributes to maintenance of sensory nerve myelination during aging. Glia *68*, 161-177. 10.1002/glia.23710.

Junge, H.J., Yang, S., Burton, J.B., Paes, K., Shu, X., French, D.M., Costa, M., Rice, D.S., and Ye, W. (2009). TSPAN12 regulates retinal vascular development by promoting Norrin- but not Wnt-induced FZD4/beta-catenin signaling. Cell *139*, 299-311. 10.1016/j.cell.2009.07.048.

Kato, M., Patel, M.S., Levasseur, R., Lobov, I., Chang, B.H., Glass, D.A., 2nd, Hartmann, C., Li, L., Hwang, T.H., Brayton, C.F., et al. (2002). Cbfa1-independent decrease in osteoblast proliferation, osteopenia, and persistent embryonic eye vascularization in mice deficient in Lrp5, a Wnt coreceptor. J Cell Biol *157*, 303-314. 10.1083/jcb.200201089.

Katsuno, T., Umeda, K., Matsui, T., Hata, M., Tamura, A., Itoh, M., Takeuchi, K., Fujimori, T., Nabeshima, Y., Noda, T., et al. (2008). Deficiency of zonula occludens-1 causes embryonic lethal phenotype associated with defected yolk sac angiogenesis and apoptosis of embryonic cells. Mol Biol Cell *19*, 2465-2475. 10.1091/mbc.E07-12-1215.

Kisanuki, Y.Y., Hammer, R.E., Miyazaki, J., Williams, S.C., Richardson, J.A., and Yanagisawa, M. (2001). Tie2-Cre transgenic mice: a new model for endothelial cell-lineage analysis in vivo. Dev Biol *230*, 230-242. 10.1006/dbio.2000.0106.

Kiss, T., Nyul-Toth, A., Balasubramanian, P., Tarantini, S., Ahire, C., DelFavero, J., Yabluchanskiy, A., Csipo, T., Farkas, E., Wiley, G., et al. (2020). Single-cell RNA sequencing identifies senescent cerebromicrovascular endothelial cells in the aged mouse brain. Geroscience *42*, 429-444. 10.1007/s11357-020-00177-1.

Knowland, D., Arac, A., Sekiguchi, K.J., Hsu, M., Lutz, S.E., Perrino, J., Steinberg, G.K., Barres, B.A., Nimmerjahn, A., and Agalliu, D. (2014). Stepwise recruitment of transcellular and paracellular pathways underlies blood-brain barrier breakdown in stroke. Neuron *82*, 603-617. 10.1016/j.neuron.2014.03.003.

Kuhnert, F., Mancuso, M.R., Shamloo, A., Wang, H.T., Choksi, V., Florek, M., Su, H., Fruttiger, M., Young, W.L., Heilshorn, S.C., and Kuo, C.J. (2010). Essential regulation of CNS angiogenesis by the orphan G protein-coupled receptor GPR124. Science *330*, 985-989. 10.1126/science.1196554.

Langen, U.H., Ayloo, S., and Gu, C. (2019). Development and Cell Biology of the Blood-Brain Barrier. Annu Rev Cell Dev Biol *35*, 591-613. 10.1146/annurev-cellbio-100617-062608.

Leino, R.L., Gerhart, D.Z., and Drewes, L.R. (1999). Monocarboxylate transporter (MCT1) abundance in brains of suckling and adult rats: a quantitative electron microscopic immunogold study. Brain Res Dev Brain Res *113*, 47-54. 10.1016/s0165-3806(98)00188-6.

Leino, R.L., Gerhart, D.Z., Duelli, R., Enerson, B.E., and Drewes, L.R. (2001). Diet-induced ketosis increases monocarboxylate transporter (MCT1) levels in rat brain. Neurochem Int *38*, 519-527. 10.1016/s0197-0186(00)00102-9.

Li, X., Vemireddy, V., Cai, Q., Xiong, H., Kang, P., Li, X., Giannotta, M., Hayenga, H.N., Pan, E., Sirsi, S.R., et al. (2021). Reversibly Modulating the Blood-Brain Barrier by Laser Stimulation of Molecular-Targeted Nanoparticles. Nano Lett. 10.1021/acs.nanolett.1c02996.

Liebner, S., Corada, M., Bangsow, T., Babbage, J., Taddei, A., Czupalla, C.J., Reis, M., Felici, A., Wolburg, H., Fruttiger, M., et al. (2008). Wnt/beta-catenin signaling controls development of the blood-brain barrier. J Cell Biol *183*, 409-417. 10.1083/jcb.200806024.

Lohrke, J., Frisk, A.L., Frenzel, T., Schockel, L., Rosenbruch, M., Jost, G., Lenhard, D.C., Sieber, M.A., Nischwitz, V., Kuppers, A., and Pietsch, H. (2017). Histology and Gadolinium Distribution in the Rodent Brain After the Administration of Cumulative High Doses of Linear and Macrocyclic Gadolinium-Based Contrast Agents. Invest Radiol *52*, 324-333. 10.1097/RLI.0000000000000344.

Luhmann, U.F., Lin, J., Acar, N., Lammel, S., Feil, S., Grimm, C., Seeliger, M.W., Hammes, H.P., and Berger, W. (2005). Role of the Norrie disease pseudoglioma gene in sprouting

angiogenesis during development of the retinal vasculature. Invest Ophthalmol Vis Sci *46*, 3372-3382. 10.1167/iovs.05-0174.

Mancuso, M.R., Kuhnert, F., and Kuo, C.J. (2008). Developmental angiogenesis of the central nervous system. Lymphat Res Biol *6*, 173-180. 10.1089/lrb.2008.1014.

Manley, G.T., Fujimura, M., Ma, T., Noshita, N., Filiz, F., Bollen, A.W., Chan, P., and Verkman, A.S. (2000). Aquaporin-4 deletion in mice reduces brain edema after acute water intoxication and ischemic stroke. Nat Med *6*, 159-163. 10.1038/72256.

Martowicz, A., Trusohamn, M., Jensen, N., Wisniewska-Kruk, J., Corada, M., Ning, F.C., Kele, J., Dejana, E., and Nyqvist, D. (2019). Endothelial beta-Catenin Signaling Supports Postnatal Brain and Retinal Angiogenesis by Promoting Sprouting, Tip Cell Formation, and VEGFR (Vascular Endothelial Growth Factor Receptor) 2 Expression. Arterioscler Thromb Vasc Biol *39*, 2273-2288. 10.1161/ATVBAHA.119.312749.

Mastroberardino, L., Spindler, B., Pfeiffer, R., Skelly, P.J., Loffing, J., Shoemaker, C.B., and Verrey, F. (1998). Amino-acid transport by heterodimers of 4F2hc/CD98 and members of a permease family. Nature *395*, 288-291. 10.1038/26246.

Mathiisen, T.M., Lehre, K.P., Danbolt, N.C., and Ottersen, O.P. (2010). The perivascular astroglial sheath provides a complete covering of the brain microvessels: an electron microscopic 3D reconstruction. Glia *58*, 1094-1103. 10.1002/glia.20990.

Mayor, S., Parton, R.G., and Donaldson, J.G. (2014). Clathrin-independent pathways of endocytosis. Cold Spring Harb Perspect Biol *6*. 10.1101/cshperspect.a016758.

Menard, C., Pfau, M.L., Hodes, G.E., Kana, V., Wang, V.X., Bouchard, S., Takahashi, A., Flanigan, M.E., Aleyasin, H., LeClair, K.B., et al. (2017). Social stress induces neurovascular pathology promoting depression. Nat Neurosci *20*, 1752-1760. 10.1038/s41593-017-0010-3.

Montagne, A., Nation, D.A., Sagare, A.P., Barisano, G., Sweeney, M.D., Chakhoyan, A., Pachicano, M., Joe, E., Nelson, A.R., D'Orazio, L.M., et al. (2020). APOE4 leads to blood-brain barrier dysfunction predicting cognitive decline. Nature *581*, 71-76. 10.1038/s41586-020-2247-3.

Muir, A.R., and Peters, A. (1962). Quintuple-layered membrane junctions at terminal bars between endothelial cells. J Cell Biol *12*, 443-448. 10.1083/jcb.12.2.443.

Munji, R.N., Soung, A.L., Weiner, G.A., Sohet, F., Semple, B.D., Trivedi, A., Gimlin, K., Kotoda, M., Korai, M., Aydin, S., et al. (2019). Profiling the mouse brain endothelial transcriptome in health and disease models reveals a core blood-brain barrier dysfunction module. Nat Neurosci *22*, 1892-1902. 10.1038/s41593-019-0497-x.

Murata, T., Lin, M.I., Huang, Y., Yu, J., Bauer, P.M., Giordano, F.J., and Sessa, W.C. (2007). Reexpression of caveolin-1 in endothelium rescues the vascular, cardiac, and pulmonary defects in global caveolin-1 knockout mice. J Exp Med *204*, 2373-2382. 10.1084/jem.20062340.

Napolitano, L., Scalise, M., Galluccio, M., Pochini, L., Albanese, L.M., and Indiveri, C. (2015). LAT1 is the transport competent unit of the LAT1/CD98 heterodimeric amino acid transporter. Int J Biochem Cell Biol *67*, 25-33. 10.1016/j.biocel.2015.08.004.

Nguyen, L.N., Ma, D., Shui, G., Wong, P., Cazenave-Gassiot, A., Zhang, X., Wenk, M.R., Goh, E.L., and Silver, D.L. (2014). Mfsd2a is a transporter for the essential omega-3 fatty acid docosahexaenoic acid. Nature *509*, 503-506. 10.1038/nature13241.

Nielsen, S., Nagelhus, E.A., Amiry-Moghaddam, M., Bourque, C., Agre, P., and Ottersen, O.P. (1997). Specialized membrane domains for water transport in glial cells: high-resolution immunogold cytochemistry of aquaporin-4 in rat brain. J Neurosci *17*, 171-180.

Nitta, T., Hata, M., Gotoh, S., Seo, Y., Sasaki, H., Hashimoto, N., Furuse, M., and Tsukita, S. (2003). Size-selective loosening of the blood-brain barrier in claudin-5-deficient mice. J Cell Biol *161*, 653-660. 10.1083/jcb.200302070.

Nusse, R., and Clevers, H. (2017). Wnt/beta-Catenin Signaling, Disease, and Emerging Therapeutic Modalities. Cell *169*, 985-999. 10.1016/j.cell.2017.05.016.

O'Brown, N.M., Megason, S.G., and Gu, C. (2019). Suppression of transcytosis regulates zebrafish blood-brain barrier function. Elife *8*. 10.7554/eLife.47326.

Oh, J., Takahashi, R., Kondo, S., Mizoguchi, A., Adachi, E., Sasahara, R.M., Nishimura, S., Imamura, Y., Kitayama, H., Alexander, D.B., et al. (2001). The membrane-anchored MMP inhibitor RECK is a key regulator of extracellular matrix integrity and angiogenesis. Cell *107*, 789-800. 10.1016/s0092-8674(01)00597-9.

Park, M.H., Lee, J.Y., Park, K.H., Jung, I.K., Kim, K.T., Lee, Y.S., Ryu, H.H., Jeong, Y., Kang, M., Schwaninger, M., et al. (2018). Vascular and Neurogenic Rejuvenation in Aging Mice by Modulation of ASM. Neuron *100*, 762. 10.1016/j.neuron.2018.10.038.

Pfeiffer, F., Schafer, J., Lyck, R., Makrides, V., Brunner, S., Schaeren-Wiemers, N., Deutsch, U., and Engelhardt, B. (2011). Claudin-1 induced sealing of blood-brain barrier tight junctions ameliorates chronic experimental autoimmune encephalomyelitis. Acta Neuropathol *122*, 601-614. 10.1007/s00401-011-0883-2.

Phelps, J.S., Hildebrand, D.G.C., Graham, B.J., Kuan, A.T., Thomas, L.A., Nguyen, T.M., Buhmann, J., Azevedo, A.W., Sustar, A., Agrawal, S., et al. (2021). Reconstruction of motor control circuits in adult Drosophila using automated transmission electron microscopy. Cell *184*, 759-774 e718. 10.1016/j.cell.2020.12.013.

Planutiene, M., Planutis, K., and Holcombe, R.F. (2011). Lymphoid enhancer-binding factor 1, a representative of vertebrate-specific Lef1/Tcf1 sub-family, is a Wnt-beta-catenin pathway target gene in human endothelial cells which regulates matrix metalloproteinase-2 expression and promotes endothelial cell invasion. Vasc Cell *3*, 28. 10.1186/2045-824X-3-28.

Pollay, M., and Stevens, F.A. (1980). Starvation-induced changes in transport of ketone bodies across the blood-brain barrier. J Neurosci Res *5*, 163-172. 10.1002/jnr.490050208.

Ransohoff, R.M., and Engelhardt, B. (2012). The anatomical and cellular basis of immune surveillance in the central nervous system. Nat Rev Immunol *12*, 623-635. 10.1038/nri3265.

Rasschaert, M., Emerit, A., Fretellier, N., Factor, C., Robert, P., Idee, J.M., and Corot, C. (2018a). Gadolinium Retention, Brain T1 Hyperintensity, and Endogenous Metals: A Comparative Study of Macrocyclic Versus Linear Gadolinium Chelates in Renally Sensitized Rats. Invest Radiol *53*, 328-337. 10.1097/RLI.0000000000000447.

Rasschaert, M., Schroeder, J.A., Wu, T.D., Marco, S., Emerit, A., Siegmund, H., Fischer, C., Fretellier, N., Idee, J.M., Corot, C., et al. (2018b). Multimodal Imaging Study of Gadolinium Presence in Rat Cerebellum: Differences Between Gd Chelates, Presence in the Virchow-Robin Space, Association With Lipofuscin, and Hypotheses About Distribution Pathway. Invest Radiol *53*, 518-528. 10.1097/RLI.0000000000000490.

Razani, B., Engelman, J.A., Wang, X.B., Schubert, W., Zhang, X.L., Marks, C.B., Macaluso, F., Russell, R.G., Li, M., Pestell, R.G., et al. (2001). Caveolin-1 null mice are viable but show evidence of hyperproliferative and vascular abnormalities. J Biol Chem *276*, 38121-38138. 10.1074/jbc.M105408200.

Reese, T.S., and Karnovsky, M.J. (1967). Fine structural localization of a blood-brain barrier to exogenous peroxidase. J Cell Biol *34*, 207-217. 10.1083/jcb.34.1.207.

Reis, M., and Liebner, S. (2013). Wnt signaling in the vasculature. Exp Cell Res *319*, 1317-1323. 10.1016/j.yexcr.2012.12.023.

Reyahi, A., Nik, A.M., Ghiami, M., Gritli-Linde, A., Ponten, F., Johansson, B.R., and Carlsson, P. (2015). Foxf2 Is Required for Brain Pericyte Differentiation and Development and Maintenance of the Blood-Brain Barrier. Dev Cell *34*, 19-32. 10.1016/j.devcel.2015.05.008.

Richter, M., Gottanka, J., May, C.A., Welge-Lussen, U., Berger, W., and Lutjen-Drecoll, E. (1998). Retinal vasculature changes in Norrie disease mice. Invest Ophthalmol Vis Sci *39*, 2450-2457.

Rossler, K., Neuchrist, C., Kitz, K., Scheiner, O., Kraft, D., and Lassmann, H. (1992). Expression of leucocyte adhesion molecules at the human blood-brain barrier (BBB). J Neurosci Res *31*, 365-374. 10.1002/jnr.490310219.

Sabbagh, M.F., Heng, J.S., Luo, C., Castanon, R.G., Nery, J.R., Rattner, A., Goff, L.A., Ecker, J.R., and Nathans, J. (2018). Transcriptional and epigenomic landscapes of CNS and non-CNS vascular endothelial cells. Elife *7*. 10.7554/eLife.36187.

Sabbagh, M.F., and Nathans, J. (2020). A genome-wide view of the de-differentiation of central nervous system endothelial cells in culture. Elife *9*. 10.7554/eLife.51276.

Sadeghian, H., Lacoste, B., Qin, T., Toussay, X., Rosa, R., Oka, F., Chung, D.Y., Takizawa, T., Gu, C., and Ayata, C. (2018). Spreading depolarizations trigger caveolin-1-dependent endothelial transcytosis. Ann Neurol *84*, 409-423. 10.1002/ana.25298.

Sagare, A.P., Bell, R.D., Zhao, Z., Ma, Q., Winkler, E.A., Ramanathan, A., and Zlokovic, B.V. (2013). Pericyte loss influences Alzheimer-like neurodegeneration in mice. Nat Commun *4*, 2932. 10.1038/ncomms3932.

Saitou, M., Furuse, M., Sasaki, H., Schulzke, J.D., Fromm, M., Takano, H., Noda, T., and Tsukita, S. (2000). Complex phenotype of mice lacking occludin, a component of tight junction strands. Mol Biol Cell *11*, 4131-4142. 10.1091/mbc.11.12.4131.

Schafer, N.F., Luhmann, U.F., Feil, S., and Berger, W. (2009). Differential gene expression in Ndph-knockout mice in retinal development. Invest Ophthalmol Vis Sci *50*, 906-916. 10.1167/iovs.08-1731.

Schoors, S., De Bock, K., Cantelmo, A.R., Georgiadou, M., Ghesquiere, B., Cauwenberghs, S., Kuchnio, A., Wong, B.W., Quaegebeur, A., Goveia, J., et al. (2014). Partial and transient reduction of glycolysis by PFKFB3 blockade reduces pathological angiogenesis. Cell Metab *19*, 37-48. 10.1016/j.cmet.2013.11.008.

Segarra, M., Aburto, M.R., Cop, F., Llao-Cid, C., Hartl, R., Damm, M., Bethani, I., Parrilla, M., Husainie, D., Schanzer, A., et al. (2018). Endothelial Dab1 signaling orchestrates neuro-glia-vessel communication in the central nervous system. Science *361*. 10.1126/science.aao2861.

Shibata, M., Yamada, S., Kumar, S.R., Calero, M., Bading, J., Frangione, B., Holtzman, D.M., Miller, C.A., Strickland, D.K., Ghiso, J., and Zlokovic, B.V. (2000). Clearance of Alzheimer's amyloid-ss(1-40) peptide from brain by LDL receptor-related protein-1 at the blood-brain barrier. J Clin Invest *106*, 1489-1499. 10.1172/JCI10498.

Skepper, J.N. (2000). Immunocytochemical strategies for electron microscopy: choice or compromise. J Microsc *199*, 1-36. 10.1046/j.1365-2818.2000.00704.x.

Sohet, F., Lin, C., Munji, R.N., Lee, S.Y., Ruderisch, N., Soung, A., Arnold, T.D., Derugin, N., Vexler, Z.S., Yen, F.T., and Daneman, R. (2015). LSR/angulin-1 is a tricellular tight junction protein involved in blood-brain barrier formation. J Cell Biol *208*, 703-711. 10.1083/jcb.201410131.

Sorensen, I., Adams, R.H., and Gossler, A. (2009). DLL1-mediated Notch activation regulates endothelial identity in mouse fetal arteries. Blood *113*, 5680-5688. 10.1182/blood-2008-08-174508.

Soto, I., Graham, L.C., Richter, H.J., Simeone, S.N., Radell, J.E., Grabowska, W., Funkhouser, W.K., Howell, M.C., and Howell, G.R. (2015). APOE Stabilization by Exercise Prevents Aging Neurovascular Dysfunction and Complement Induction. PLoS Biol *13*, e1002279. 10.1371/journal.pbio.1002279.

Srinivasan, B., Kolli, A.R., Esch, M.B., Abaci, H.E., Shuler, M.L., and Hickman, J.J. (2015). TEER measurement techniques for in vitro barrier model systems. J Lab Autom *20*, 107-126. 10.1177/2211068214561025.

Stahl, A., Connor, K.M., Sapieha, P., Chen, J., Dennison, R.J., Krah, N.M., Seaward, M.R., Willett, K.L., Aderman, C.M., Guerin, K.I., et al. (2010). The mouse retina as an angiogenesis model. Invest Ophthalmol Vis Sci *51*, 2813-2826. 10.1167/iovs.10-5176.

Stamatovic, S.M., Martinez-Revollar, G., Hu, A., Choi, J., Keep, R.F., and Andjelkovic, A.V. (2019). Decline in Sirtuin-1 expression and activity plays a critical role in blood-brain barrier permeability in aging. Neurobiol Dis *126*, 105-116. 10.1016/j.nbd.2018.09.006.

Stamos, J.L., and Weis, W.I. (2013). The beta-catenin destruction complex. Cold Spring Harb Perspect Biol *5*, a007898. 10.1101/cshperspect.a007898.

Stan, R.V., Kubitza, M., and Palade, G.E. (1999). PV-1 is a component of the fenestral and stomatal diaphragms in fenestrated endothelia. Proc Natl Acad Sci U S A *96*, 13203-13207. 10.1073/pnas.96.23.13203.

Stan, R.V., Tkachenko, E., and Niesman, I.R. (2004). PV1 is a key structural component for the formation of the stomatal and fenestral diaphragms. Mol Biol Cell *15*, 3615-3630. 10.1091/mbc.e03-08-0593.

Stenman, J.M., Rajagopal, J., Carroll, T.J., Ishibashi, M., McMahon, J., and McMahon, A.P. (2008). Canonical Wnt signaling regulates organ-specific assembly and differentiation of CNS vasculature. Science *322*, 1247-1250. 10.1126/science.1164594.

Sweeney, M.D., Sagare, A.P., and Zlokovic, B.V. (2018). Blood-brain barrier breakdown in Alzheimer disease and other neurodegenerative disorders. Nat Rev Neurol *14*, 133-150. 10.1038/nrneurol.2017.188.

Tam, S.J., Richmond, D.L., Kaminker, J.S., Modrusan, Z., Martin-McNulty, B., Cao, T.C., Weimer, R.M., Carano, R.A., van Bruggen, N., and Watts, R.J. (2012). Death receptors DR6 and TROY regulate brain vascular development. Dev Cell *22*, 403-417. 10.1016/j.devcel.2011.11.018.

Tang, M., Park, S.H., Petri, S., Yu, H., Rueda, C.B., Abel, E.D., Kim, C.Y., Hillman, E.M., Li, F., Lee, Y., et al. (2021). An early endothelial cell-specific requirement for Glut1 is revealed in Glut1 deficiency syndrome model mice. JCI Insight *6*. 10.1172/jci.insight.145789.

Tao-Cheng, J.H., Nagy, Z., and Brightman, M.W. (1987). Tight junctions of brain endothelium in vitro are enhanced by astroglia. J Neurosci *7*, 3293-3299.

Tarlungeanu, D.C., Deliu, E., Dotter, C.P., Kara, M., Janiesch, P.C., Scalise, M., Galluccio, M., Tesulov, M., Morelli, E., Sonmez, F.M., et al. (2016). Impaired Amino Acid Transport at the Blood Brain Barrier Is a Cause of Autism Spectrum Disorder. Cell *167*, 1481-1494 e1418. 10.1016/j.cell.2016.11.013.

Tran, K.A., Zhang, X., Predescu, D., Huang, X., Machado, R.F., Gothert, J.R., Malik, A.B., Valyi-Nagy, T., and Zhao, Y.Y. (2016). Endothelial beta-Catenin Signaling Is Required for Maintaining Adult Blood-Brain Barrier Integrity and Central Nervous System Homeostasis. Circulation *133*, 177-186. 10.1161/CIRCULATIONAHA.115.015982.

Valenta, T., Hausmann, G., and Basler, K. (2012). The many faces and functions of beta-catenin. EMBO J *31*, 2714-2736. 10.1038/emboj.2012.150.

Vanlandewijck, M., and Betsholtz, C. (2018). Single-Cell mRNA Sequencing of the Mouse Brain Vasculature. Methods Mol Biol *1846*, 309-324. 10.1007/978-1-4939-8712-2_21.

Vanlandewijck, M., He, L., Mae, M.A., Andrae, J., Ando, K., Del Gaudio, F., Nahar, K., Lebouvier, T., Lavina, B., Gouveia, L., et al. (2018). A molecular atlas of cell types and zonation in the brain vasculature. Nature *554*, 475-480. 10.1038/nature25739.

Vannucci, S.J., and Simpson, I.A. (2003). Developmental switch in brain nutrient transporter expression in the rat. Am J Physiol Endocrinol Metab *285*, E1127-1134. 10.1152/ajpendo.00187.2003.

Veys, K., Fan, Z., Ghobrial, M., Bouche, A., Garcia-Caballero, M., Vriens, K., Conchinha, N.V., Seuwen, A., Schlegel, F., Gorski, T., et al. (2020). Role of the GLUT1 Glucose Transporter in Postnatal CNS Angiogenesis and Blood-Brain Barrier Integrity. Circ Res *127*, 466-482. 10.1161/CIRCRESAHA.119.316463.

Villasenor, R., Ozmen, L., Messaddeq, N., Gruninger, F., Loetscher, H., Keller, A., Betsholtz, C., Freskgard, P.O., and Collin, L. (2016). Trafficking of Endogenous Immunoglobulins by Endothelial Cells at the Blood-Brain Barrier. Sci Rep *6*, 25658. 10.1038/srep25658.

Villasenor, R., Schilling, M., Sundaresan, J., Lutz, Y., and Collin, L. (2017). Sorting Tubules Regulate Blood-Brain Barrier Transcytosis. Cell Rep *21*, 3256-3270. 10.1016/j.celrep.2017.11.055.

Wang, Y., Cho, C., Williams, J., Smallwood, P.M., Zhang, C., Junge, H.J., and Nathans, J. (2018). Interplay of the Norrin and Wnt7a/Wnt7b signaling systems in blood-brain barrier and

blood-retina barrier development and maintenance. Proc Natl Acad Sci U S A *115*, E11827-E11836. 10.1073/pnas.1813217115.

Wang, Y., Huso, D., Cahill, H., Ryugo, D., and Nathans, J. (2001). Progressive cerebellar, auditory, and esophageal dysfunction caused by targeted disruption of the frizzled-4 gene. J Neurosci *21*, 4761-4771.

Wang, Y., Macke, J.P., Abella, B.S., Andreasson, K., Worley, P., Gilbert, D.J., Copeland, N.G., Jenkins, N.A., and Nathans, J. (1996). A large family of putative transmembrane receptors homologous to the product of the Drosophila tissue polarity gene frizzled. J Biol Chem *271*, 4468-4476. 10.1074/jbc.271.8.4468.

Wang, Y., Rattner, A., Zhou, Y., Williams, J., Smallwood, P.M., and Nathans, J. (2012). Norrin/Frizzled4 signaling in retinal vascular development and blood brain barrier plasticity. Cell *151*, 1332-1344. 10.1016/j.cell.2012.10.042.

Wang, Y., Sabbagh, M.F., Gu, X., Rattner, A., Williams, J., and Nathans, J. (2019). Beta-catenin signaling regulates barrier-specific gene expression in circumventricular organ and ocular vasculatures. Elife *8*. 10.7554/eLife.43257.

Wang, Z., Liu, C.H., Huang, S., Fu, Z., Tomita, Y., Britton, W.R., Cho, S.S., Chen, C.T., Sun, Y., Ma, J.X., et al. (2020). Wnt signaling activates MFSD2A to suppress vascular endothelial transcytosis and maintain blood-retinal barrier. Sci Adv *6*, eaba7457. 10.1126/sciadv.aba7457.

Westergaard, E. (1980). Transport of microperoxidase across segments of cerebral arterioles under normal conditions. Neuropathol Appl Neurobiol *6*, 267-277. 10.1111/j.1365-2990.1980.tb00211.x.

Winkler, E.A., Nishida, Y., Sagare, A.P., Rege, S.V., Bell, R.D., Perlmutter, D., Sengillo, J.D., Hillman, S., Kong, P., Nelson, A.R., et al. (2015). GLUT1 reductions exacerbate Alzheimer's disease vasculo-neuronal dysfunction and degeneration. Nat Neurosci *18*, 521-530. 10.1038/nn.3966.

Winkler, E.A., Sengillo, J.D., Bell, R.D., Wang, J., and Zlokovic, B.V. (2012). Blood-spinal cord barrier pericyte reductions contribute to increased capillary permeability. J Cereb Blood Flow Metab *32*, 1841-1852. 10.1038/jcbfm.2012.113.

Xia, C.H., Liu, H., Cheung, D., Wang, M., Cheng, C., Du, X., Chang, B., Beutler, B., and Gong, X. (2008). A model for familial exudative vitreoretinopathy caused by LPR5 mutations. Hum Mol Genet *17*, 1605-1612. 10.1093/hmg/ddn047.

Xu, Q., Wang, Y., Dabdoub, A., Smallwood, P.M., Williams, J., Woods, C., Kelley, M.W., Jiang, L., Tasman, W., Zhang, K., and Nathans, J. (2004). Vascular development in the retina and inner ear: control by Norrin and Frizzled-4, a high-affinity ligand-receptor pair. Cell *116*, 883-895. 10.1016/s0092-8674(04)00216-8.

Yamazaki, Y., Baker, D.J., Tachibana, M., Liu, C.C., van Deursen, J.M., Brott, T.G., Bu, G., and Kanekiyo, T. (2016). Vascular Cell Senescence Contributes to Blood-Brain Barrier Breakdown. Stroke *47*, 1068-1077. 10.1161/STROKEAHA.115.010835.

Yang, A.C., Stevens, M.Y., Chen, M.B., Lee, D.P., Stahli, D., Gate, D., Contrepois, K., Chen, W., Iram, T., Zhang, L., et al. (2020). Physiological blood-brain transport is impaired with age by a shift in transcytosis. Nature *583*, 425-430. 10.1038/s41586-020-2453-z.

Yao, Y., Chen, Z.L., Norris, E.H., and Strickland, S. (2014). Astrocytic laminin regulates pericyte differentiation and maintains blood brain barrier integrity. Nat Commun *5*, 3413. 10.1038/ncomms4413.

Ye, X., Smallwood, P., and Nathans, J. (2011). Expression of the Norrie disease gene (Ndp) in developing and adult mouse eye, ear, and brain. Gene Expr Patterns *11*, 151-155. 10.1016/j.gep.2010.10.007.

Ye, X., Wang, Y., Cahill, H., Yu, M., Badea, T.C., Smallwood, P.M., Peachey, N.S., and Nathans, J. (2009). Norrin, frizzled-4, and Lrp5 signaling in endothelial cells controls a genetic program for retinal vascularization. Cell *139*, 285-298. 10.1016/j.cell.2009.07.047.

Zhang, C., Lai, M.B., Pedler, M.G., Johnson, V., Adams, R.H., Petrash, J.M., Chen, Z., and Junge, H.J. (2018). Endothelial Cell-Specific Inactivation of TSPAN12 (Tetraspanin 12) Reveals Pathological Consequences of Barrier Defects in an Otherwise Intact Vasculature. Arterioscler Thromb Vasc Biol *38*, 2691-2705. 10.1161/ATVBAHA.118.311689.

Zhang, Y., Chen, K., Sloan, S.A., Bennett, M.L., Scholze, A.R., O'Keeffe, S., Phatnani, H.P., Guarnieri, P., Caneda, C., Ruderisch, N., et al. (2014). An RNA-sequencing transcriptome and splicing database of glia, neurons, and vascular cells of the cerebral cortex. J Neurosci *34*, 11929-11947. 10.1523/JNEUROSCI.1860-14.2014.

Zhao, L., Li, Z., Vong, J.S.L., Chen, X., Lai, H.M., Yan, L.Y.C., Huang, J., Sy, S.K.H., Tian, X., Huang, Y., et al. (2020). Pharmacologically reversible zonation-dependent endothelial cell transcriptomic changes with neurodegenerative disease associations in the aged brain. Nat Commun *11*, 4413. 10.1038/s41467-020-18249-3.

Zhou, Y., and Nathans, J. (2014). Gpr124 controls CNS angiogenesis and blood-brain barrier integrity by promoting ligand-specific canonical wnt signaling. Dev Cell *31*, 248-256. 10.1016/j.devcel.2014.08.018.

Zhou, Y., Wang, Y., Tischfield, M., Williams, J., Smallwood, P.M., Rattner, A., Taketo, M.M., and Nathans, J. (2014). Canonical WNT signaling components in vascular development and barrier formation. J Clin Invest *124*, 3825-3846. 10.1172/JCI76431.